Universitätsklinikum Hamburg-Eppendorf

Zentrum für Experimentelle Medizin,
Institut für Experimentelle Pharmakologie und Toxikologie

Institutsdirektor: Prof. Dr. Thomas Eschenhagen

Konstitutive Phosphorylierung von cMyBP-C als Behandlung der Hypertrophischen Kardiomyopathie?

Dissertation

zur Erlangung des Grades eines Doktors der Medizin
an der Medizinischen Fakultät der Universität Hamburg

vorgelegt von

Alexander Dutsch
aus Henstedt-Ulzburg

Hamburg 2017

Angenommen von der
Medizinischen Fakultät der Universität Hamburg am: 10.10.2017

Veröffentlicht mit Genehmigung der
Medizinischen Fakultät der Universität Hamburg.

Prüfungsausschuss, der/die Vorsitzende: Prof. Dr. Lucie Carrier

Prüfungsausschuss, zweite/r Gutachter/in: Prof. Dr. Heimo Ehmke

Table of Contents

1 Introduction 1

1.1 Cardiomyopathies 1

1.2 Hypertrophic Cardiomyopathy (HCM) 2

1.3 The sarcomere - contractile unit of the muscle 5

1.4 Excitation contraction coupling (ECC) 6

1.5 β-Adrenergic signaling in cardiac myocytes and impact on ECC 7

1.6 Cardiac myosin-binding protein C (cMyBP-C) 8

1.6.1 Role in contraction and relaxation 9

1.6.2 Phosphorylation – a posttranslational modification 10

1.6.3 *MYBPC3* mutations and links to HCM 12

1.7 Current therapies 13

1.8 Gene therapy 14

1.9 Engineered heart tissues (EHTs) 17

1.10 Aim of the study 18

2 Material and Methods 19

2.1 Recombinant adeno-associated virus 19

2.2 Bacterial strains 19

2.3 Chemicals and solutions 19

2.4 Laboratory equipment 21

2.5 Consumable material 23

2.6 Antibodies 24

2.6.1 Western Blot 24

2.6.1.1 Primary antibodies 24

2.6.1.2 Secondary antibodies 25

2.6.2 Immunofluorescence 25

2.6.2.1 Primary antibodies 25

2.6.2.2 Secondary antibodies 25

2.7 Primers 25

2.7.1 Primers for site-directed PCR mutagenesis 25

2.7.2 *Mybpc3* primer sequences for sequencing and PCR 26

2.7.3 *Mybpc3* primer and probe sequences for qPCR 26

2.8 Restriction Enzymes 27

2.9 Homozygous *Mybpc3*-targeted knock-in (KI) mouse model 28

2.10 Production of recombinant adeno-associated virus serotype 6 28

2.11 Murine EHTs 29

2.11.1 Solutions for EHTs 29

2.11.2 Isolation of neonatal mouse cardiac myocytes 30
2.11.3 Generation of mouse EHTs in a 24-well format 31
2.11.4 AAV6-mediated gene transfer in EHTs 32
2.11.5 EHTs culture 33
2.11.6 Harvesting of EHTs 33
2.11.7 EHTs contraction analysis 34
2.11.7.1 Spontaneous contractions 34
2.11.7.2 Electrical pacing 36
2.12 DNA and RNA analysis 38
2.12.1 Site-directed mutagenesis PCR 38
2.12.2 Preparation of plasmid DNA 39
2.12.3 Restriction digestion 39
2.12.4 RNA extraction from EHTs 40
2.12.5 Determination of DNA and RNA concentrations 40
2.12.6 Reverse transcription 41
2.12.7 Polymerase Chain Reaction 41
2.12.8 Quantitative PCR 42
2.12.9 Agarose gel electrophoresis 44
2.12.10 Sequencing of DNA 44
2.13 Protein analysis 44
2.13.1 Protein extraction from EHTs 44
2.13.2 SDS-PAGE 45
2.13.3 Western Blot analysis 46
2.13.4 Immunoflourescence analysis of EHTs 47
2.14 Statistical analysis 48
3 Results 49
3.1 Introducing the mutation Ser282Asp in WT *Mybpc3* cDNA 49
3.2 Generation of EHTs 50
3.3 Measurements of contractile parameters under spontaneous contraction 52
3.4 Analysis of contractile parameters 53
3.5 Measurement of contractile parameters under electrical pacing 56
3.5.1 Analysis of contractile parameters 58
3.5.2 Response to rising external [Ca^{2+}] and calcium sensitivity 60
3.5.3 Response to isoprenaline at submaximal external [Ca^{2+}] 61
3.5.4 Response to EMD 57033 at submaximal external [Ca^{2+}] 64
3.6 Evaluation of *Mybpc3* and hypertrophic markers 66
3.6.1 Total *Mybpc3* mRNA and prevention of accumulation of mutant mRNAs 66

3.6.2 Evaluation of mutant *Mybpc3* mRNAs 68
3.6.3 Hypertrophic markers 69
3.7 Evaluation of cMyBP-C protein level 70
3.8 Evaluation of phosphorylation state of serine residues in the Mybpc-Motif 70
3.9 Sarcomeric localization of cMyBP-C in EHTs 72
4 Discussion 76
4.1 Mouse-EHTs – a relatively young model 77
4.2 Hypercontractile HCM-phenotype of KI-EHTs 79
4.2.1 Feasibility of AAV6-mediated gene therapy in EHTs 80
4.2.2 Rescue of the hypercontractile phenotype in KI-EHTs 81
4.2.3 Impact of constitutive phosphorylation *in vitro* 84
4.3 Role of M-Motif serine 282: trigger or serine as any other? 85
4.4 From bench to bedside – HCM gene therapy in humans 87
4.5 Conclusion and future directions 88
5 Zusammenfassung 89
6 Summary 91
7 Literature 93
8 Own publications 104
9 Acknowledgements 105
10 Curriculum vitae 107
11 Appendix 108
11.1 List of abbreviations 108
11.2 SI Prefixes 111
Eidesstattliche Versicherung 112

1 Introduction

The heart is the central organ in living beings since it is the engine for the whole body maintaining a proper function of the other organs. Many limiting diseases are cardiovascular diseases – or heart diseases.

1.1 Cardiomyopathies

Diseases of the circulatory system are still the main cause of death (40%, Figure 1) in an industrial nation, such as Germany.

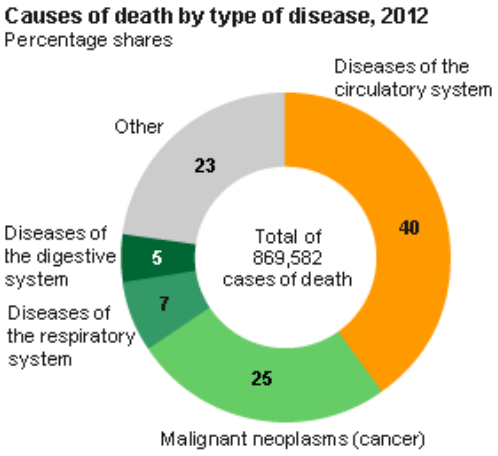

Figure 1: Causes of death by type of disease in Germany (2012). 40% of deaths in Germany in both sexes were caused by diseases of the circulatory system (2012), from: Statistisches Bundesamt, visited: 2014.

Here cardiomyopathies play a major role. Forty years ago, there was not much known about cardiomyopathies and thus the term was used to describe myocardial diseases that could not be classified in another way (Elliott et al. 2008). Until now the knowledge about etiology and pathophysiology of different cardiomyopathies has grown. To date they are classified according to the 'European Society of Cardiology Working Group on Myocardial and Pericardial Diseases'. In order to provide relevance to everyday clinical practice, cardiomyopathies shall be specified by morphological and functional properties that are either of familial or non-familial origin (Figure 2).

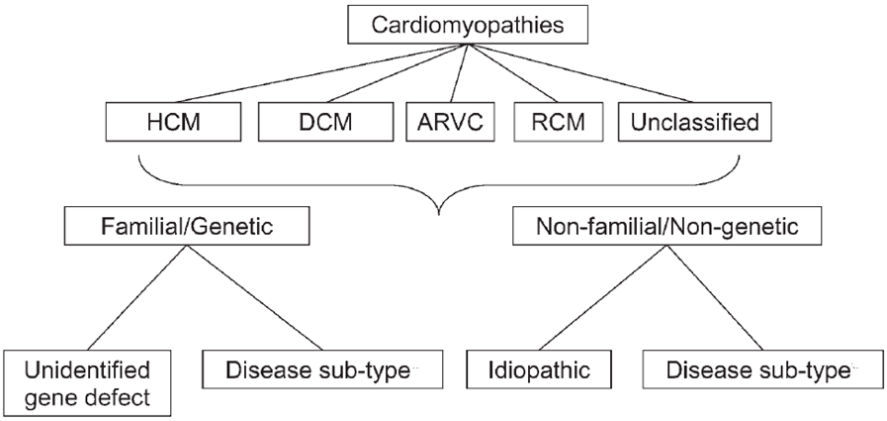

Figure 2: Classification of cardiomyopathies by the 'European Society of Cardiology Working Group on Myocardial and Pericardial Diseaes'. HCM, hypertrophic cardiomyopathy; DCM, dilated cardiomyopathy; ARVC, arrhythmogenic right ventricular cardiomyopathy; RCM, restrictive cardiomyopathy (Elliott et al. 2008).

1.2 Hypertrophic Cardiomyopathy (HCM)

Hypertrophic cardiomyopathy (HCM) is the most common inherited cardiac disease with a prevalence in the general population of 0.2%, affecting both sexes (Maron et al. 1995). The number of undetected cases may be higher because many patients do not show symptoms (Maron et al. 2014). Symptomatic patients mainly complain about chest pain and dyspnea during exercise. Syncopes are also observed, but to a much lower extent (Elliott and McKenna 2004). HCM was first described as an asymmetrical hypertrophy of the heart (Teare 1958). Today much more about pathophysiological alterations is known; however, the knowledge is still incomplete. HCM is clinically characterized by an unexplained increase of the thickness of the left-ventricular wall (≥15 mm in adults) and a hypertrophy of the left ventricle (LV, Figure 3), verified by cardiac imaging techniques. Increase of LV thickness often leads to an outflow obstruction, which is mainly responsible for the symptoms in patients.

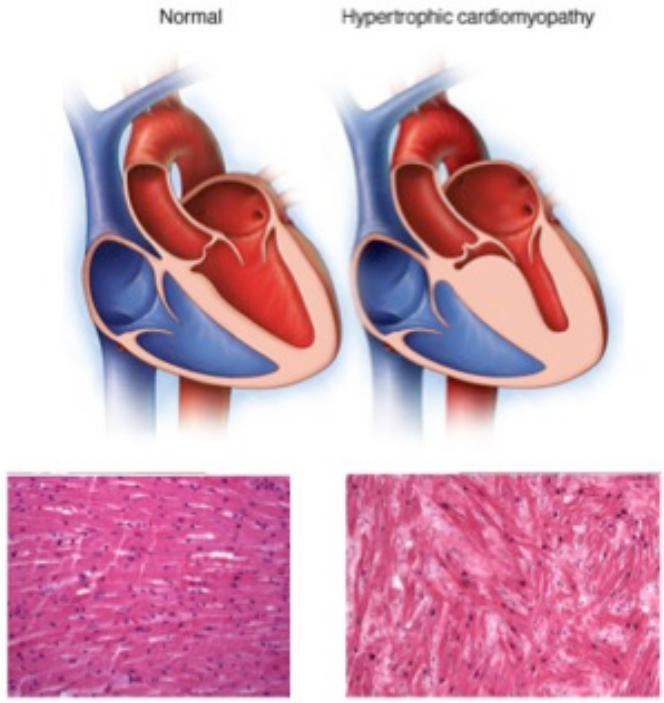

Figure 3: Morphological characteristics of HCM. Comparison of a normal and a heart showing typical features of HCM (upper part). In the bottom part: histological sections (stained with hematoxylin and eosin); adapted from the Mayo Clinic website (upper part, visited: September 2014) and bottom part from (Ho 2010).

The right ventricle can be affected in some cases, but never without involvement of the LV. Many patients show asymmetric LV-hypertrophy, most commonly including the interventricular septum (Maron et al. 2014). On histological level HCM is characterized by a disarray of the cardiomyocytes and interstitial fibrosis (Figure 3). In combination with dilatation of the atria this might be the cause for arrhythmias in patients, generally presented as atrial fibrillation. In addition to the involvement of the cardiac muscle, also vascular and microvascular changes can be observed in HCM hearts. This contributes to myocardial ischemia (Elliott and McKenna 2004). Systolic function remains normal until a late stage of the disease, whereas diastolic function is impaired quite early (Lekanne Deprez et al. 2006). The main devastating consequence of HCM, besides the transition to heart failure, is the appearance of sudden cardiac death especially in young competing athletes (Maron et al. 1996).

Less is known about neonatal forms of HCM. These are severe states of the disease and affected children do not survive their first year of life (Xin et al. 2007). A study presenting 4 children with proven *MYBPC3* mutations showed problems with feeding, failure to thrive and dyspnea. All of them died from cardiac failure before 13 weeks of age (Wessels et al. 2015).

HCM is transmitted via an autosomal-dominant inheritance pattern. Mutations in at least 19 genes, encoding sarcomeric proteins are known to cause the disease (Table 1).

Table 1: Sarcomeric genes in which mutations lead to HCM (Schlossarek et al. 2011).

Gene name	Symbol	Number of mutations
β-myosin heavy chain	*MYH7*	218
Cardiac myosin-binding protein C	*MYBPC3*	185
Cardiac troponin T	*TNNT2*	36
Cardiac troponin I	*TNNI3*	30
α-tropomyosin	*TPM1*	12
Regulatory myosin light chain	*MYL2*	10
Cardiac α-actin	*ACTC1*	7
Essential myosin light chain	*MYL3*	5
α-actinin 2	*ACTN2*	4
Muscle LIM protein	*CSRP3*	3
Muscle RING-finger protein 1	*TRIM63*	3
Myozenin 2 (calsarcin 1)	*MYOZ2*	2
Nexilin	*NEXN*	2
Telethonin	*TCAP*	2
Titin	*TTN*	2
Vinculin	*VCL*	2
Cardiac troponin C	*TNNC1*	1
α-myosin heavy chain	*MYH6*	1
Obscurin	*OBSCN*	1

In more than 60% of genotyped HCM cases the main affected genes are *MYH7* and *MYBPC3* coding for beta-myosin heavy chain (β-MHC) and cardiac myosin-binding protein C (cMyBP-C), respectively. Mutations in *MYBPC3* are the major cause of the disease. In contrast to HCM patients with *MYH7* mutations, many patients with *MYPBC3* mutations show a later onset, lower penetrance and an overall more benign phenotype. *MYBPC3* mutations, however, are mainly linked to a significant morbidity and mortality (Harris et al. 2011). Most of the patients are heterozygotes for *MYBPC3* mutations, nonetheless up to 6% (Richard et al. 2003) are either compound-heterozygotes or homozygotes for mutations leading to HCM and thus present a severe phenotype (cave: severity is depending on form of mutation, if missense or truncating), especially seen at neonatal stage (Lekanne Deprez et al. 2006, Xin et al. 2007, Wessels et al. 2015). A relation between genetic state, severity of the disease or contractile function is not possible, neither in children nor in adults (Morita et al. 2008). Taken together, this suggests additional factors like environment, microRNAs or posttranslational modifications to be responsible for the onset and manifestation of the disease (Schlossarek et al. 2011).

1.3 The sarcomere - contractile unit of the muscle

The sarcomere is composed of thick and thin filaments that form a contractile unit within a myocyte. The close interaction of the filaments enables the contraction of cardiomyocytes. Simplified due to microscopy nomenclature, the sarcomere is defined as the unit between two neighbouring Z-lines. In between two Z-lines, the I-band (mainly formed by the thin filament actin) and the A-band (mainly formed by the thick filaments, myosin) with C-zone (formed by cMyBP-C) and M-line complete the sarcomere (Figure 4).

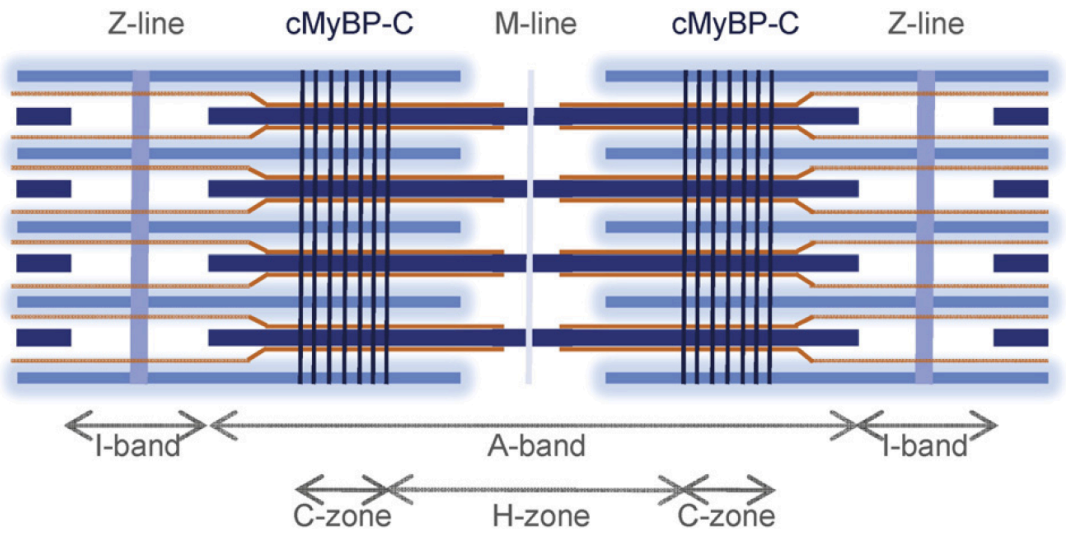

Figure 4: Schematic illustration of the sarcomere. Two Z-lines form the sarcomere, containing the I-band (composed of thin filaments; light blue) and the A-band (composed of thick filaments, dark blue). In addition, the titin forms the third elastic filament (orange lines; adapted from Carrier et al. 2015).

The actin filaments consist of small globular units with specific binding sites for myosin, fixed at the Z-discs. Additional proteins that are part of the thin filament are the troponin complex (cardiac troponin T (cTnT), cardiac troponin C (cTnC), cardiac troponin I (cTnI)) and tropomyosin. Myosin filaments consist of heavy chains with attached heads for binding to actin (α/β-myosin heavy chain) and both regulatory and essential light chains (MLC). The thick filaments are stabilized and fixed to the Z-discs via a giant protein, titin, which stands between the thin and thick filaments. Interaction of myosin and actin leads to shortening of the sarcomere, which is the main mechanism of contraction. This is triggered by an increase in intracellular [Ca^{2+}] concentration, which when bound to cTnC releases the binding site on actin for myosin, usually blocked by α-tropomyosin. The hydrolysis of adenosinetriphosphate

(ATP) by an intrinsic ATPase activity of myosin initiates several steps of conformational changes that finally lead to a migration of myosin heads on actin filaments, representing the contraction on molecular level. Active decrease in intracellular [Ca^{2+}] concentration via different mechanisms, such as sarcoplasmic reticulum ATPase (SERCA), sodium-calcium exchanger (NCX), mitochondrial uniport or cell membrane located calcium ATPases finish the mentioned cycle of contraction (Figure 5). Increase in intracellular [Ca^{2+}] concentration then leads to a reentry of the cycle.

1.4 Excitation contraction coupling (ECC)

The cardiac contraction is enabled by the transformation of an electrical signal into the interaction of the contractile filaments, supported by changes of intracellular [Ca^{2+}] concentration. This process is known as excitation contraction coupling (ECC, reviewed in Bers 2002). An incoming action potential leads to a depolarization of the cell membrane. This induces an intake of calcium into the cytosol of a cardiac myocyte via voltage sensitive calcium channels that are located in the cell membrane. The increase in intracellular [Ca^{2+}] concentration leads to an activation of cardiac ryanodine receptors (RyR) that are located on the sarcoplasmic reticulum (SR). The RyR simultaneously act as calcium channels and induce a further release of calcium from the SR, known as calcium-induced calcium release. The increase in [Ca^{2+}] concentration corresponds to the plateau of the action potential and enables the interaction of the myofilaments for contraction (Figure 5). The active decrease in [Ca^{2+}] concentration finishes the contraction cycle.

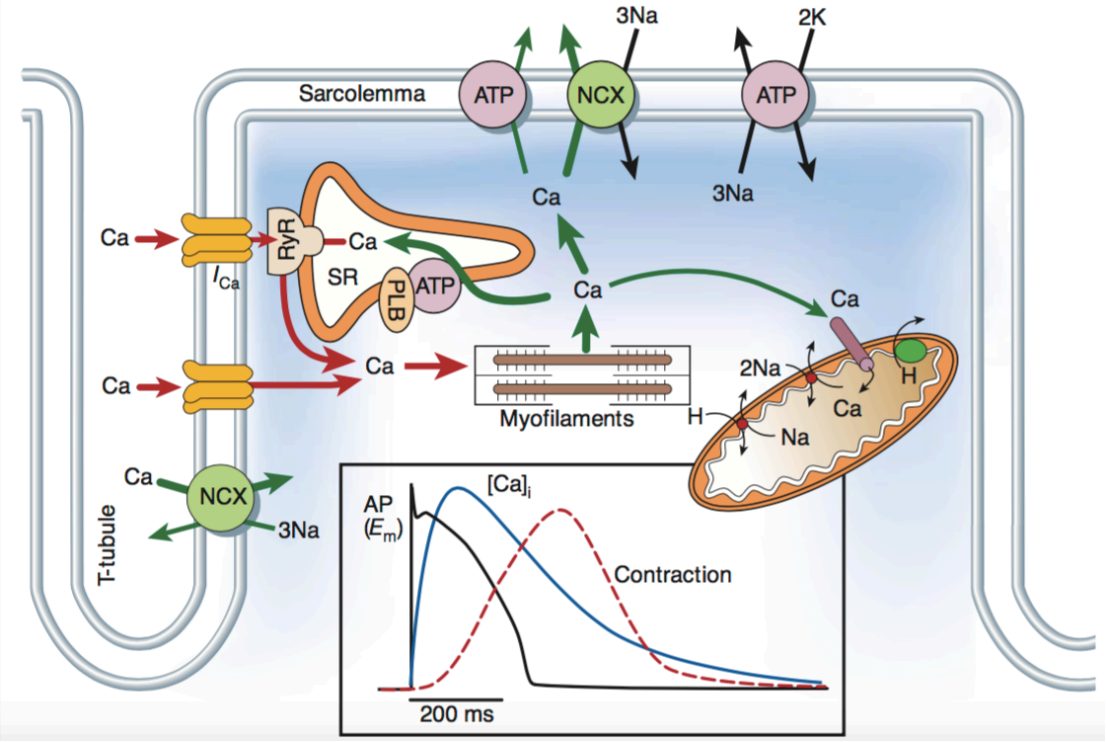

Figure 5: Excitation contraction coupling cycle of calcium intake and release from the cytosol in a cardiac myocyte. An incoming action potential (AP) induces a membrane depolarization and the intake of calcium via voltage sensitive calcium channels. The increase in [Ca^{2+}] concentration induces a further release from the sarcoplasmic reticulum by caradiac ryanodine receptors (RyR, calcium induced calcium release) and interaction of the myofilaments. Active decrease of [Ca^{2+}] concentration finishes the cycle of contraction. AP, action potential; ATP, adenosine triphosphate; PLB, phospholamban; SR, sarcoplasmic reticulum; RyR, ryanodine receptor; NCX, sodium-calcium exchanger (adapted from: Bers 2002).

1.5 β-Adrenergic signaling in cardiac myocytes and impact on ECC

Stimulation of β-adrenergic receptors in the heart increases the force of contraction (inotropy), the heart rate (chronotropy), the electrical conductivity (bathmotropy) and the speed of relaxation (lusitropy). Especially inotropy and lusitropy are relevant in the ventricular myocardium. β-Adrenergic receptor stimulation activates a stimulating GTP-binding protein (G_s), which induces the adenelyl cyclase to produce cyclic adenosine monophosphate (cAMP) from ATP. cAMP then stimulates cAMP-dependent protein kinase A (PKA) to phosphorylate downstream targets, such as voltage sensitive calcium channels, the cardiac ryanodine receptor, cMyBP-C, cTnI or phospholamban. Phosphorylation of voltage sensitive calcium channels and the ryanodine receptor increases their open probability for calcium transmission into the cytosol. This additional cytosolic calcium availability increases both the maximal force generation and the sensitivity towards calcium. Phosphorylation of phospholamban reduces its repressing impact on SERCA. This accelerates the calcium uptake into

the sarcoplasmatic reticulum and supports relaxation. The whole process can be inhibited by activation of M2-muscarinic receptors and the stimulation of an inhibitory GTP-binding protein (G_i). G_i reduces the adenylyl cyclase activity and in this way the concentration of cAMP (Figure 6, reviewed in Bers 2002).

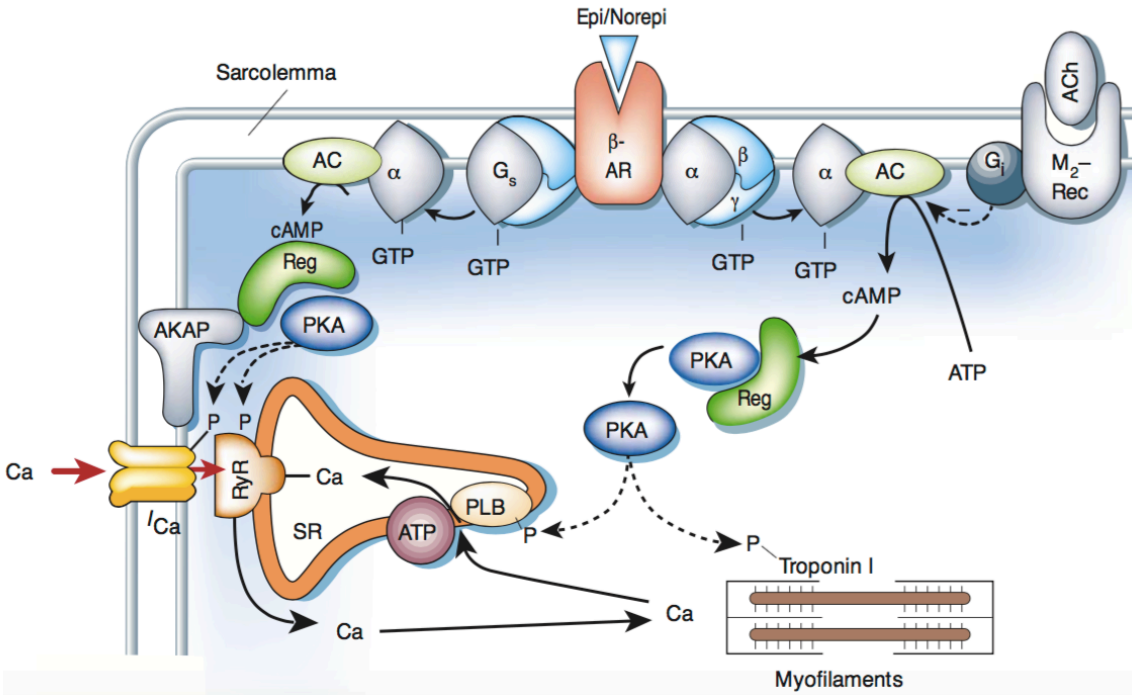

Figure 6: β-Adrenergic signaling in cardiac myocytes and impact on ECC. β-Adrenergic and M2-muscarinic signaling in cardiac myocytes and the downstream targets of PKA phosphorylation with impact on ECC cycle. AC, adenylyl cyclyase; β-AR, β-adrenergic receptor; ACh, acetylcholine; ATP, adenosine triphosphate; GTP, guansine triphosphate; AKAP, A kinase anchoring protein; Reg, PKA regulatory subunit; M_2-Rec, M_2-muscarinic receptor; G_s, stimulating GTP-binding protein; G_i, inhibitory GTP-binding protein; PLB, phospholamban; SR, sarcoplasmatic reticulum; RyR, ryanodine receptor; PKA, protein kinase A (adapted from: Bers 2002).

1.6 Cardiac myosin-binding protein C (cMyBP-C)

A first general description of a c-MyBP-C or C-protein was made by Offer and colleagues (Offer et al. 1973). There are three isoforms of myosin-binding protein C, the fast-skeletal, slow-skeletal and the cardiac (Yamamoto and Moos 1983), which are highly conserved through all species. The first description of the whole sequence of the human *MYBPC3* gene was made by Lucie Carrier and colleagues. It was shown that the gene, located on chromosome 11, consists of more than 21000 bp, with 35 exons, of which only 34 are coding (Carrier et al. 1997). The cardiac isoform (150 kDa) is exclusively expressed in the heart (Fougerousse et al. 1998) and consists of 8 immunoglobulin-like domains and 3 fibronectin-like domains. The N-terminal domains mainly interact with actin and myosin (fragment S2). The COOH-

terminal domains interact with myosin (LMM) and titin (Figure 7). The tight regulated interaction has a direct impact on the contraction.

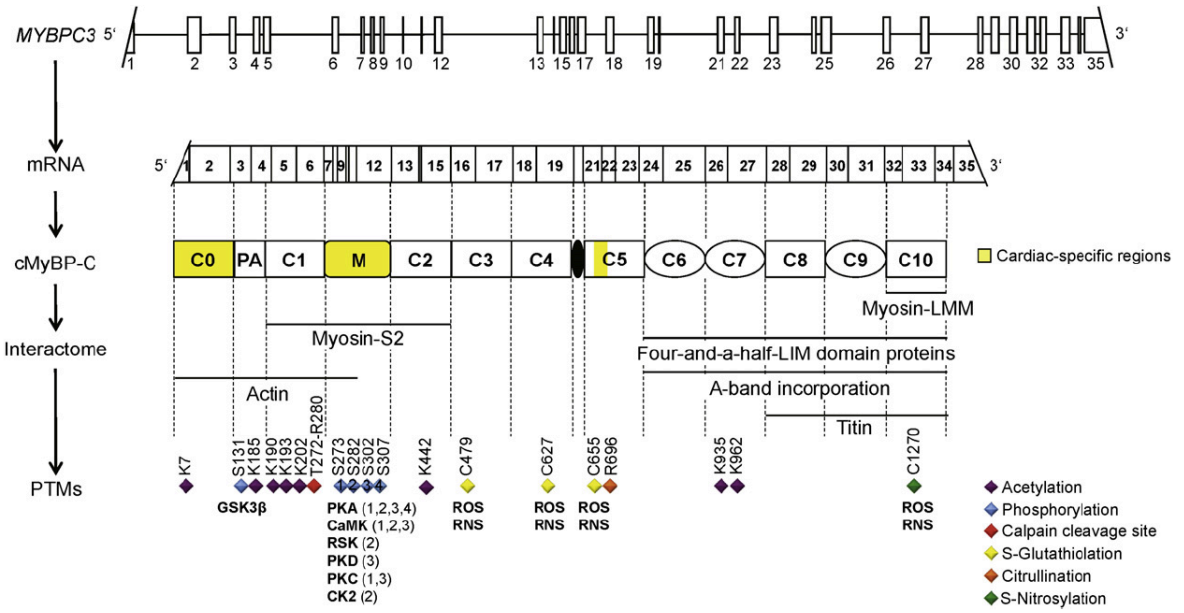

Figure 7: Schematic illustration of murine *MYBPC3*, mRNA and cMyBP-C and its interaction sites with contractile proteins and its posttranslational modifications. *MYBPC3* contains 21 kbp in 35 exons. The cMyBP-C consists of 8 immunoglobulin-like domains (squares) and 3 fibronectin-like domains (ovals). The cardiac specific regions are shown in yellow. The M-Motif (M), with the four phosphorylatable serine residues (S273, S282, S302 and S307) is shown in yellow as a cardiac specific region. cMyBP-C is a target for many forms of posttranslational modifications, indicated by the differentially coloured hashes. CaMK, calcium calmodulin-dependent protein kinase; CK2, casein kinase II; GSK3β, glycogen-synthase kinase isoform 3β; PKA, cAMP activated protein kinase; PKD, protein kinase D; PKC, protein kinase C; ROS, reactive oxygen species; RNS, reactive nitrogen species; RSK, ribosomal S6 kinase (adapted from: Carrier et al. 2015).

Unique elements of the cardiac isoform are an additional IgC2-like domain (C0) at the N-terminus, four phosphorylation sites in the Mybpc-Motif (M-Motif) and the insertion of 28 amino acids in the C5 domain (reviewed in Flashman et al. 2004, Oakley et al. 2004, Schlossarek et al. 2011). The phosphorylation of the four serine residues is mediated by a variety of different kinases (Figure 7). The correct organization of cMyBP-C in the sarcomere is still not completely understood (reviewed in Schlossarek et al. 2011). The arrangement in preference is a trimeric collar formation around the myosin filament backbone in which three cMyBP-C molecules bind with their C5-C10 domains to myosin and reach with the domains C0-C4 into the interfilament space, for the interaction with actin and the myosin fragment S2 (Winegrad 1999).

1.6.1 Role in contraction and relaxation

cMyBP-C is a regulator of contraction and relaxation in cardiomyocytes (reviewed in Sadayappan and de Tombe 2012). Lessons learned from knock-in (KI), knock-out

(KO) and transgenic mice suggest an impact on cardiac function (reviewed in Harris et al. 2011). A lack of C-protein leads to an increase in the binding probability of myosin heads to actin, disabling a proper relaxation of cardiomyocytes (Pohlmann et al. 2007). This suggests that cMyBP-C has an important influence on regulation of the relaxation of the heart (reviewed in Schlossarek et al. 2011). Regulation of the diastole is most likely mediated via the binding site to actin within the C0-C1 domain (Herron et al. 2006, Mun et al. 2014) as well as the S2 fragment of myosin filaments via the C1-M-C2 domain. The interaction with the S2 fragment is essential for regulation of both contraction and relaxation. This is mainly depending on the phosphorylation state of the M-Motif serines (reviewed in Flashman et al. 2004). Phosphorylation leads to a weakening of the cMyBP-C attachment to the S2 fragment and to actin. This increases the probability of myosin heads binding to actin and promotes the contraction (Figure 8). That implicates a regulatory function on the cross-bridge cycle, increasing the speed of interaction.

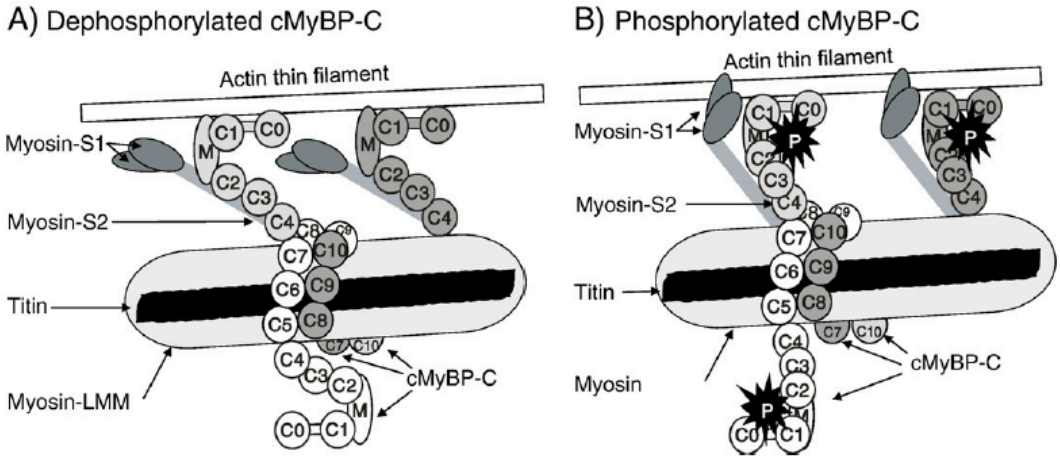

Figure 8: Interaction of cMyBP-C with actin and myosin and role of phosphorylation. [A] Three cMyBP-C molecules are bound with their C-terminal domains around the thick filament backbone (light-meromyosin, Myosin-LMM) from there reaching to the thin filament (interaction with N-terminal domains). The M-Motif is interacting with the Myosin-S2 fragment. **[B]** Phosphorylation in the M-Motif weakens the binding of cMyBP-C to actin, enabling myosin-heads to interact with actin (Schlossarek et al. 2011).

1.6.2 Phosphorylation – a posttranslational modification

Proper function of the sarcomeric proteins is closely related to the posttranslational modifications of the interacting proteins (see Figure 7 for cMyBP-C). In the center of attention is the phosphorylation, since a dysfunction is closely related to the phosphorylation state of different proteins (Kuster et al. 2012). Especially phosphorylation of cMyBP-C was shown to be essential for maintaining a normal

cardiac function, even at rest (Barefield and Sadayappan 2010, James and Robbins 2011, Bardswell et al. 2012, Sadayappan and de Tombe 2012). The main investigations were made on the phosphorylation of the M-Motif serine residues, since they have a main influence on contractility. In general, cMyBP-C phosphorylation was shown to be cardioprotective (Sadayappan et al. 2006) and protects the protein itself from degradation, which might preserve cardiac contractility (Barefield and Sadayappan 2010). Therefore it seems reasonable that phosphorylation of cMyBP-C is reduced in human and experimental model of heart failure (El-Armouche et al. 2007). The four M-Motif serines are phosphorylated by different protein kinases (Figure 7). Upon β-adrenergic stimulation and activation of PKA all serine residues can be phosphorylated (Gautel et al. 1995, Jia et al. 2010). This leads to an increase in cross-bridge-kinetics and thus quicker contraction, relaxation and a higher force development. It is still not clear, whether PKA-induced phosphorylation of cMyBP-C directly affects myofilament Ca^{2+} sensitivity, has a modulating influence on it or whether myofilament Ca^{2+} sensitivity is mainly controlled by cTnI phosphorylation (Barefield and Sadayappan 2010, Bardswell et al. 2012, Kuster et al. 2012).

Besides PKA, cMyBP-C is also known to be phosphorylated by the calcium calmodulin-dependent protein kinase II (CaMKII) (Schlender and Bean 1991). CaMKII phosphorylates Ser-273, Ser-282 and Ser-302, of which Ser-282 phosphorylation seems to be necessary at least for Ser-302 phosphorylation (Sadayappan et al. 2011). Other kinases, known to phosphorylate cMyBP-C, are protein kinase C (PKC) and protein kinase D (PKD). While PKC phosphorylates Ser-273 and Ser-302 (Sadayappan et al. 2011), PKD exclusively phosphorylates Ser-302 (Bardswell et al. 2010). Recently the ribosomal S6 kinase (RSK) and casein kinase II (CK2) were identified as additional kinases acting only on Ser-282 phosphorylation (Cuello et al. 2011, Kooij et al. 2013). Since Gautel found first hints for a regulation of the M-Motif phosphorylation (Gautel et al. 1995), much investigation has been performed on the detection of a potential hierarchy between the M-Motif serines. Among these, the phosphorylation of Ser-282 might have a regulatory role on the phosphorylation of the remaining serine residues (Sadayappan et al. 2011, Gupta et al. 2013). A loss of the ability of Ser-282 phosphorylation in mice, however, was recently shown to have no major effect on the phosphorylation of neighbouring serine

residues upon PKA-phosphorylation. This might argue against a role of Ser-282 as a trigger for phosphorylation of Ser-273 and Ser-302 (Gresham et al. 2014).

1.6.3 *MYBPC3* mutations and links to HCM

Many mutations in the *MYBPC3* gene are known to cause HCM (Table 1). Most of them (>60%) are truncating nonsense mutations and lead to a frameshift. Both nonsense and frameshift mutations, which result in a premature termination codon (PTC) in the mRNA, produce a C-terminally truncated protein (Schlossarek et al. 2011, Sadayappan and de Tombe 2012). These resulting proteins miss binding sites for titin and light meromyosin, which are normally present in full-length cMyBP-C. Many patients are heterozygotes for *MYBPC3* mutations. In these patients a lower amount of wild-type (WT) cMyBP-C was found and truncated proteins were not detected (Marston et al. 2009). This strongly suggests haploinsufficiency as the main causal mechanism of the disease. Lack of cMyBP-C disturbs the composition of the sarcomere stoichiometry, impairs its function and by that induces stress signaling and hypertrophy, finally causing HCM (Richard et al. 2006, Schlossarek et al. 2011). A summary is given in Figure 9.

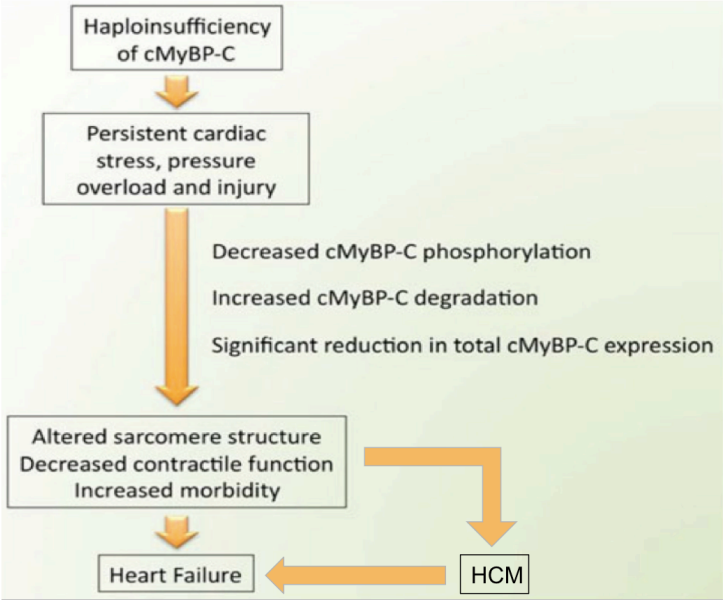

Figure 9: Pathophysiology, induced by haploinsufficiency in HCM. Due to a mutation in *MYBPC3* the remaining wild-type (WT) allele is not sufficient to compensate the loss of cMyBP-C (haploinsufficiency). This leads to cardiac stress, which induces further changes on cMyBP-C, such as decreased phosphorylation and cMyBP-C proteolysis, ending in heart failure (adapted from: Sadayappan and de Tombe 2012).

Confirmations for these assumptions were obtained in experiments with different animal models for HCM. Homozygous *Mybpc3*-targeted knock-in (KI) mice carrying a frequent founder mutation found in humans in Tuscany (Girolami et al. 2006) showed

reduced levels of total *Mybpc3* mRNAs and cMyBP-C proteins. Homozygous KI mice show typical features of HCM, such as LV hypertrophy, systolic and diastolic dysfunction and an increase in calcium-sensitivity (Vignier et al. 2009, Fraysse et al. 2012). In addition to haploinsufficiency, the presence of poison polypeptides that result from different reading frames in mutant mRNAs may be involved in disease pathogenesis (Figure 10).

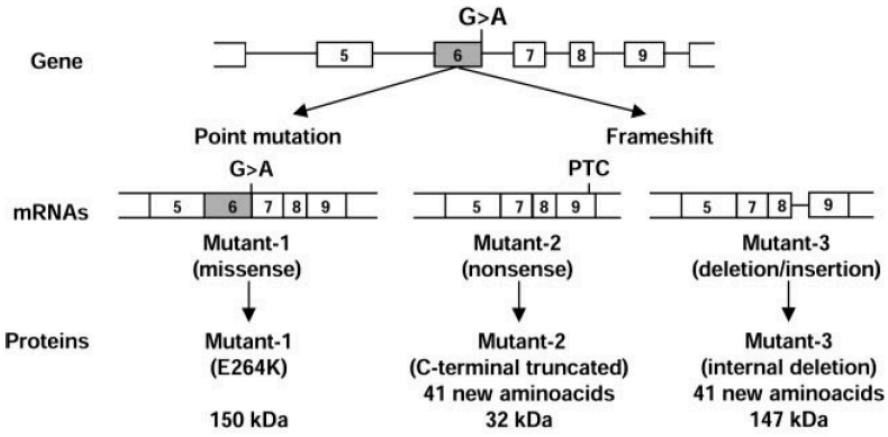

Figure 10: *Mybpc3* mutation (G>A transition) and its consequences on mRNA and protein level. G>A transition at the last nucleotide of exon 6 in the *Mybpc3* gene leads to 3 different mutant mRNAs and 3 different mutant proteins (Vignier et al. 2009).

This does also implicate an involvement of the nonsense-mediated mRNA decay as well as the ubiquitin-proteasome system and the autophagy-lysosome pathway (Sarikas et al. 2005, Schlossarek et al. 2014) in the development of HCM and makes the disease and its causing factors even more complex.

1.7 Current therapies

Although HCM and its devastating consequences are known for long, there are only symptomatic, empirically based therapies available to treat the disease (Authors/Task Force et al. 2014). Depending on the presented symptoms of the patients these can be either pharmacological or surgical treatments. According to the ESC guidelines of 2014, the drug therapy is mainly based on usage of β-blockers, calcium channel blockers and anti-arrhythmics. β-blockers, such as propranolol, alleviate the resting obstruction, improve relaxation and can provide systolic benefits (Adelman et al. 1970). They additionally suppress arrhythmic events (Tendera et al. 1993). Calcium channel blockers, such as verapamil or diltiazem can increase the exercise capacity and improve or normalize the LV diastolic filling, comparable to β-

blockers. These recommendations are suitable both for children and adults (Shaffer et al. 1988, Authors/Task Force et al. 2014). Antiarrhythmic drugs, such as disopyramide (class IA anti-arrhythmic) or amiodarone (class III anti-arrhythmic) are used to prevent supraventricular arrhythmic events, as well as ventricular arrhythmias (Robinson et al. 1990). Another drug that has been shown to be useful in HCM treatment, is perhexiline, which is used to improve energy depletion that is observed in HCM patients reflected by lower ratios of phosphocreatine to ATP (Abozguia et al. 2010). However, this drug is not approved for clinical use in Germany.

Surgical therapies are used in patients that do not benefit from drug therapies anymore or to relieve LV obstruction. Today's gold standard method is the septal myectomy with removal of excessive cardiac tissue (Authors/Task Force et al. 2014). Another approach is the septal alcohol ablation (TASH). Herein alcohol is subjected to a septal perforatory artery and causes a septal scar. With this procedure, however, up to 20% of the patients present an atrio-ventricular (AV) block as a complication. Patients at risk for sudden cardiac death due to their epicrisis should get an implanted cardioverter defibrillator (ICD; Elliott and McKenna 2004, Authors/Task Force et al. 2014).

The last treatment option, available for patients, that neither benefit from drug therapy nor from surgeries, is the heart transplantation (Harris et al. 2006, Maron et al. 2010, Maron and Maron 2013).

1.8 Gene therapy

Definiton of 'Gene therapy' is the delivery of DNA or RNA via specific vector systems either to prevent, treat or cure human inherited diseases. Many tools, vectors and strategies were developed to achieve these goals (Kaufmann et al. 2013). Conventional gene therapy involves the transfer of a whole gene (i.e. the whole cDNA) in order to substitute a defect gene in the targeted cell.

Initially gene therapy was thought to be used for the treatment of primary immunodeficiencies, but the principle of gene therapy is experimentally used in many

diseases today, becoming clinical reality with the approval of Glybera for the treatment of a lipoproteinlipase deficiency in 2012 (Pleger et al. 2013). The field is constantly growing. Another approach that took the obstacle to a phase 2 trial, is the gene therapy of SERCA2a for the treatment of heart failure patients (Jessup et al. 2011). The supporting company Celladon, however, stopped further research and development (press release 06/26/2015).

Especially inherited cardiomyopathies seem to be suitable candidates for gene therapy since they are often monogenic diseases (Mamidi et al. 2014). In regards to HCM, a recently published proof-of-concept study from the group around Lucie Carrier dealt with the adeno-associated virus (AAV) mediated transfer of a full-length *Mybpc3* cDNA. This way of gene therapy in homozygous *Mybpc3*-targeted KI mice prevented the development of an HCM-phenotype, implicating an even more feasible way of treatment with the possibility for the transition to the clinics (Mearini et al. 2014). Another group used a lentiviral-driven transfer of full-length *Mybpc3* into cMyBP-C deficient (cMyBP-C$^{-/-}$) mice via direct cardiac injection. After transduction mice displayed an improved contractile function with proper incorporation of exogenous cMyBP-C (Merkulov et al. 2012).

As mentioned above, there are different ways of application of gene therapy. Both viral and non-viral vector systems exist (reviewed in Vannucci et al. 2013, Wang et al. 2013). Many non-viral methods like administration of plasmid DNA provide almost unlimited sizes of delivered genes, however they show low transduction efficiency, short-term expression and unspecific tropism. In contrast, viral vectors provide a specific tropism for target cells, show long-term expression of the transgene and often only need a single administration for a sufficient treatment (Pleger et al. 2013, Mearini et al. 2014). Particularly AAVs are the main used viruses in gene therapy today, since they show a high efficiency of transduction of both dividing and non-dividing cells with a great tissue specificity (Table 3) and long term effect. In addition to that, AAVs induce only a low immune response (Vannucci et al. 2013). Advantages and disadvantages of AAVs are summarized in Table 2.

Table 2: Advantages and disadvantages of AAV in gene therapy (Vannucci et al. 2013).

Advantages	*Disadvantages*
Transduce non-dividing and dividing cells	Carry up to 5 Kbp heterologous DNA
Parental virus apathogenic	High vector titers difficult to achieve
Wide cellular tropism	Need co-infection by helper virus (adenovirus or herpes simplex virus)
Potential site-specific integration	
Low immunogenic	

WT AAV genome consists of *rep* and *cap* genes flanked by two inverted terminal repeats (ITR). These genes can be exchanged for the production of recombinant AAV with the therapeutic nucleic acid sequence of interest and the desired promoter upstream. Uptake of AAV occurs via endocytosis (Figure 11). Even though packaging capacity up to 5 kbp has been described, our group showed that AAV can carry even up to 5.4 kbp of heterologous DNA (Mearini et al. 2014).

Table 3: Tissue tropism of different AAV serotypes (Davis et al. 2008).

Tissue	AAV Serotype
Cardiac muscle	AAV9, AAV8, AAV6, AAV1, AAV7, AAV5, AAV2
Skeletal muscle	AAV1, AAV7, AAV6, AAV8, AAV9
Vascular endothelium	AAV1, AAV2, AAV5
Vascular smooth muscle	AAV2
CNS	AAV5, AAV1, AAV4, AAV2
Midbrain	AAV2
Ependyma / astrocytes	AAV4
Eye	
Retina	AAV5, AAV4
Photoreceptors	AAV5
Cochlear hair cells	AAV3
Lung	AAV9, AAV6, AAV5
Liver	AAV9, AAV8, AAV6, AAV2, AAV1
Pancreas	AAV8, AAV1, AAV2, AAV6
Kidney	AAV2, AAV9 (neonatal)

An increased cell tropism can be obtained by using specific promoter sequences. A promoter that could be shown to exclusively lead to expression in cardiomyocytes is the human cadiac troponin T promoter (*TNNT2*; Prasad et al. 2011).

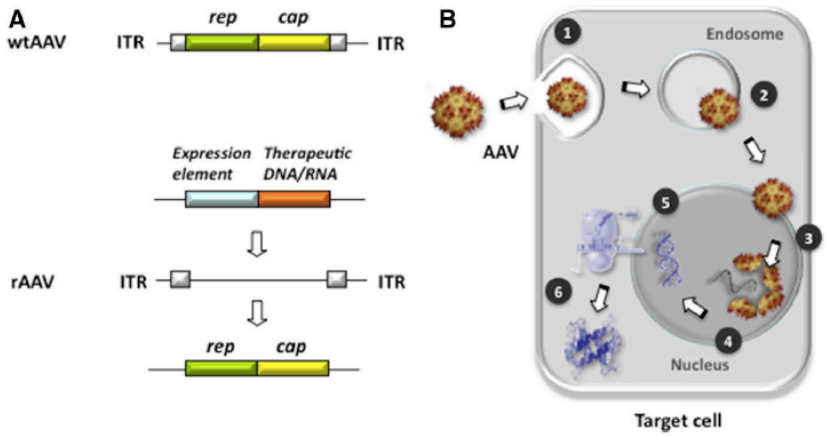

Figure 11: Genetic elements of AAV, recombination possibilities and cell cycle. [A] WT Adeno-associated virus (wtAAV) containing *rep* and *cap* genes that are flanked by to inverted terminal repeats (ITR). *Rep* and *cap* genes can be exchanged by therapeutic nucleic acids of interest during recombination. **[B]** Cell cycle of AAV in the targeted cell, uptake (1), release from endosome (2), enter of nucleus (3), release of viral DNA (4), gene expression (5,6; Pleger et al. 2013).

In general, AAVs are an ideal tool for gene therapy, because they can easily be modified (Vannucci et al. 2013).

1.9 Engineered heart tissues (EHTs)

The engineering of 3-dimensional (3D) models of the heart (EHTs) has several implications. First they provide the opportunity to serve as potential tissue grafts for patients, that lost substantial parts of the heart, e.g. after a myocardial infarction. Second they give a closer insight into the physiology of the cardiomyocytes working together as a network, and third pharmacological studies aiming for therapeutic or toxic effects can be performed in bigger cohorts (reviewed in Hirt et al. 2014). First heart tissues were engineered from chicken cardiomyocytes in a collagen-based matrix (Eschenhagen et al. 1997). For more than 10 years the method was optimized and EHTs were produced using rat cardiomyocytes in a fibrin-based matrix (Hansen et al. 2010). Since genetic engineering in rats is impossible, but feasible in mice, production of murine EHTs was quite attractive. This challenging task was first overcome by A. Stöhr in our Department of Experimental Pharmacology and Toxicology, in Hamburg-Eppendorf (Stohr et al. 2013). For the first time murine EHTs from WT and KI mice were characterized under different conditions, paving the way for this work.

1.10 Aim of the study

The current treatment for HCM is based on relief of symptoms but lacks a causal strategy and thus remains insufficient. The use of conventional gene therapy was recently shown to successfully prevent the HCM phenotype in both KI and KO EHTs as well as in KI-mice that all display typical features of human HCM, such as hypercontractility, cardiac hypertrophy and both systolic and diastolic dysfunction (Stohr et al. 2013, Mearini et al. 2014, Wijnker et al. 2016). In the last few years many studies have been published, dealing with the phosphorylation of cMyBP-C and its beneficial functional role on contraction. However phosphorylation of cMyBP-C has not been used in any study as a target for HCM treatment.

Therefore the aim of this study was to evaluate, whether a constitutively phosphorylated cMyBP-C was able to rescue the HCM phenotype of KI-EHTs. Due to the idea that a certain hierarchy among the phosphorylatable M-Motif serines exists, the first serine to be phosphorylated, Ser-282, was chosen for constitutive phosphorylation, by site-directed mutagenesis.

According to previous work that was performed in the group (Stohr et al. 2013, Mearini et al. 2014, Wijnker et al. 2016), the construct was packaged in adeno-associated virus serotype 6 (AAV6) and used for transduction of KI-EHTs.
The main question addressed by my project is:

> Does the transduction of AAV6 encoding a consitutively phosphorylated cMyBP-C lead to a rescue of the HCM phenotype in KI-EHTs? And beyond this question: Is there any difference to transduction of WT cMyBP-C into KI-EHTs?
> If yes, which treatment is more appropriate?

2 Material and Methods

2.1 Recombinant adeno-associated virus

AAV	Manufacturer
AAV6-*TNNT2*-FLAG-WT-*Mybpc3*	C. Schob, UKE-HEXT, Hamburg
AAV6-*TNNT2*-FLAG-WT-*Mybpc3*-Ser282Asp	C. Schob, UKE-HEXT, Hamburg
AAV6-CMV	I. Braren, UKE-HEXT, Hamburg

2.2 Bacterial strains

Bacterial strain	Manufacturer
XL10-GOLD ultracompetent cells	Agilent
One Shot® TOP10 Chemically Competent *E. coli*	Invitrogen

2.3 Chemicals and solutions

Product	Manufacturer
4-(2-hydroxyethyl)piperazine-1-ethanesulfonic acid (HEPES)	Roth
Acrylamide/bis solution (29:1)	Bio-Rad
Agarose (UltraPure™)	Invitrogen
Agarose, 2% (PBS)	Invitrogen
Amersham™ ECL™ Prime Western Blotting Detection Reagent	GE Healthcare
Ammonium persulfate (APS)	Bio-Rad
Ampicilline trihydrate	Serva
AmpliTaq Gold® DNA Polymerase	Applied Biosystems
Aprotinin, 2 mg/ml (Aqua ad injectibilia)	Sigma-Aldrich
Aqua ad injectibilia	Baxter GmbH
Ascorbic acid	Merck
Bacto™ Agar	Becton
Bacto™ Tryptine	Becton
Bovine fibrinogen	Sigma

Bovine serum albumin (BSA)	Sigma
Calcium chloride dihydrage ($CaCl_2$-$2H_2O$)	Sigma
Collagenase type II	Worthington
Cytosine β-D-arabinofuranoside (Ara-C)	Sigma
Deoxyribonucleotide triphosphate (dNTP) mix (dATP, dCTP, dGTP, dTTP)	Applied Biosystems
Difco™ trypsin 250	Becton
Dimethyl Sulfoxide (DMSO)	Sigma
DRAQ5™	BioStatus Limited
Dulbecco's modified Eagle medium (DMEM)	Gibco
EMD 57033 ((+)-5-(1-(3,4-dimethoxybenzoyl)-1,2,3,4-tetrahydroquinolin-6-yl)-6-methyl-3,6-dihydro-2H-1,3,4-thiadiazin-2-one)	Merck
Ethanol (96%)	Geyer GmbH & CoKG
Ethanol (99%)	Geyer GmbH & CoKG
Ethidium bromide	Fluka
Ethylenediaminetetraacetic acid (EDTA)	Sigma
Fetal bovine or calf serum (FBS or FCS)	Biochrom
Gene Ruler™ 100 bp, 1 kb DNA ladder	Fermentas
Glucose	Sigma
Glycerol	Merck
Glycine	Roth
Hank's balanced salt solution (HBSS), calcium/magnesium-free	Gibco
Histofix®	Roth
Horse Serum	Biochrom
Hydrochloric acid, 37% solution	Merck
Insulin (human)	Sigma
Isoprenaline hydrochloride	Sigma
Isopropyl alcohol	Merck

Loading dye, 6x	Fermentas
Lysogeny broth medium	own production
M199 with Earl' salt and L-glutamine	Gibco
Magnesium chloride hexahydrate ($MgCl_2$-$6H_2O$)	Merck
Matrigel	BD Bioscience
Methanol	J.T. Baker
Milk powder	Roth
Mowiol	own production
N,N,N',N'-Tetramethylethylenediamine (TEMED)	Bio-Rad
Penicillin/Streptomycin	Gibco
Phosphate buffered saline (PBS)	Biochrom
Polyoxyethylene (20) sorbitan monolaurate (Tween® 20)	Sigma
Ponceau S	Sigma
Potassium chloride (KCl)	Merck
Power SYBR® Green PCR Master Mix	Invitrogen
Precision Plus Protein Standard™	Bio-Rad
Sodium chloride (NaCl)	J.T. Baker
Sodium dodecyl sulphate (SDS)	Roth
Sodium hydrogen carbonate ($NaHCO_3$)	Merck
Sodium dihydrogen phosphate monohydrate (NaH_2PO_4-H_2O)	Merck
TaqMan® Universal PCR Master Mix	Applied Biosystems
Thrombin	Sigma
Trishydroxymethylaminomethane (Tris) base	Sigma
Triton X-100	Sigma
TRIzol®	Invitrogen

2.4 Laboratory equipment

Product	Manufacturer

Accu-jet pipetting aid	Brand GmbH
Agarose GEL Electrophoresis System GT	Bio-Rad
Analytic balance (GENIUS)	Sartorius AG
Beckmann-Centrifuge (J-6B)	Thermo scientific
Benchtop centrifuge	Sarstedt AG & Co.
Blotting system (Mini Trans-Blot® cell)	Bio-Rad
Carbon electrodes (CG 1290)	Carbon Graphite Consulting Klein
Chemie Genius^2 Bio imaging system with Gene Tools software	Syngene
Electrophoresis system (Mini PROTEAN® 3 electrophoresis cell)	Bio-Rad
Electrophoresis system (Sub-Cell GT)	Bio-Rad
Generation I (Set-up for video optical recording)	own production with CTMV software
Ice machine	Scotsman
Incubator shaker (C25 classic)	New Brunswick Scientific
Incubators (B 5050 E and Hera cell 240)	Heraeus Instruments
Magnetic stirrer (IKAMAG® RCT)	Janke & Kunkel GmbH
Mastercycler® pro (vapo.protect)	Eppendorf AG
MC 6 Centrifuge (90.186100)	Sarstedt AG & Co.
Microscope (Axiovert 200 M) with a 40x-oil objective, with LSM 5	Zeiss
Microwave	Sharp
Minicentrifuge (C-1200)	National Labnet Co.
Nano Drop spectrometer	ThermoFisher scientific
Neubauer chamber	Glaswarenfabrik Karl Hecht KG
PCR cycler (2720 Thermal cycler)	Applied Biosystems
PCR cycler (GeneAmp® PCR system 9700)	Applied Biosystems
Pipettes (10, 100, 1000 µl)	Eppendorf AG
Precision balance (Precision advanced)	Ohaus®
S88X Dual Output Square Pulse Stimulator	GRASS Technologies
Sterile work bench (Lamin Air HB 2448)	Heraeus Instruments

Surgical instruments	Karl Hammacher GmbH
Taqman ABI Prism 7900HT sequence detection system with ABI 7900HT SDS	Applied Biosystems
Thermomixer comfort	Eppendorf AG
Tissue Lyzer	Qiagen
Ulra-pure water system Mili-Q plus	Millipore
Vortex-Genie 2	Scientific industries
Water bath	GFL
Microscope (Axiovert 25)	Zeiss
Centrifuge (Universal 30 RF)	Hettich Zentrifugen
Centrifuge (5810 R)	Eppendorf AG
Centriuge (5415 D)	Eppendorf AG
Power supply	Bio Rad

2.5 Consumable material

Product	Manufacturer
12 ml Cell Culture Tube	Greiner Bio-One
Blotting paper (Whatman 3MM)	Schleicher & Schuell
Cell strainer (70 µm, Nylon)	Falcon
Coverslips (∅ 10 mm)	Glaswarenfabrik Karl Hecht KG
Culture plates (6-well, 24-well)	Nunc
Disposable syringes	Braun
Falcon tubes (15 and 50-ml)	Sarstedt AG & Co.
Glassware	Schott Duran
Latex Medical Examination Gloves	Supermax Glove Manufacturing Sdn. Bhd.
Micro tubes (1.5 and 2.0-ml)	Sarstedt AG & Co.
Microscope slides	Paul Marienfeld
Nitril powder-free examination gloves	Ansell
Nitrocellulose membrane (Portran® BA 85)	Schleicher & Schuell
PCR tubes	Sarstedt AG & Co.
Petri dishes, 10 mm	Sarstedt AG & Co.

Pipette tips (for 10, 100, 1000 µl pipettes)	Sarstedt AG & Co.
Serological pipette (10 ml wide mouth)	Becton Dickinson
Serological pipettes (1, 2, 5, 10, 25, 50 ml)	Sarstedt AG & Co.
Sterile filter (0.22 µm)	Sarstedt AG & Co.
Vacuumfiltration rapid filtermax (100, 250, 500 ml)	TPP®

2.6 Antibodies

2.6.1 Western Blot

2.6.1.1 Primary antibodies

Detected protein	Primary antibody	Company	Dilution
cMyBP-C	M-Motif; rabbit polyclonal	Gift of W. Linke	1:1,000
pSer-273-cMyBP-C	phosphorylated Ser-273 in M-Motif, rabbit polyclonal	Gift of S. Sadayappan	1:2,000
pSer-282- cMyBP-C	phosphorylated Ser-282 in M-Motif, rabbit polyclonal	Eurogentec	1:1,000
pSer-302- cMyBP-C	phosphorylated Ser-302 in M-Motif, rabbit polyclonal	Gift of S. Sadayappan	1:10,000
α-actinin	α-actinin, mouse monoclonal	Sigma	1:1,000
FLAG-cMyBP-C	FLAG-Tag, mouse monoclonal	Sigma	1:5,000

2.6.1.2 Secondary antibodies

Secondary antibody	Company	Dilution
anti-rabbit IgG	Sigma	1:6,000
anti-mouse IgG	Dianova	1:20,000

2.6.2 Immunofluorescence

2.6.2.1 Primary antibodies

Detected protein	Primary antibody	Company	Dilution
cMyBP-C	M-Motif; rabbit polyclonal	Gift of W. Linke	1:200
FLAG-cMyBP-C	FLAG-Tag, mouse monoclonal	Sigma	1:800
	FLAG-Tag, rabbit polyclonal		
α-actinin	α-actinin, mouse monoclonal	Sigma	1:200

2.6.2.2 Secondary antibodies

Secondary antibody	Company	Dilution
anti-rabbit IgG, Alexa Fluor 546	Molecular Probes	1:800
anti-mouse IgG, Alexa Fluor 488	Molecular Probes	1:800

2.7 Primers

2.7.1 Primers for site-directed PCR mutagenesis

Primer	Sequence (5' to 3')
Mybpc3 S282D F	GAGCAGGTCGGAGAACCGATGACAGCCATGAAGATG
Mybpc3 S282D R	CATCTTCATGGCTGTCATCGGTTCTCCGACCTGCTC

2.7.2 *Mybpc3* primer sequences for sequencing and PCR

Primer	Sequence (5' to 3')
FLAG F	GGATTACAAGGATGACGACGA
GAPDH F	ATTCAACGGCACAGTCAAG
GAPDH R	TGGCTCCACCCTTCAAGT
Mybpc3 ex.1 F	CACCCCTGGTGTGACTGTTCTCAA
Mybpc3 ex.2 R	GTCATCAGGGCTCGCATC
Mybpc3 ex.2 R	CTGACCGCTCCGTCTCAG
Mybpc3 ex.4 F	TCTTTCTGATGCGACCACAG
Mybpc3 ex.6 F	TGCTCAGACCACTTCTGCTG
Mybpc3 ex.9 R	TCCAGAGTCCCAGCATCTTC
Mybpc3 ex.17 F	ATGCAGTACGCACAAGTGGA
Mybpc3 ex.21 F	AACCTCCCAAGATCCACTT
Mybpc3 ex.21 R	AAGTGGATCTTGGGAGGTTC
Mybpc3 ex.27 F	GGTGAAGGACCTACCCACTG
Mybpc3 ex.33 F	GGGAGTATTGACCCTGGAGATCAG
Mybpc3 ex.34 R	TTCGACGGATCCCTGGTCACTGAGGAACTCG

2.7.3 *Mybpc3* primer and probe sequences for qPCR

Gene	Full name	Primer/Probe	Sequence (5' to 3')
Acta1	α-skeletal Actin (mouse)	Primer Forward	CCCCTGAGGAGCACCCGACT
		Primer Reverse	CGTTGTGGGTGACACCGTCCC
Gnas	Guanine nucleotide-binding protein, alpha stimulating (mouse)	Forward	CAAGGCTCTGTGGGAGGAT
		Reverse	CGAAGCAGGTCCTGGTCACT
		GαS Probe	FAM-GCTGATTGACTGTGCCCAGTACTTCCT-TAMRA
Mybpc3	Myosin-binding	Mutant 1 F	GTGTCTACCAAGGACAAATTTGACA

	protein C, cardiac (mouse)	Mutant 1 R	CCAGGTCTCCAGAACCAATG
		Mutant 1 Probe 1	VIC-CTCACTGTCCATAAGG-MGB
		Mutant 1 Probe 2	FAM-AACCTCACTGTCCATGAG-MGB
		Mutant 2/3 F	TGGACCTGAGCAGCAAAGTG
		Mutant 2/3 R	GGTCCAGGTCTCCAGAACCA
		Mutant 2/3 Probe	FAM-CCAGCAAGAGGCCA-MGB
		Mutant 3 F	AGAGCCAGCAAGAGGCCATT
		Mutant 3 R	TCCAGAGTCCCAGCATCTTC
		Mutant 3 Probe	TCGGAGAACCAGCCCCTGCTAGCTC
		Wt-*Mybpc3* F	GATGCGAGCCCTGATGAC
		Wt-*Mybpc3* R	GACTTGAGACACTTTCTTCC
Myh7	Myosin, heavy chain 7, cardiac (mouse)	Primer Forward	GAGGAGAGGGCGGACATC
		Primer Reverse	GGAGCTGGGTAGCACAAGAG
NppA	Atrial natriuretic peptide (mouse)	Primer Forward	ATCTGCCCTCTTGAAAAGCA
		Primer Reverse	ACACACCACAAGGGCTTAGG

2.8 Restriction Enzymes

Restriction enzymes with supplied buffer	**Manufacturer**
FastDigest® NheI	Fermentas
FastDigest® NotI	Fermentas
FasDigest® SmaI	Fermentas

2.9 Homozygous *Mybpc3*-targeted knock-in (KI) mouse model

The investigations were performed according to the guidelines for care and use of laboratory animals published by the NIH (Publication No. 85-23, revised 1985). A mouse model was developed by our group in 2009, showing the typical molecular and phenotypic features of HCM (Vignier et al. 2009). It is based on a genetic knock-in (KI) of the most frequent mutation found in Tuscany (Girolami et al. 2006) into the *Mybpc3* gene. In brief, by using the Cre/lox system for gene targeting, a G to A transition was introduced on the last nucleotide of exon 6. This mutation results in 2 frameshift and 1 missense mutant mRNAs and lower amounts of mutant mRNAs and cMyBP-C than corresponding WT mRNA and cMyBP-C amounts in WT mice (Vignier et al. 2009). Homozygous KI mice develop both hypertrophy and cardiac dysfunction, displayed by an increased LV mass to body weight (LVM/BW)-ratio and a reduced fractional area shortening at an early stage of life, respectively (Vignier et al. 2009, Mearini et al. 2013). Both WT and KI mice were bred on a Black Swiss genetic background.

2.10 Production of recombinant adeno-associated virus serotype 6

The protocol for production of recombinant AAV serotype 6 is adapted from the PhD thesis of Doreen Stimpel (Hamburg, 2013). The production of recombinant AAV serotype 6 (AAV6) was performed at the Center for Experimental Therapy Research (HEXT) Vector Core Unit of the University Medical Center Hamburg-Eppendorf (Claudia Schob). In brief, the AAV6 was produced by a double-transfection of HEK293 cells with two plasmids. On the one hand the transfer plasmid of interest (either WT *Mybpc3*, constitutively phosphorylated WT *Mybpc3* or empty, containing a CMV promoter only, Figure 12) which is between two AAV2 inverted terminal repeats (ITR) and on the other hand the AAV packaging plasmid pD6rs containing AAV2 *rep* and AAV6 *cap* genes as well as adenoviral helper functions, were used in the double-transfection process. HEK293 ($1.5x10^7$) cells were seeded on 15-cm plates and transfected with polyehtylenimine. The titers of the different AAV6 were determined by qPCR using the SYBR® Green technology with specific primers for the promoter sequences.

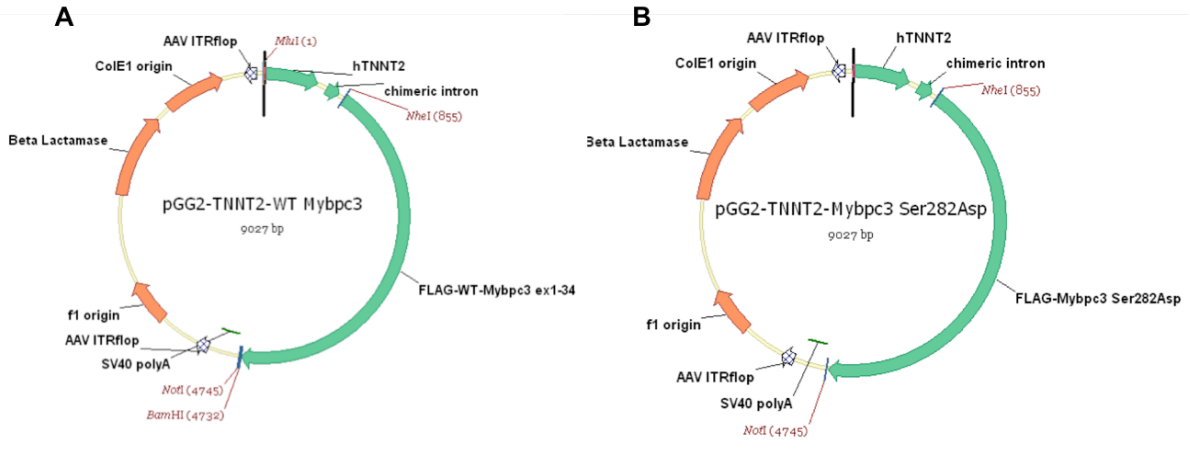

Figure 12: Vector map illustration for the two *Mybpc3* constructs. [A] Vector map for the expression vector pGG2 encoding FLAG *Mybpc3* (S282) and **[B]** vector map for the expression vector pGG2 encoding FLAG *Mybpc3* Ser282Asp (D282).

2.11 Murine EHTs

2.11.1 Solutions for EHTs

EHT culture medium:

DMEM (including 1 g/l D-glucose, 3.7 g/l $NaHCO_3$)

10% Horse serum (heat inactivated)

2% Chicken embryo extract

1% Penicillin/streptomycin

0.1% Insulin (10 µg/ml)

0.1% Aprotinin (33 µg/ml)

Isoprenaline hydrochloride (SIGMA®) was dissolved in aqua bidest (10 mM final stock concentration) and stabilized with 1 M HCl (40 µl in 10 ml aqua bidest with isoprenaline). Aliquots were made and both the stock solution and the aliquots were kept at -20 °C for further use, but not longer than one month.

5-(1-(3, 4-dimethoxybenzoyl)-1, 2, 3, 4-tetrahydroquinolin-6-yl)-6-methyl-3, 6-dihydro-2H-1, 3, 4-thiadiazin-2-one (EMD 57033) was dissolved in DMSO (10 mM final stock concentration). According to the manufacturers' instructions aliquots were made and stored at -20 °C protected from light for further use.

2.11.2 Isolation of neonatal mouse cardiac myocytes

Cardiac cells were isolated from at least 25 neonatal mice (0 to 1 day-old) according to the protocol of our group (Vignier et al. 2009). Both WT and KI mice were sacrificed by decapitation. The hearts were extracted under semi-sterile conditions with autoclaved instruments and kept in Ca^{2+}/Mg^{2+} free Hank's balanced salt solution (HBSS) on ice. Non-cardiac tissue was removed with a forceps and the cleaned hearts were washed once in 7-10 ml fresh Ca^{2+}/Mg^{2+} free HBSS on ice. Then each heart was cut into 3-4 pieces and predigested in a trypsin-HBSS solution (0.5 mg/ml) continuously under gentle agitation at 4 °C overnight. A wide mouth pipette was used in every pipetting step to reduce damage to the cardiac cells. The trypsin predigestion was followed by five rounds of 240 U/ml collagenase type II (Worthington) digestion in a water bath at 37 °C. In order to warm up the tissue, to increase the collagenase digestion efficiency and to wash out the trypsin from the tissue, it was collected in warm light medium (DMEM:M199, 3:1; 1% penicillin/streptomycin; 1 mM HEPES, pH 7.4) in a 50-ml falcon tube and incubated for 3 min. Afterwards, cells were dissociated with collagenase in HBSS at 37 °C for 9 min each time. The supernatants were collected on ice in pre-chilled dark medium (5-7 ml, DMEM:M199, 3:1, 10% horse serum, 5% FCS, 1% penicillin/streptomycin, 1 mM HEPES, pH 7.4). After the digestion, cell suspension was centrifuged for 8 min at 600 rpm at room temperature. Cell pellets were kept on ice and the supernatant was centrifuged again for 5 min at 600 rpm. Cell pellets were pooled, suspended in 25 ml warm dark medium and counted in a Neubauer chamber. Fourty µl of cell suspension were mixed with 40 µl dark medium and 20 µl trypthan blue. Twenty to fourty µl of that suspension were pipetted onto the chamber and vital cells (not blue) were counted in the 8 big squares calculating the average.

The cell number was calculated as follows:

$$counting\ average \times 2.5 \times 10^4 = number\ of\ cells/ml$$

2.5: dilution factor

10^4: chamber factor

$$number\ of\ cells/ml \times 25 = total\ number\ of\ cells$$

25: total volume of suspension

Usually 0.5 – 0.7 x 10^6 cells per heart were obtained.

2.11.3 Generation of mouse EHTs in a 24-well format

The generation of mouse EHTs was recently established by A. Stöhr (Stohr et al. 2013). The following protocol is adapted from her PhD thesis (Hamburg, 2012). To obtain the correct number of cells for EHTs, 25 ml cell suspension was spinned for 8 min at 600 rpm and the pellet was resuspended to a final cell density with the removed supernatant. Molds were casted in a 24-well plate using 1.6 ml/well of 60 °C warm and sterile agarose (2%, Invitrogen, solved in PBS). Teflon spacers were used in order to create rectangular molds (Figure 13). After solidification of the agarose the spacers were carefully removed. Subsequently silicone racks for attachment of the EHTs were placed into the molds with one pair of posts for each casting mold (Figure 13). Spacers and silicone racks were boiled twice and autoclaved before use.

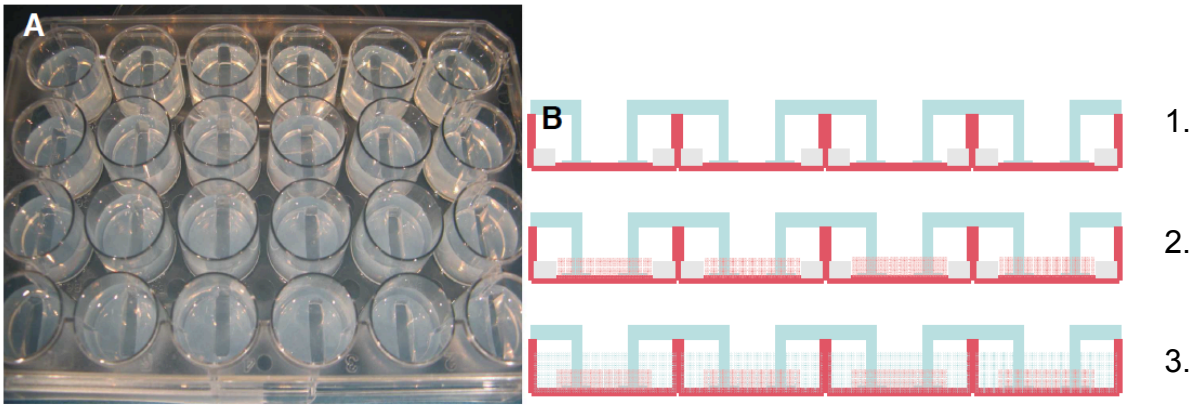

Figure 13: EHT generation steps. [A] 24-well plate with agarose casting molds after removal of the spacers. **[B]** Steps for generation of EHTs: 1. Silicone racks placed in the agarose casting molds. 2. EHT mastermix is pipetted into the molds. 3. Solid EHTs are transferred to a new 24-well plate containing fresh EHT medium (adapted from: Stohr et al. 2013).

During agarose's solidification the EHT mastermix was prepared on ice:

EHT mastermix (final volume 100 µl/EHT):	
Cell suspension ($0.68x10^6$ cells/EHT)	680 µl
2x DMEM	55 µl
Bovine fibrinogen	25 µl
Matrigel	100 µl
Non cardiac myocyte medium (NKM)	110 µl
	for 10 EHTs

Thrombin (3 U/µl)	30 µl (not to the mastermix, but for calculation)

2x DMEM:	NKM:
20% 10x DMEM	10% fetal calf serum (inactivated)
20% horse serum (heat inactivated)	1% penicillin/streptomycin
2% penicillin/streptomycin	1% L-Glutamine in DMEM
4% chicken embryo extract	
in aqua ad injectabilia	

Fibrinogen was added as last component to the mastermix and immediately resuspended until it was completely dissolved and the whole mix was homogenous. To prevent clotting of fibrinogen already in the mastermix, EHTs needed to be generated quickly after its addition. One hundred µl of the mastermix were resuspended in 3 µl thrombin (aliquots, ready to use). The resuspended mix was then quickly pipetted with the same tip into the agarose casting molds. After generation of 4 EHTs the mastermix was resuspended again to maintain homogeneity of the suspension. After casting, the EHTs were kept for solidification under cell culture conditions (37 °C, 21% O_2, 7% CO_2, humidity >90%) for 1.5-2 hours. In this time thrombin converted fibrinogen into fibrin, which resulted in the formation of a rectangular three dimensional (3D) matrix and the adhesion to the flexible silicone posts. Every EHT was then covered with 0.5 ml warm EHT culturing medium and incubated for 15 min to facilitate the transfer from the casting molds to new 24-well plates. The new plates were already prepared with 1.5 ml warm and fresh EHT culturing medium per well.

2.11.4 AAV6-mediated gene transfer in EHTs

AAV6-transduction of EHTs was performed by addition of the virus directly to the cell suspension for 30 min on ice before the preparation of the EHT mastermix. Viruses were all used at a multiplicity of infection (MOI) of 1000 vg/cell (transduction scheme Figure 14). The volume of NKM in the mastermix was adapted to the volume of virus used to match the final volume of 100 µl/EHT. All viruses were produced by the HEXT Core Facility, UKE, Hamburg.

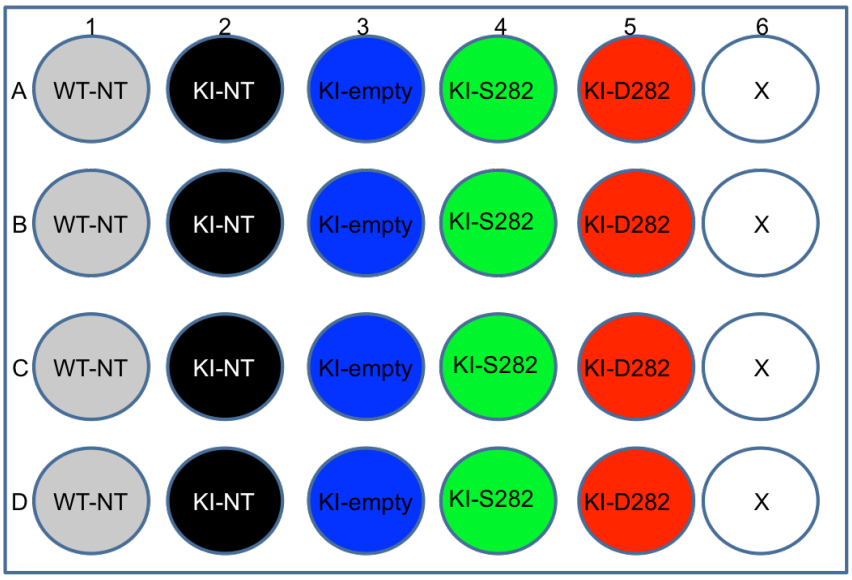

Figure 14: Scheme for transduction of EHTs in a 24-well plate. Each column represents transduction with a specific virus except NT. WT, wild-type; NT, non-transduced; KI, knock-in; S282, Virus encoding WT-cMyBP-C; D282, Virus encoding WT-Ser282Asp-cMyBP-C.

2.11.5 EHTs culture

After generation the EHTs were kept under cell culture conditions (37 °C, 21% O_2, 7% CO_2, humidity >90%) for 3-4 weeks. Medium was changed one day after generation and from then on every other day (usually Monday, Wednesday and Friday). On day 5 of culture, 25 µM cytosine arabinoside (Ara-C) was added to the medium for 48 hours to avoid an overgrowth of non-cardiac cells, such as fibroblasts. Between day 5 and day 8 of culture contractile areas formed in EHTs. Maximum beating forces were usually reached at day 14-15 of culture. Only EHTs beating synchronously were taken into consideration for further analysis.

2.11.6 Harvesting of EHTs

Between week 3-4 of culture EHTs were harvested. In general EHTs were washed twice 5 min in PBS at room temperature and depending on the further analysis differently treated afterwards (see associated paragraphs). In brief, EHTs were detached from the posts using a forceps, transferred into 2-ml tubes, shock-frozen in liquid nitrogen and stored at -80 °C for further usage (Figure 15).

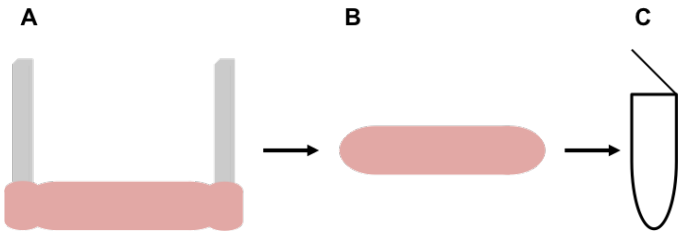

Figure 15: Harvest of an EHT. [A] Attached EHT is **[B]** removed from the post with a forceps and **[C]** directly transferred to a 2-ml tube for storage.

2.11.7 EHTs contraction analysis

2.11.7.1 Spontaneous contractions

The main parameters of interest in cardiac tissue are the contractile parameters, which reflect the viability and the quality of the tissue. In order to measure these parameters (force, velocities and times of both contraction and relaxation) within the EHT during the time of culture, a system for video-optical recording was established in our Department (Hansen et al. 2010). With this system it was possible to measure the contractions under sterile cell culture conditions either spontaneous or with electrical stimulation. The following protocol is adapted from the Master thesis of Julia Mourot (Hamburg, 2012) and the PhD thesis of Andrea Stöhr (Hamburg, 2012). For the measurements, 24-well plates with EHTs were placed in a miniature cell incubator, adjustable in terms of temperature and gas supply, with a glass roof. Above the roof a Basler-camera (type A 602f-2) was attached to a x-, y-, z-device (IAI Corporation) maneuverable by a computer that allowed to focus and record every single EHT by itself. Illumination of EHTs was possible via LED-lights underneath every well that were switched on during the measurement and then off to prevent overheating of the medium. The video-optical measurements were performed with a custom-made software (CTMV) that allowed automatic recognition of the silicone posts with a contour-recognition algorithm. Accuracy and position of the figure-recognition were adjusted before every measurement with the software to enable the best recording. Every EHT was then individually recorded, with a real time depiction of the peaks of contraction within the software (Figure 16). The change in distance of the silicone posts during the beating of the EHTs was automatically transformed into force value. Based on the geometry and consistency of the silicone posts (Sylgards 184, Young's modulus = 2.6 kPa) the forces were calculated using the following formula published by Vandenburgh and colleagues (Vandenburgh et al. 2008):

$$F = \frac{3EI\delta}{L^3},$$

F= force,

E= Young modulus of the silicone,

I= moment of inertia of the area, with $I = 0.25\pi R^4$, with R= radius (mm) and π= Pi,

δ= deflection of the silicone posts,

L= length of the silicone posts.

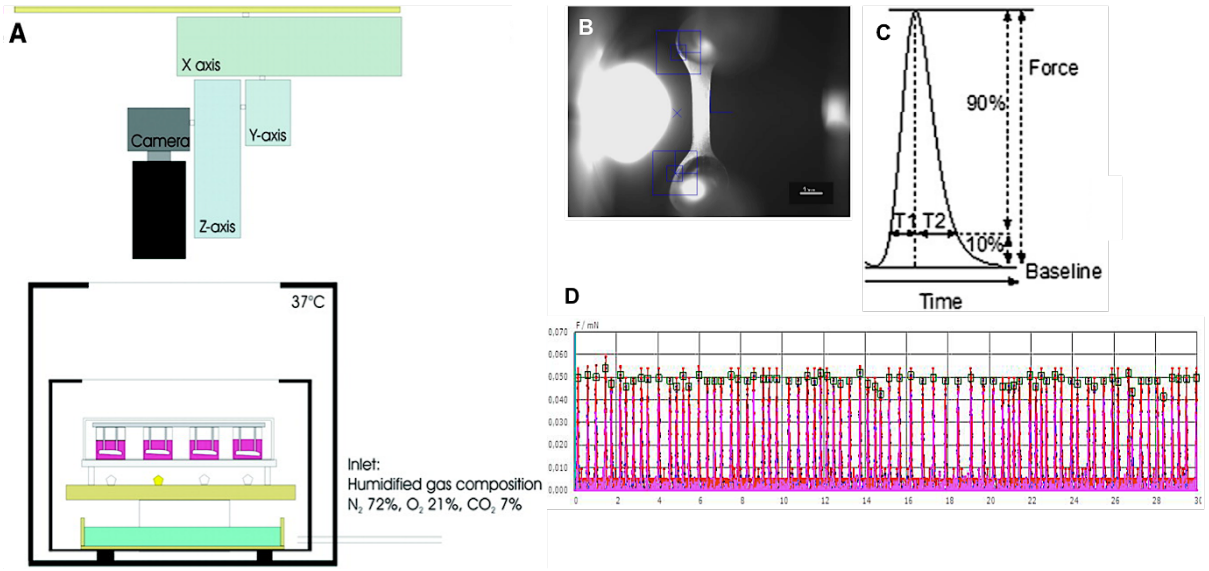

Figure 16: Measurement in a video-optical recording setup for the 24-well format. [A] The 24-well plate is placed in a mini-incubator underneath a glass rooftop enabling the camera to focus single EHTs, illuminated by a LED-light source below the specific EHT. Water is filled to the bottom of the mini-incubator to maintain a certain humidity. Gas is delivered through flexible tubes (adapted from Hansen et al. 2010). **[B]** The depiction of a recording of an EHT is shown. The blue boxes in the recording picture are the fixing points of the software for the force calculation. **[C]** Kinetics of contraction: Time to contraction (T1) and time to relaxation (T2) are shown (adapted from Stohr et al. 2013). **[D]** The corresponding contraction peaks of a measurement (force on y-axis, recognized peak is marked with a green square) displayed over time (x-axis).

Besides force there are other contractile parameters that can be analyzed with this setup, such as contraction and relaxation velocities and time to contraction (T1) and time to relaxation (T2). T1 indicates the time to 10, 20 or 50% of maximal force whereas T2 indicates the time to 50, 80 or 90% of maximal relaxation of the EHTs (Figure 16C). With this setup up to 24 EHTs can be measured one after the other. Recording time was 30 sec. Before each run the settings for the recognition of the EHTs were defined. The threshold for force recognition of the force was set to 0.015 mN from day 9 of EHT culture, to exclude those EHTs that did not synchronously beat. A report, including the contractile parameters of every individual measurement, was created in a PDF file subsequently.

2.11.7.2 Electrical pacing

Electrical pacing of EHTs was performed with the application of carbon electrodes, based on a recently developed method (Hirt et al. 2014). Here two stainless steel square bars (astenitic grade EN 1.4301, UNS S30400; Koch + Krupitzer, Germany) served both as conducting material and as scaffold for four pairs of carbon electrodes (CG 1290 Carbon Graphite Consulting Klein, Siegen, Germany). Two stainless steel square bars were used in a way to fit onto one row of a 24-well plate with one pair of carbon electrodes per well. The electrodes were attached to the bars via stainless steel screws. Symmetric biphasic pulses (2 – 7 V) of 4-msec duration were applied, generated by a Grass S88 X Dual Output Square Stimulator (Natus Neurology Incorporated Warwick, USA, Figure 17).

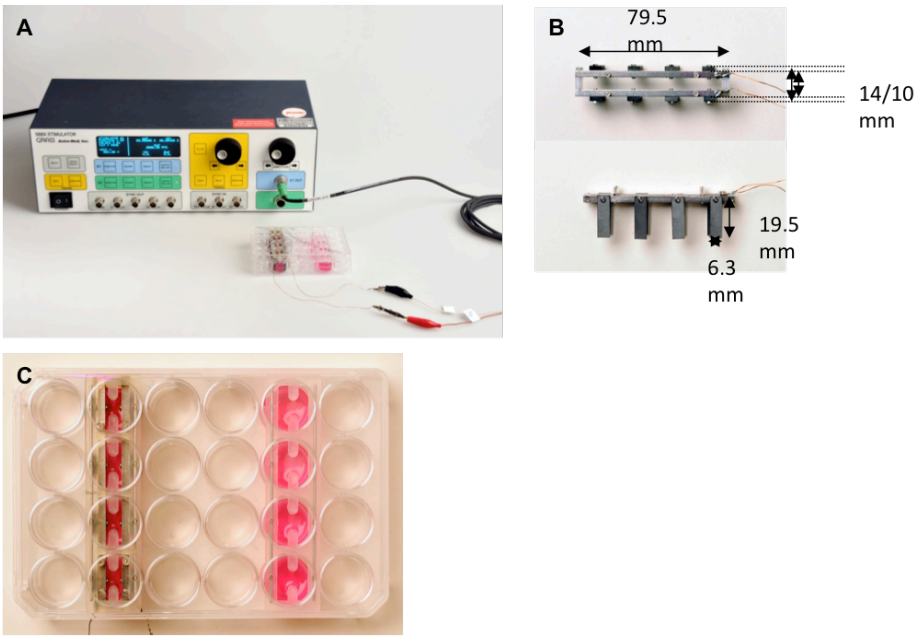

Figure 17: Devices and instruments for pacing of EHTs in sterile conditions. [A] Dual Output Square Stimulator for generation of electric pulses. **[B]** Pacing unit with carbon electrodes mounted on stainless steel racks for pacing of 4 EHTs in parallel. **[C]** 24-well plate containing a column of EHTs with pacing units mounted on the silicone racks (left) and without pacing units (right; adapted from: Hirt et al. 2014).

Pacing experiments of EHTs were performed in Tyrode's solution (in mM: NaCl 120, KCl 5.4, $MgCl_2$ 1.0, $CaCl_2$ 0.0 – 1.8, NaH_2PO_4, $NaHCO_3$ 22.6, glucose 5.0, Na_2EDTA 0.05, ascorbic acid 0.3). Tyrode's solution without [Ca^{2+}] was freshly prepared the day before the measurement. Two ml of this calcium-free solution were pipetted into each well of a 24-well plate and put to the same culture conditions like EHTs (37 °C, 21% O_2, 7% CO_2). Additionally, working solutions of Tyrode's solution containing either 0.4 mM or 20 mM [Ca^{2+}] were prepared diluting [Ca^{2+}] from a 2.25 M stock (in

water). Then another 24-well plate was filled with 2 ml of the 0.4 mM [Ca^{2+}] Tyrode' working solution.

For the measurements, EHTs were first transferred to the 24-well plate containing [Ca^{2+}]-free Tyrode's solution. The steel bars with the electrodes were mounted on the EHTs and connected to the stimulator (Figure 17). Then EHTs were paced (10 sec/measurement) and forces were recorded until their disappearance. Subsequently the EHTs were transferred to a new 24-well plate containing 2 ml [Ca^{2+}]-free Tyrode's solution/well. Then [Ca^{2+}] was added from the 20 mM working solution to the EHTs (starting from 0.1 mM up to 1.8 mM external [Ca^{2+}]). EHTs were incubated for 10 min in every new dilution. After the measurement at 1.8 mM external [Ca^{2+}] the EHTs were transferred to a new 24-well plate containing 2 ml [Ca^{2+}]-free Tyrode's solution/well. Forces were measured again until their disappearance. Subsequently [Ca^{2+}] was added from the 20 mM working solution to a final concentration of 0.4 mM external [Ca^{2+}]/well. The EHTs were measured again and forces were compared with the previous measurements at 0.4 mM external [Ca^{2+}]. Thereafter the EHTs were transferred to a new 24-well plate containing fresh Tyrode's solution of 0.4 mM [Ca^{2+}] (2 ml/well). Then forces were directly measured under pacing. This was followed by another measurement after 15 min. Subsequently isoprenaline (stock concentration 10 mM in water) or EMD 57033 (stock concentration 10 mM in DMSO) were added to the EHTs. EMD 57033 was directly added to the Tyrode's solution at a final concentration of 10 µM (1:1000). Isoprenaline was first diluted 1:100 in Tyrode's solution (0.4 mM [Ca^{2+}]) and then added to the EHTs to a final concentration of 100 nM (1:1000). The EHTs were measured 15 and 30 min after the addition of the drugs (Figure 18).

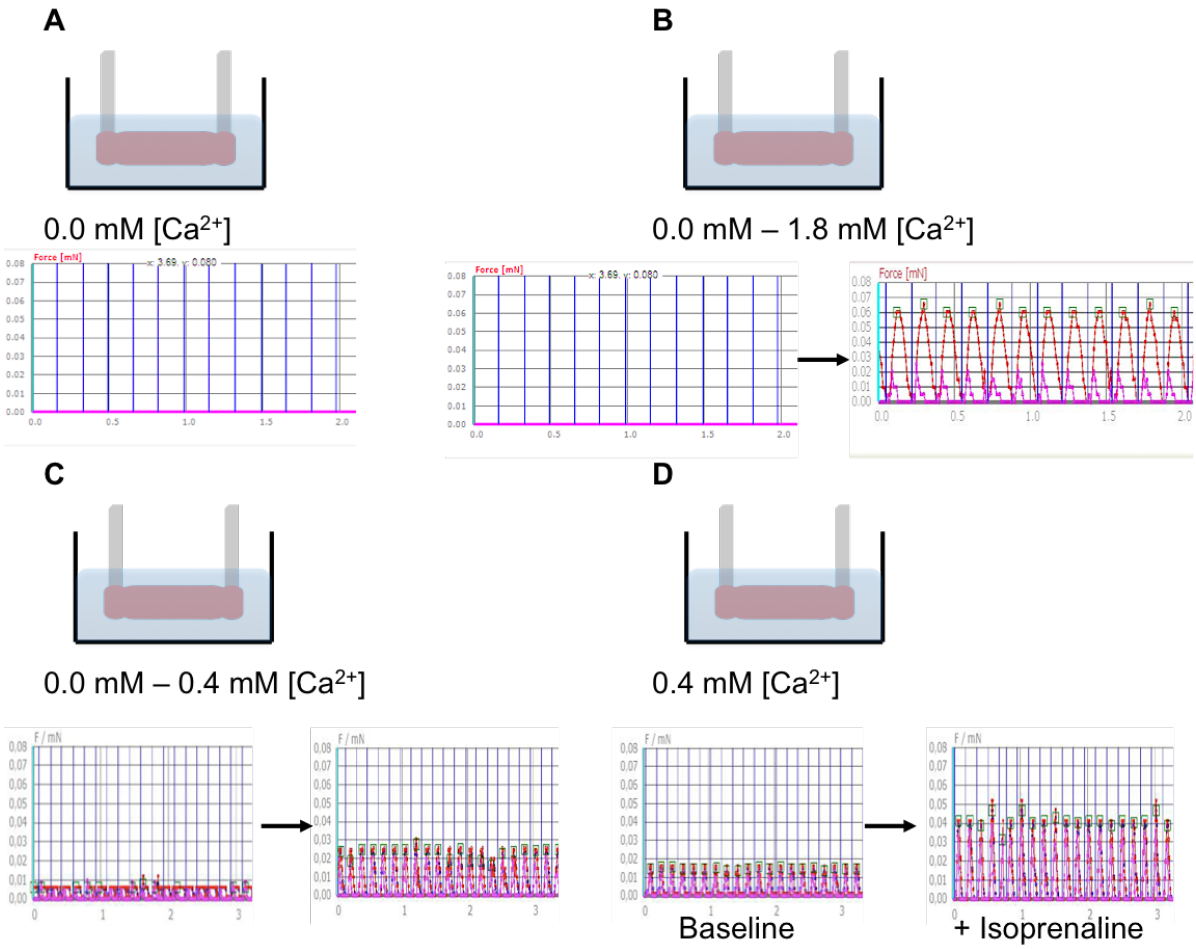

Figure 18: Scheme for [Ca2+] measurements under pacing. [A] After transfer from EHT culture medium to [Ca^{2+}]-free Tyrode's solution, EHTs were washed under pacing at 6 Hz. **[B]** EHTs were transferred to a new 24-well plate containing fresh [Ca^{2+}]-free Tyrode's solution. [Ca^{2+}] was added incrementally up to 1.8 mM. **[C]** EHTs were transferred to a new 24-well plate containing fresh [Ca^{2+}]-free Tyrode's solution and [Ca^{2+}] was added to a final concentration of 0.4 mM. Forces were compared to the previous measurement at 0.4 mM [Ca^{2+}]. **[D]** EHTs were transferred to a new 24-well plate containing fresh Tyrode's solution with 0.4 mM [Ca^{2+}]. First they were measured at baseline and then after the addition of either isoprenaline (final conc. 100 nM) or EMD 57033 (final conc. 10 µM).

2.12 DNA and RNA analysis

2.12.1 Site-directed mutagenesis PCR

For introducing a specific mutation into the WT *Mybpc3* cDNA, the QuickChange II XL Site-Directed Mutagenesis Kit (Agilent Technologies) was used following the manufacturers' instructions. The primers (Eurofins Genomics GmbH) were designed according to the protocol and 125 ng of each were used. An additional reaction with a control plasmid (contained in the kit) was performed as a control for the mutagenesis. Cycling parameters were as follows:

Table 4: Cycling parameters for the QuickChange II XL method.

Segment	Cycles	Temperature	Time
1	1	95 °C	1 min
2	18	95 °C	50 sec
		60 °C	50 sec
		68 °C	2.5 min/kb of plasmid length (here template of 9 kb → 22.5 min)
3	1	68 °C	7 min

The PCR-products were subjected to digestion with *Dpn* I (10 U/µl), which eliminates methylated and hemi-methylated parental template DNA. Four µl of the digested PCR products were then transformed into XL10-Gold ultracompetent cells. As a control for transformation the pUC18 plasmid (contained in the kit) was additionally transformed into XL10-Gold cells. The cells were incubated in SOC-medium (250 µl) for 1 h at 37 °C under gentle agitation and disseminated on ampicillin agar plates.

2.12.2 Preparation of plasmid DNA

Bacterial clones picked from agar plates were cultured at 37 °C under agitation in lysogeny broth (LB) medium with ampicillin overnight. Bacterial suspensions were taken for the isolation of plasmid DNA using the commercial NucleoSpin®Plasmid Kit (Machery-Nagel). In brief, the bacterial suspension was spinned 30 sec at 11.000 rpm, the supernatant was removed and the pellet was resuspended in 250 µl Buffer A1. Then Buffer A2 and Buffer A3 were added for cell lysis. Subsequently the lysed cell suspension was given to spin columns and DNA, bound to the silica membrane of the columns, was purified in several centrifugation steps. Finally the DNA was eluted with 30 µl aqua bidest and the concentration was measured with a spectrophotometer (NanoDrop™ ND-1000 PeqLab).

2.12.3 Restriction digestion

Restriction digestion was performed in order to discriminate the different DNA fragments (vector and insert) in size. Usually 100 µg DNA were used in 2 µl 10x

Digestion Buffer Green, 1 U/µl for each restriction digestion (usually 1 µl) enzyme and aqua bidest to a total volume of 20 µl. Incubation conditions (time and temperature) were adjusted to the optimal working conditions for each enzyme (usually Fast digest). The products were directly loaded on an agarose gel for electrophoresis.

2.12.4 RNA extraction from EHTs

Total RNA was extracted from single EHTs with the TRIzol® reagent (Invitrogen, 300 µl/EHT) following the manufacturers' instructions. The EHTs were homogenized using the TissueLyser® (Qiagen) and a lysing frequency of 30 Hz for 2 min with a steel bead. The steel beads were removed, 60 µl chloroform was added to the solution and it was homogenized on a vortex for 30 sec. Subsequently the solution was incubated for 3 min at room temperature and centrifuged for 15 min. All centrifugation steps were performed at 12.000 rpm between 4-15 °C. Then the clear upper phase (containing RNA) was removed and 150 µl isopropanol were added to it. Another 10 min of incubation at room temperature was followed by a second centrifugation for 10 min. The supernatant was discarded and the pellet was washed with 300 µl of 75% ethanol. This was followed by a third centrifugation for 5 min. The ethanol was removed and the pellet, containing RNA, was dried and dissolved in 30 µl water. RNA concentrations were determined by a spectrophotometer and extracted RNA samples were stored at -80 °C.

2.12.5 Determination of DNA and RNA concentrations

Both DNA and RNA concentrations were determined by measurement of the absorbance at a wavelength of 260 and 280 nm with a spectrophotometer (NanoDrop™ ND-1000 PeqLab). It was assumed that 1 unit of absorbance corresponds to 50 µg/ml and 40 µg/ml for DNA and RNA, respectively. The ratio A_{260}/A_{280} was automatically calculated to check the purity of the samples. Ratios below 1.8 indicated contaminations with proteins.

2.12.6 Reverse transcription

cDNA was synthesized from either single samples or pools of RNA's extracted from EHTs following the manual of the SuperScript™ III First-Strand Synthesis System (Invitrogen). Reverse transcription was performed using oligo (dT) primers and dNTP's provided with the kit. For reverse transcription 200 ng RNA were used. To exclude genomic contamination a control reaction without the reverse transcriptase was performed in parallel.

2.12.7 Polymerase Chain Reaction

For the amplification of specific cDNA fragments the polymerase chain reaction was performed. The reaction mixes were prepared using the AmpliTaq Gold® polymerase kit (Applied Biosystems®) regarding to the manufactures' instructions. One µl of cDNA template was used in a total volume of 20 µl reaction mix. Primers were used at a concentration of 0.4 µM each. The elongation time was adjusted relative to the length of the expected DNA amplicons. The synthesis rate was estimated to be 1 kb/min, unless notified otherwise by the manufacturer.

Table 5: Standard PCR program (touch-down) used for AmpliTaq Gold® DNA Polymerase.

PCR step	Temperature	Time	Cycles
Initial denaturation	94 °C	5 min	1
Denaturation	94 °C	30 sec	11
Annealing	65 °C – 60 °C or 60 °C – 55 °C	30 sec	
Elongation	72 °C	1 min	
Denaturation	94 °C	30 sec	24
Annealing Elongation	60 °C or 55 °C	30 sec	
	72 °C	1 min	
Final extension	72 °C	10 min	1
Final hold	4 °C	∞	

2.12.8 Quantitative PCR

Quantitative PCR (qPCR) experiments were performed according to the PhD thesis of Doreen Stimpel (Hamburg, 2013). The mRNA levels of different samples were determined by quantitative PCR using either SYBR® Green or TaqMan® probes (Figure 19). This was performed on the TaqMan® ABI Prism® 7900HT sequence detection system (Applied Biosystems®).

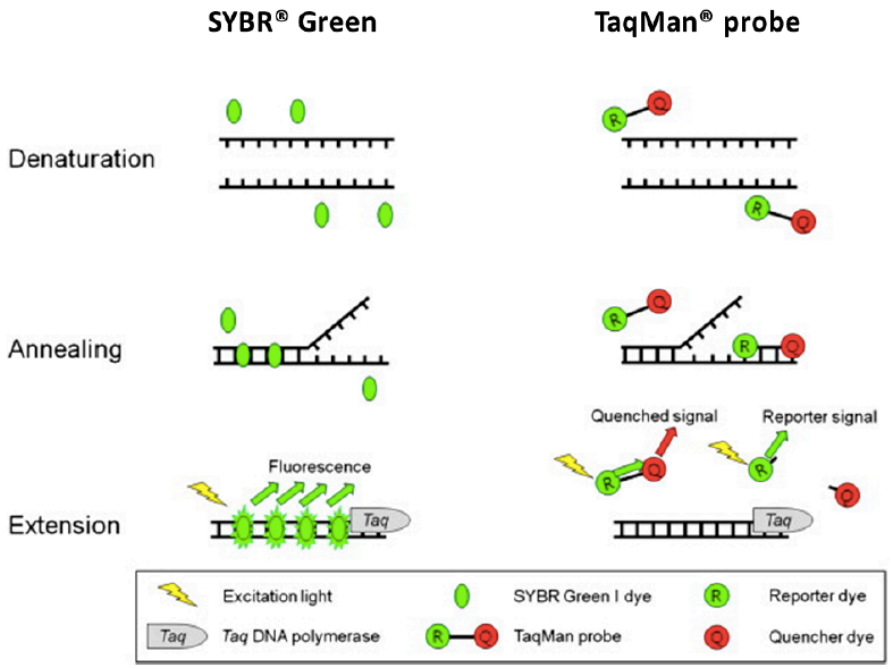

Figure 19: SYBR® Green and TaqMan® probe chemistries for qPCR analysis. SYBR Green unspecifically binds double-stranded DNA via intercalation in the sample that is analyzed. During the amplification more SYBR green binds to double-stranded DNA. Intercalation induces the emission of a fluorescent signal. The degree of emission increases with the degree of intercalated SYBR Green. The TaqMan probe contains a reporter dye at the 5'-terminus and a quencher dye at the 3'-terminus. During amplification the specific primers and probe hybridize to the maternal DNA strand and the DNA-polymerase extends the strand creating a double-strand. If the probe is intact, excitation induced by light is suppressed by the quencher. If the probe is cleaved due to the exonuclease activity of the DNA-polymerase, exciting light leads to the emission of the reporter creating a detectable signal proportional to the factor of amplification (Kim et al. 2013).

For the analysis, the cDNA was diluted 1:2 in nuclease-free water and specific TaqMan® probes were used for the quantification of the mutant and WT *Mybpc3* mRNAs levels. SYBR® Green was used for the quantification of total *Mybpc3* mRNA levels as well as the hypertrophic gene markers (*Acta1*, *Myh7* and *NppA*). Probes and primers are listed in paragraph 2.7 and were used at a concentration of 0.5 µM and 0.9 µM in a total volume of 10 µl, respectively. The different PCR programs are shown in Table 6 and 7.

Table 6: PCR program for qPCR using specific TaqMan probes, relative quantification method.

PCR step	Temperature	Time	Cycles
Stage 1	50 °C	2 min	1
Stage 2	95 °C	10 min	1
Stage 3	95 °C	15 sec	45
	62 °C	1 min	

Table 7: PCR program for qPCR using SYBR Green, absolute quantification method.

PCR step	Temperature	Time	Cycles
Stage 1	50 °C	2 min	1
Stage 2	95 °C	10 min	1
Stage 3	95 °C	15 sec	45
	60 °C	1 min	
Stage 4	95 °C	15 sec	1
	60 °C	15 sec	
	95 °C	15 sec	

All measurements were performed in triplicate and normalized to *Gnas* encoding GαS as endogenous control. The mRNA amounts are determined on a logarithmic scale, plotting the fluorescence signal against the cycle number during the exponential phase. The cycle threshold (C_t) is set at that point, where the fluorescence signal exceeds the background signal. Quantification of the mRNA levels was done using the $2^{-\Delta\Delta Ct}$ method. The C_t values of the endogenous control were subtracted from the C_t values of the gene of interest. The mean ΔC_t of the reference was subsequently subtracted from each ΔC_t value of the analyzed samples, resulting in the $\Delta\Delta C_t$. The calculation of $2^{-\Delta\Delta Ct}$ provides the amount of mRNA for each sample.

The analysis was performed with the Sequence Detection Software, version 2.4.

2.12.9 Agarose gel electrophoresis

Analysis of digested DNA and PCR products was achieved via an agarose gel electrophoresis. Digested DNA was either pipetted directly on an agarose gel (loading dye included in the digestion buffer) or PCR products were mixed with 2x loading dye and then pipetted on an agarose gel (0.8-2% (in TAE: 40 mM Tris base; 20 mM acetic acid; 1 mM EDTA, pH 8.0), depending on the size of fragments) containing ethidium bromide (0.8 µM) as a DNA intercalating agent. The electrophoresis was performed in 1x TAE buffer with 80 to 120 V. To discriminate the different fragments in terms of size, DNA ladders (Gene Ruler™) of 100 bp or 1 kbp were used. The DNA fragments on the gels were visualized by ultraviolet light with the Chemie Genius^2 Bio imaging system.

2.12.10 Sequencing of DNA

DNA sequencing analysis was performed by Eurofins MWG Operon according to the instructions of their sample submission guidelines, which are available online (http://www.mwg-biotech.com).

2.13 Protein analysis

2.13.1 Protein extraction from EHTs

Prior to the extraction of proteins from EHTs a master mix consisting of a commercial protein extraction buffer M-PER, 1 tablet complete mini + EDTA and 1 tablet PhosphoSTOP (each dissolved in M-PER) in a ratio 10:1, was produced. Seventy µl of the master mix and a steel bead were added to each EHT and homogenized with a TissueLyzer (Qiagen®) two times for 30 sec at a frequency of 30 Hz. The steel beads were removed afterwards and the samples were centrifuged for 5 minutes at 10.000 rpm at 4 °C. The resulting pellet was resuspended in the supernatant to reduce loss of protein. Susbequently 60 µl of the solution were added to 12 µl 6x Laemmli buffer for a 6:1 ratio. The samples were then denaturated at 95 °C for 5 min and stored at -20 °C for further use.

6x Laemmli buffer:

SDS	1.2 g
Gylcerol	6 g
Tris base (pH 6.8, 0.5 M)	1.2 ml
DTT	0.93 g
Bromophenol blue	6 mg
Aqua bidest.	ad 10 ml

2.13.2 SDS-PAGE

Separation of proteins according to their different molecular weights is achieved by using the SDS-PAGE method (Sodium dodecyl sulfate polyacrylamide gel electrophoresis). SDS covers the intrinsic charges of the proteins forming protein micellular structures, which are then able to migrate in an electric field that is applied to the proteins. Proteins dissolved in 1x Laemmli buffer were separated on 10-12 % polyacrylamide gels (consisting of an upper stacking and a lower running gel) by electrophoresis, initially at 80 V for 10 min and then at 150 V for at least 1.5 h in 1x electrophoresis buffer. The Precision Plus Protein Standard™ was used as a molecular weight marker.

Stacking gel (final volume 10 ml):

Acrylamide/bis solution (29:1, 40%)	1.28 ml (final concentration: 5.1%)
Tris base (0.5 M, pH 6.8)	2.5 ml
SDS	0.1 ml (final concentration: 10%)
APS	0.1 ml (final concentration: 10%)
TEMED	0.01 ml (final concentration: 1%)
Aqua bidest.	6.03 ml

Running gel (final volume 10 ml):

Acrylamide/bis solution (29:1, 40%)	2.5 ml (final concentration10%)
Tris base (1.5 M, pH 8.8)	2.5 ml
SDS	0.1 ml (final concentration: 10%)
APS	0.1 ml (final concentration: 10%)
TEMED	0.004 ml (final concentration: 0.04%)
Aqua bidest.	4.8 ml

Running gel (final volume 10 ml):

Acrylamide/bis solution (29:1, 40%)	3 ml (final concentration: 12%)
Tris base (1.5 M, pH 8.8)	2.5 ml
SDS	0.1 ml (final concentration: 10%)
APS	0.1 ml (final concentration: 10%)
TEMED	0.004 ml
Aqua bidest.	4.3 ml

10x Electrophoresis buffer:

Tris base (250 mM)	30.2 g
Gylcin (1.92 M)	144 g
SDS	10 g (final concentration: 1%)
Aqua bidest.	ad 1000 ml

2.13.3 Western Blot analysis

After the separation on the gel, the proteins were transferred onto a nitrocellulose membrane by wet-electroblotting at 300 mA for 2 h at 4 °C in a Mini Trans-blot chamber system with specific transfer buffer (1x Blot buffer II). After blotting, the membrane was stained with Ponceau S to verify the successful transfer of the proteins onto the membrane. Then the membrane was washed 3x 5 min with 1x TBS-T. To prevent unspecific antibody binding the membrane was blocked for 1 h at room temperature in 5% milk solution in 1x TBS-T. After a washing step the primary antibody solution was given to the membrane and incubated overnight at 4 °C under gentle agitation. After washing 3x 5 min in 1x TBS-T the membrane was incubated with the corresponding secondary antibody for at least 1 h at room temperature under gentle agitation. This was followed by a final washing step. The detection of proteins was performed using the ECL-Prime Kit according to the manufacturers' instructions. The chemoluminescent signals were detected with the Chemie Genius^2 Bio Imiganing System at different time points (6 sec to 5 min).

For additional staining the antibodies were removed from the membranes using the Restore™ PLUS Western Blot Stripping Buffer (Thermo scientific). Membranes were incubated in 5 ml stripping buffer for 30 min at room temperature under gentle

agitation. Thereafter another blocking step was performed and antibodies were added as described above.

5x Blot Buffer II:

Tris base (250 mM)	58 g
Glycin (1.9 M)	290 g
SDS	10 g (final concentration: 0.5%)
Aqua bidest.	ad 2000 ml

10x TBS:

Tris base	121.1 g
NaCl	87.66 g
HCl (37%)	adjust pH to 7.5
Aqua bidest.	ad 1000 ml

1x TBS-Tween 0.1%:

10x TBS	100 ml
Tween 20	1 ml
Aqua bidest.	900 ml

5% Milk powder solution:

Milk powder, not fat, dry (blotting grade)	2.5 g
1x TBS-T 0.1%	50 ml

2.13.4 Immunoflourescence analysis of EHTs

On the day of the harvest, EHTs were washed in PBS and fixed in 2 ml Roti-Histofix (Carl Roth®) at 4 °C overnight. Subsequently the EHTs were cut off the posts and transferred to 1.5-ml Eppendorf tubes with 1 ml blocking solution (Solution A) overnight. All incubation and washing steps were performed under gentle agitation at 4 °C. After the incubation the EHTs were washed 3x for at least 30 min in Solution B and then transferred to PCR tubes. One hundred µl of Solution B and the primary antibodies were added to the EHTs and incubated overnight. Another washing step in Solution B was performed in 1.5-ml Eppendorf tubes. For addition of the secondary antibodies and DRAQ5™, the EHTs were transferred to PCR tubes and 100 µl of

Solution B containing the secondary antibodies and DRAQ5™ (1:1000) were added. Incubation was performed overnight protected from light. In the next step the EHTs were washed 3x in 1x PBS for at least 30 min protected from light and finally transferred to object slides fixed with Mowiol 488 using cover slips (26 x 76 mm, two molds, Thermo Scientific). They were stored overnight at 4 °C protected from light. Confocal images were obtained with a Zeiss Axiovert microscope with a 40x-oil objective and recorded with a Zeiss LSM 710 system.

Solution A:

FCS	500 µl (10%)
BSA	250 µl (5%)
Triton X-100	25 µl (0.5%)
1x PBS	4225 µl

Solution B:

BSA	1.5 ml (5%)
Triton X-100	150 µl (0.5%)
1x PBS	28.35 ml

2.14 Statistical analysis

All data were expressed as mean ± SEM and analyzed with the software GraphPad Prism 5. Statistical analysis comparing the effect in the same group over time was done using the paired Student's t-test. More than two groups were statistically analyzed by a one-way ANOVA analysis with Bonferroni post-test. Multiple comparisons were performed using the two-way ANOVA analysis with Bonferroni post-test. Calcium sensitivity curves were analyzed by the F-test. A value of $p<0.05$ was considered statistically significant.

3 Results

3.1 Introducing the mutation Ser282Asp in WT *Mybpc3* cDNA

In order to obtain a constitutively phosphorylated cMyBP-C at Ser-282, a site-directed mutagenesis PCR was performed using the full-length WT *Mybpc3* cDNA. Here an exchange from AG to GA was done, resulting in a nucleotide triplet encoding aspartic acid instead of serine. This is thought to mimick a phosphorylation state (D282).

Prior to validation of the mutation site via sequencing, the plasmid DNA containing the desired mutation was transformed into competent bacterial cells. The DNA was purified and analyzed to check whether the expected fragments (insert (3890 bp) containing *Mybpc3* DNA with mutation and vector (5137 bp)) were still present. In 9 out of 12 clones the existence of both expected fragments was observed (Figure 20).

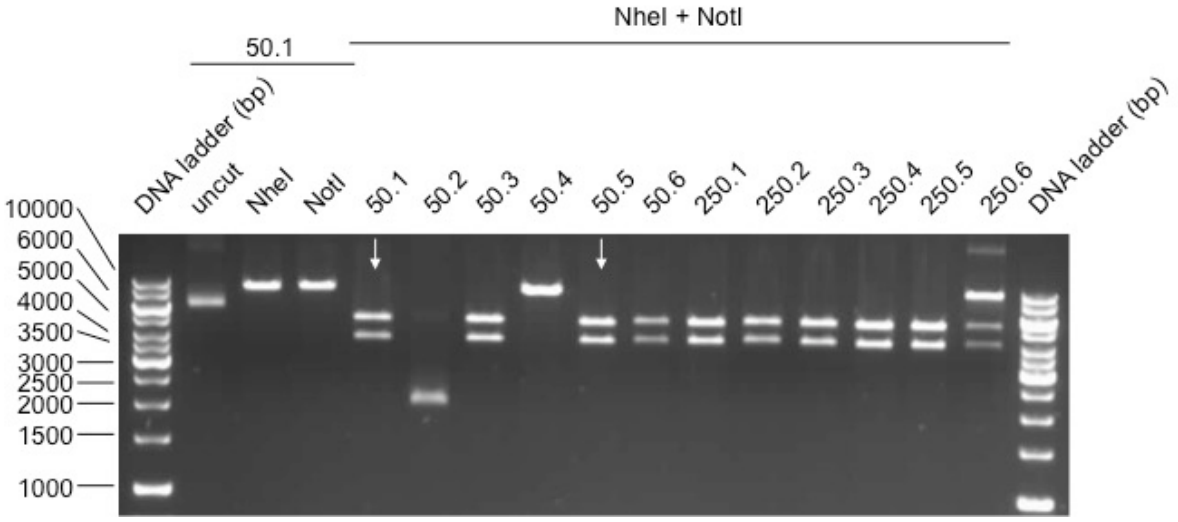

Figure 20: Analytic agarose gel for validation of presence of vector and insert. Bacterial clones transformed with D282 *Mybpc3* cDNA were picked from agar plates, inoculated with different amount of bacterial suspension. Plasmid DNA was purified and subjected to restriction digestion (NheI and NotI). The digested DNA was loaded on a 1% agarose gel containing ethidiumbromid. The expected fragment sizes are 3890 bp for the insert (D282 *Mybpc3* cDNA) and 5137 bp for the vector. Clone 50.1 was either loaded uncut, single cut or double cut. Nine out of twelve clones show the presence of both insert and vector.

Sequencing was done at first around the mutation and the clone 50.1 resulted to be positive (Figure 21). To verify that no other mutation was introduced during mutagenesis, the clone was sequenced with several primers covering the whole insert. No other mutation was found (data not shown).

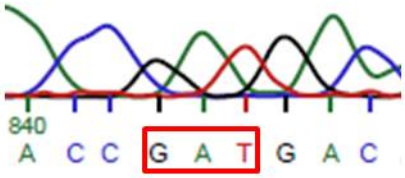

Figure 21: Result from sequencing. Sequencing peaks with neighbouring codons of the region surrounding the mutation from AG to GA shown. Codon for aspartic acid marked with a red rectangle.

SmaI restriction digestion was done to verify integrity of ITR sequences, necessary for an efficient virus production. DNA purified from the bacterial clone showed the presence of the expected fragments (5302 bp, 3703 bp, Figure 22).

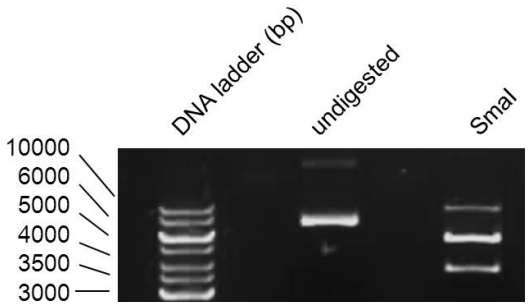

Figure 22: Analytic agarose gel for validation of *SmaI* restriction digestion. Plasmid containing the mutation (D282) from clone 50.1 either uncut or digested with *SmaI* was loaded on a 1% agarose gel containing ethidiumbromid. The expected fragment sizes are 5302 bp, 3703 bp. The *SmaI*-digested DNA shows the presence of both predicted fragments; bp: base pair.

3.2 Generation of EHTs

The generation of mouse EHTs was performed following the protocol established by A. Stöhr (Stohr et al. 2013). For successful generation of EHTs at least 25 mouse pups, between 0- and 1-day-old, were needed.

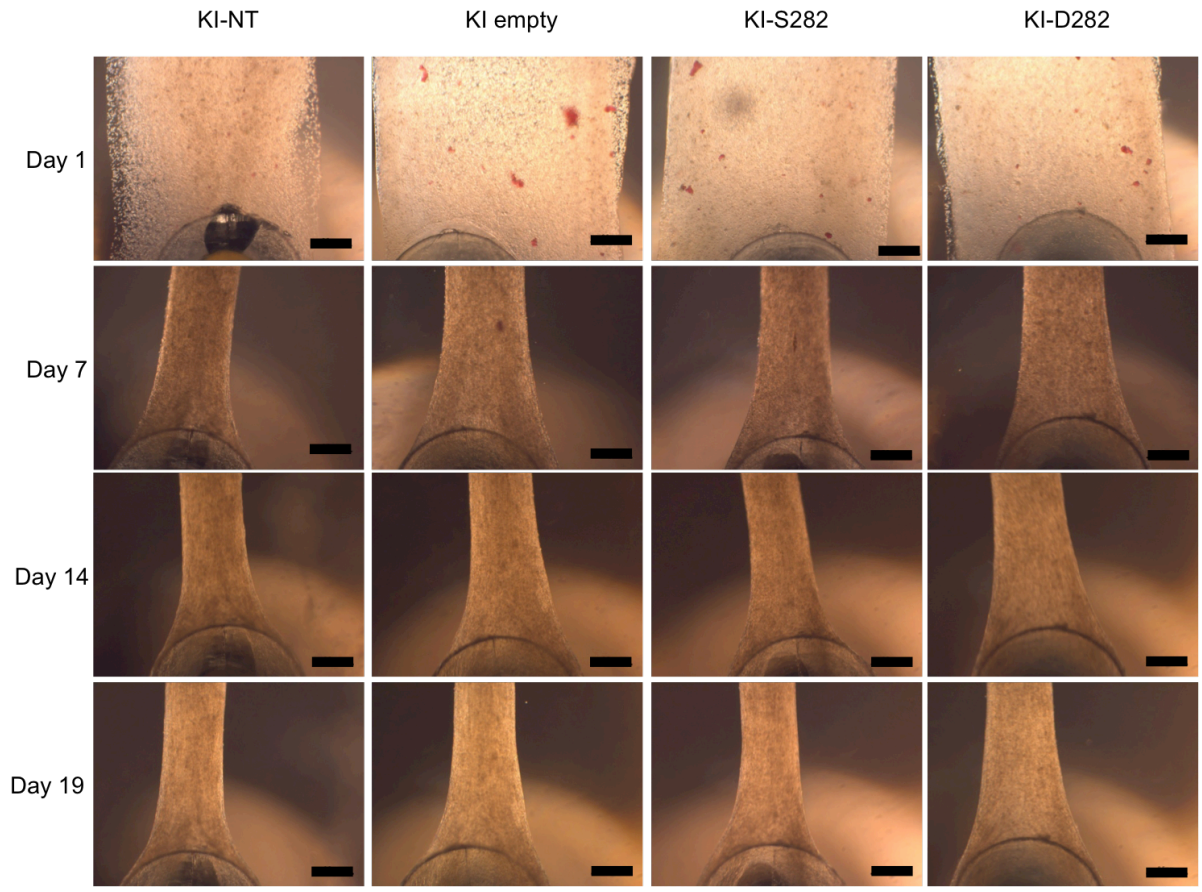

Figure 23: Development and maturation of EHTs. EHTs were remodeled over time becoming thinner from day 1 to day 19 of culture. On day 1 some EHTs showed red spots (most likely red blood cells) that disappeared over time and did not seem to have an influence on function. KI, knock-in; NT, non-transduced; S282, WT cMyBP-C with Ser282; D282, transgenic cMyBP-C with Asp282. Scale bar, 0.5 mm.

At day 1 of culture the EHTs maintained the shape of the agarose mould. During maturation a remodeling of the fibrin matrix was visible in all EHTs, which became thinner until the day of harvest between day 19 – 21 (Figure 23). With the start of coherent beating an alignment of the cell mixture in line of force was observed. Under the microscope the EHTs did not differ between the genotypes (Figure 23). WT-EHTs developed in the same way as KI-EHTs (data not shown).

The development of force in EHTs from different batches was not consistent. In some batches contractile areas were visible already at day 3 and coherent contractions of the whole EHTs with measurable forces at day 5, whereas other batches showed coherent contractions only at day 9 or later (data not shown). One WT batch did not develop force. Generally the maximal of force was reached between day 12 - 16 and continuously declined after day 16 in every group (data not shown).

3.3 Measurements of contractile parameters under spontaneous contraction

In mouse EHTs forces were seen to be quite low (0.04-0.05 mN) but with a non-stop beating (Stohr et al. 2013). This was different than rat EHTs, where obtained forces were rather high (up to 0.2 mN) but beats showed burst-like patterns (Hansen et al. 2010). The mouse EHT beating pattern was confirmed in this work. To answer the question if there were changes in contractile parameters between the different groups of EHTs, their spontaneous beating activity was measured with video-optical recording in EHT culturing medium, containing 1.8 mM external [Ca^{2+}], every other day 2 h after change of the EHT culture medium. Representative recordings are shown in Figure 24. Recordings were analyzed for all contractile parameters (force, velocities and times of both contraction and relaxation) with the customized CTMV software.

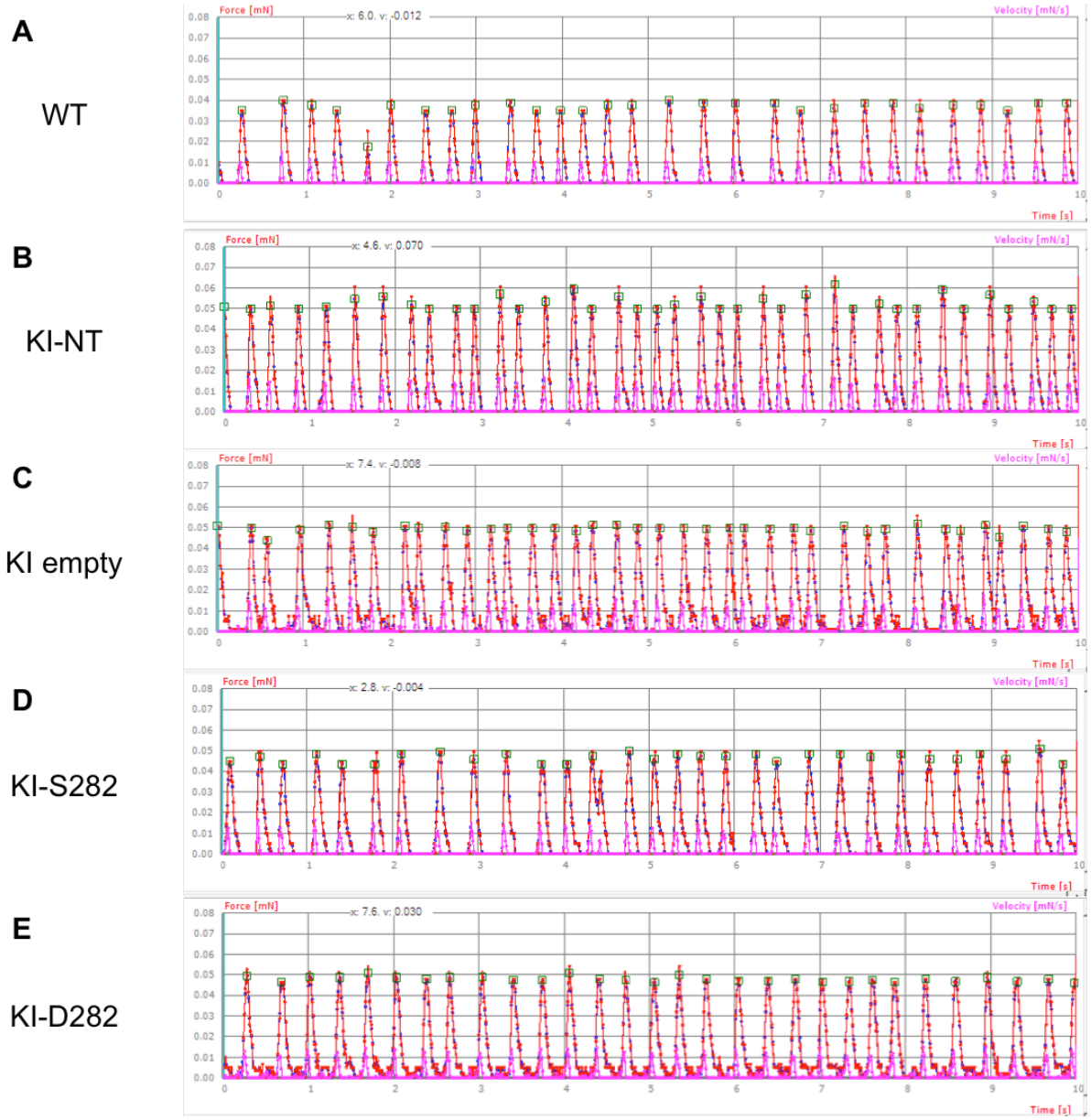

Figure 24: Spontaneous activity of WT, KI-NT and transduced KI EHTs. Representative 10 sec segments of recordings for **[A]** WT, **[B]** KI-NT, **[C]** KI empty, **[D]** KI-S282 and **[E]** KI-D282. All EHTs showed permanent beating through the whole time of recording.

To exclude EHTs that did not beat coherently, only those EHTs, correctly attached to both silicone posts, reaching a frequency of ≥ 50 bpm and with forces of ≥ 0.015 mN spontaneous beating activity were taken into account for the analysis.

3.4 Analysis of contractile parameters

KI-EHTs were known to show a hypercontractile phenotype with higher forces and velocities of contraction (CV) and relaxation (RV) in spontaneous beating activity compared to the WT. To assess whether this phenotype was prevented by treatment

with AAV6 encoding either KI-S282 (WT cMyBP-C with Ser282) or KI-D282 (transgenic cMyBP-C with Asp282), the spontaneous beating activity in each group was measured in EHT culture medium, containing 1.8 mM external [Ca^{2+}], with video-optical recording. The data obtained from different batches were pooled for maximal forces. This was usually reached between day 12 and 19 of culture.

In contrast to previous results, KI-NT only showed a tendency to higher forces in spontaneous beating activity than WT. Overall the maximal force did not differ between the groups (Figure 25).

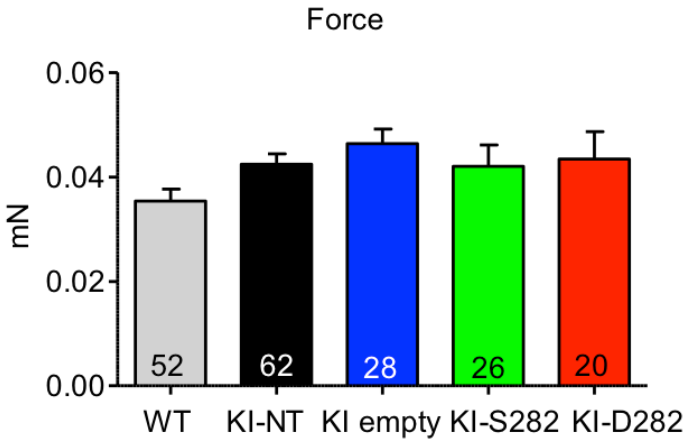

Figure 25: Maximal forces of EHTs under spontaneous beating activity. Forces of several EHTs in all groups were analyzed. Maximal force values were pooled for each batch on the day of highest force development. Measurement was performed with video-optical recording in EHT culturing medium containing 1.8 mM external [Ca^{2+}]. Numbers of analyzed EHTs are indicated in the bars. Data are expressed as mean±SEM. WT, wild-type; KI, knock-in; NT, non-transduced.

CV and RV were also not different between the groups. Only the CV of KI empty was 45% higher than the WT (Figure 26).

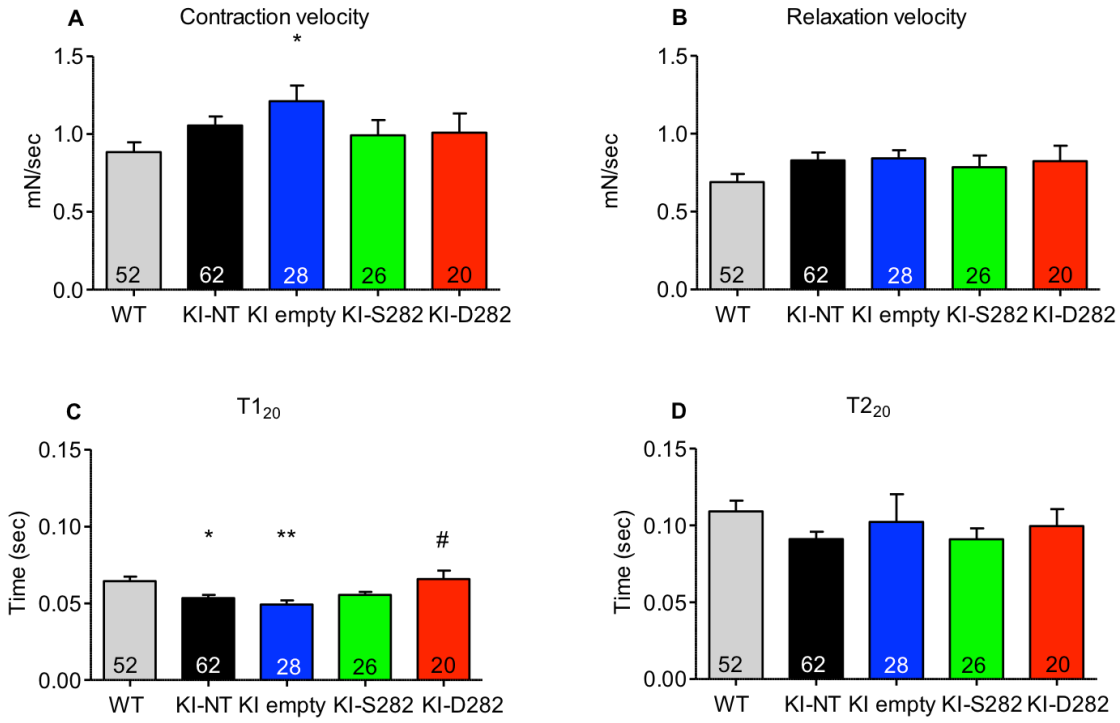

Figure 26: Contractile parameters of spontaneous beating activity in EHTs. EHTs in the groups from different batches were pooled according the day of maximal force development for **[A]** CV, **[B]** RV, **[C]** $T1_{20}$ and **[D]** $T2_{20}$. Measurements were performed with video-optical recording in EHT culturing medium containing 1.8 mM external [Ca^{2+}]. Numbers of analyzed EHTs are indicated in the bars. Data are expressed as mean±SEM. **P*<0.05, ***P*<0.01 vs. WT; #*P*<0.05 vs. KI empty (one-way ANOVA plus Bonferroni post test). WT, wild-type; KI, knock-in; NT, non-transduced.

Nevertheless time of contraction $T1_{20}$ was 17% lower in the KI-NT and 25% lower in the KI empty than in the WT. The decrease in T1 might reflect a quicker contraction in the KI-NT and KI empty, which was only visible in the KI empty (Figure 26 A, C). In the KI-D282 $T1_{20}$ was 38% higher than in the KI empty. It remains unexplainable why there was a significant difference seen in $T1_{20}$ between KI-D282 and KI empty. In terms of $T2_{20}$ there was only a tendency of a reduced time in the KI-NT compared to the WT. Similarly there was no correction of the phenotype visible in the KI-S282 or KI-D282.

The influence of the viral transduction on the frequency of EHTs was also investigated. Frequency in all groups showed a Gaussian distribution. WT and KI-D282 had lower frequencies (17% and 19%, respectively) than the KI-NT. No major differences were detected between the remaining groups (Figure 27).

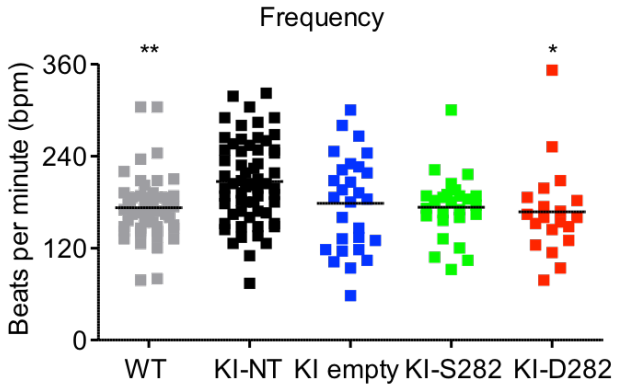

Figure 27: Frequency of EHTs under spontaneous contractile activity. Frequency for several EHTs on the day where they reached their maximal forces are shown. Black line indicates mean. *P<0.05, **P<0.01 vs. KI-NT (one-way ANOVA plus Bonferroni post test). WT, wild-type; KI, knock-in; NT, non-transduced.

3.5 Measurement of contractile parameters under electrical pacing

Since there was no correction of hypercontractility in KI-D282 and KI-S282 in spontaneous contractile activity, more challenging experimental conditions were chosen. Therefore EHTs were subjected to electrical pacing in Tyrode's solution (at different external [Ca^{2+}]). Based on former experiments, a pacing rate of 6 Hz was chosen (Stohr et al. 2013). This should exclude the confounding effect of frequency. An established protocol, based on the continuous perfusion with Tyrode's solution and performed under unsterile conditions, was chosen. In three different runs, however, EHTs were not capable to survive the whole experimental procedure (data not shown). Therefore electrical stimulation was performed in the same setup as used for measurements of spontaneous activity. Pacing electrodes were mounted under sterile conditions on the EHTs and raising external [Ca^{2+}] (0.2-1.8 mM) in the Tyrode's solution were obtained by addition from a defined $CaCl_2$ working solution. Under these conditions EHTs were capable to endure the whole experimental procedure (Figure 28).

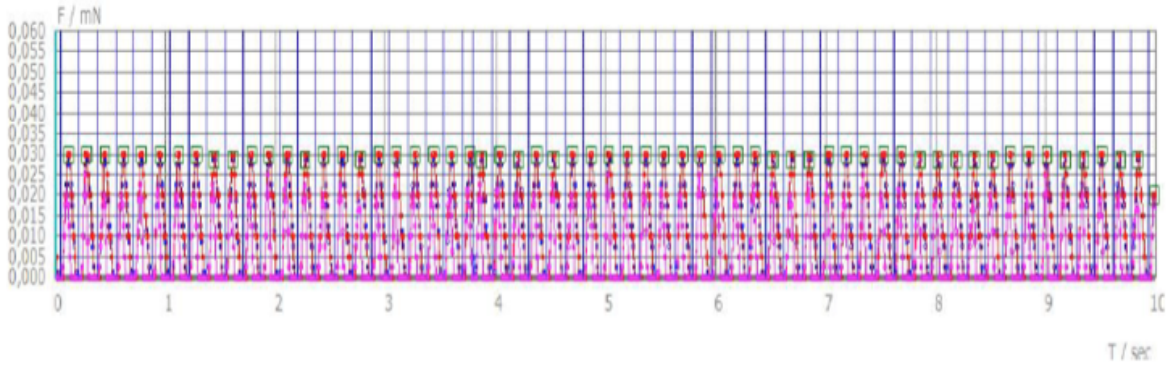

Figure 28: Force of an EHT under electrical pacing (6 Hz). Recording of an EHT under electrical stimulation (6 Hz) in Tyrode's solution (1.8 mM external [Ca^{2+}]). Measurement duration was 10 sec. Blue lines in front of the contraction curve indicate the pulse of the pacing unit.

Nevertheless, in some cases it was impossible to successfully record the EHTs due to difficulties in figure recognition (Figure 29). These EHTs were not taken into account for the analysis. Additionally, in some cases EHTs did not properly follow the pacing of 6 Hz but became arrhythmic and were not analyzed. EHTs were usually measured between day 14 and 16 of culture.

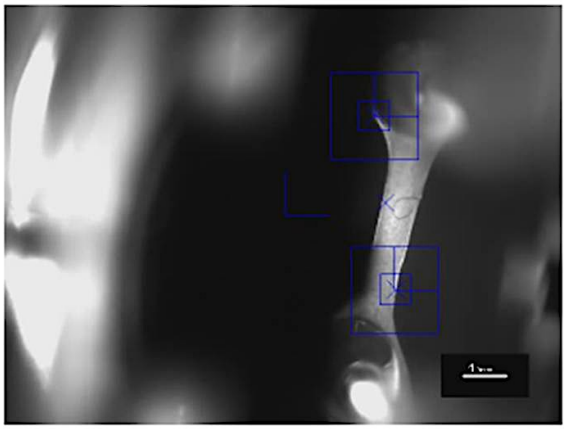

Figure 29: Bad figure recognition of EHTs under electrical pacing. EHT was not recorded vertically and the blue figure recognition squares were not aligned on the same side of the EHT. Thus a convenient figure recognition was impossible. Scale bar 1 mm.

3.5.1 Analysis of contractile parameters

In order to investigate the effect of gene therapy treatment and to unmask the phenotype of the different groups, EHTs were not only paced at 6 Hz, they were also subjected to challenging conditions, such as different external [Ca^{2+}] (0.1-1.8 mM) in Tyrode's solution. At low external [Ca^{2+}] EHTs did not develop force. With the raise of external [Ca^{2+}], EHTs began to beat again, following the pacing rhythm in most cases. External [Ca^{2+}] was increased until concentrations of standard culture medium (1.8 mM) were reached (Figure 30).

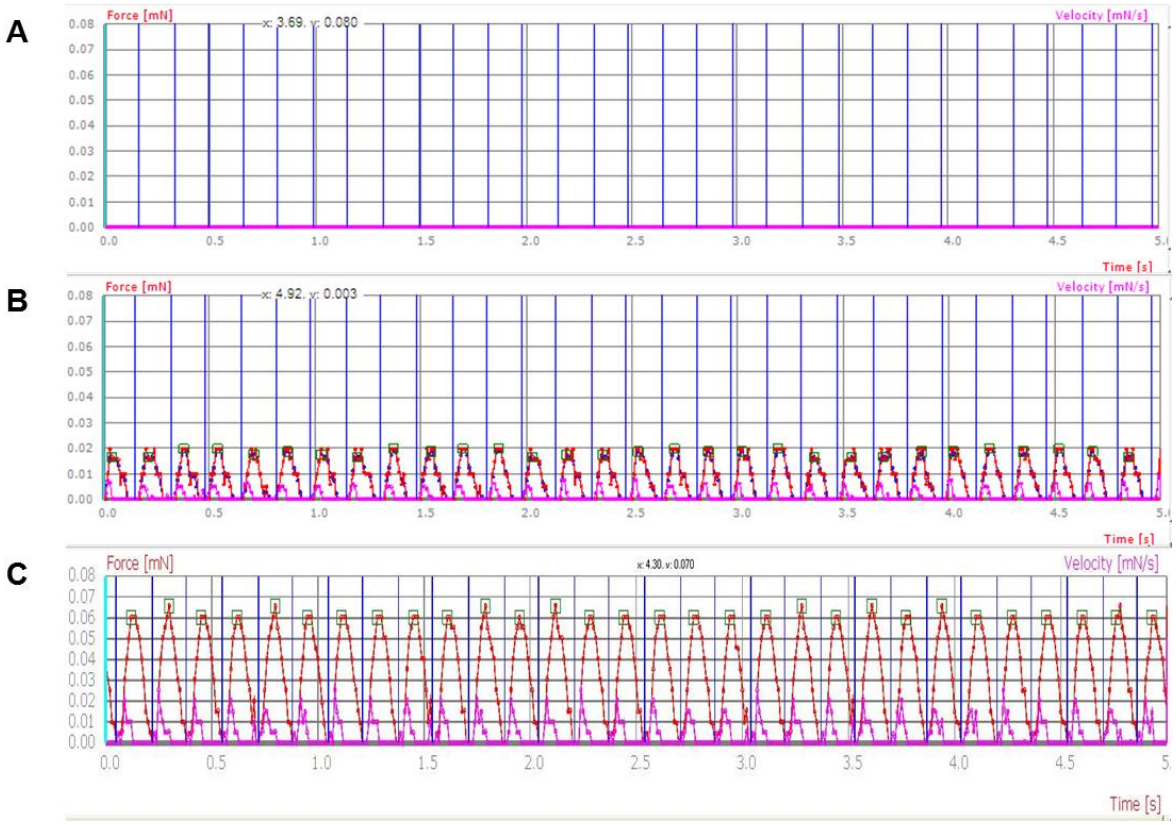

Figure 30: Contraction peaks with rising external [Ca^{2+}]. Representative 5 sec traces for a KI-EHT at different external [Ca^{2+}] of **[A]** 0.1 mM, **[B]** 0.4 mM and **[C]** 1.8 mM under electrical pacing of 6 Hz is shown. Blue lines indicate the pulse of the pacing unit.

Overall KI-NT showed 2.8 (0.2 mM) – 1.4 (1.8 mM)-fold higher forces than the WT, reflecting their hypercontractile phenotype. The same increase in force was shown by KI empty EHTs. Forces developed by KI-S282 were not different from the WT but were significantly lower than the KI-NT. Forces developed by KI-D282 were between WT and KI-NT (Figure 31).

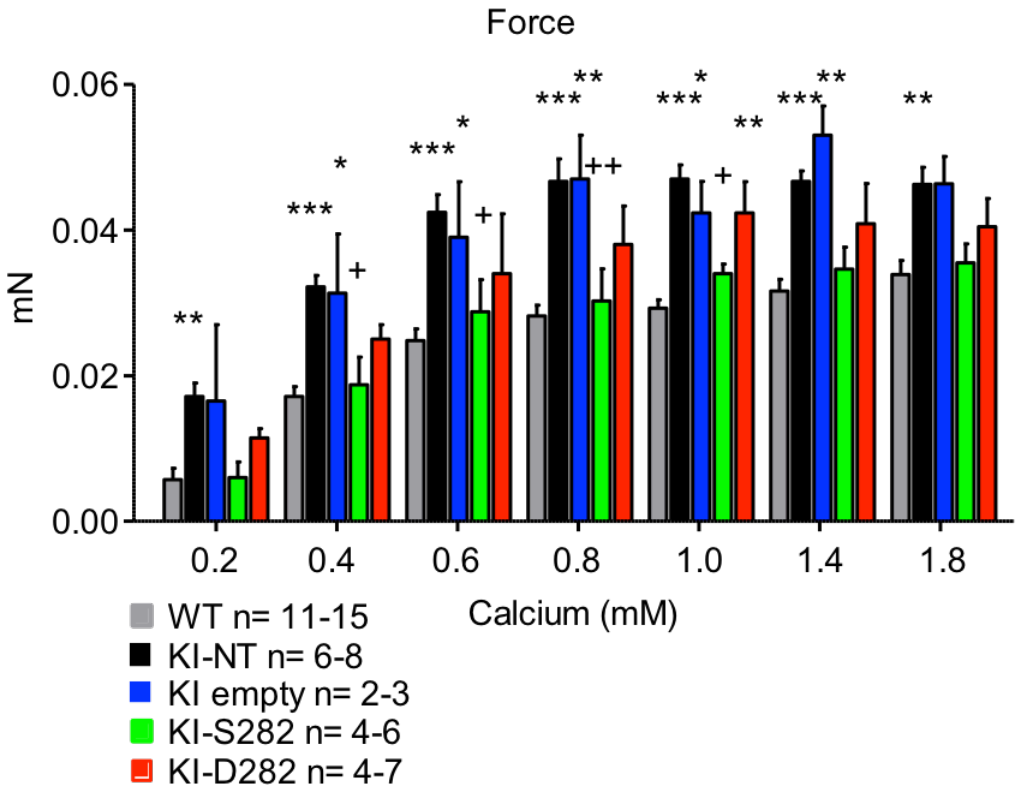

Figure 31: Contractile phenotype in terms of force of EHTs with electrical pacing (6 Hz) in Tyrode's solution. Development of force in the different groups of EHTs at different concentrations of external [Ca^{2+}] in Tyrode's solution under electrical pacing (6 Hz). Data are expressed as mean±SEM. *P<0.05, **P<0.01, ***P<0.001 vs. WT, same condition; +P<0.05, ++P<0.01 vs. KI-NT, same condition (two-way ANOVA plus Bonferroni post test). WT, wild-type; KI, knock-in; NT, non-transduced.

Consistent with higher forces, KI-NT showed also faster kinetics of contraction under electrical pacing than the WT. Contraction velocities were at least 1.3-fold higher than in the WT at all external [Ca^{2+}]. Relaxation velocities were at least 1.5-fold higher than in WT except for 1.4 mM and 1.8 mM external [Ca^{2+}], where only a tendency was seen. KI empty EHTs showed faster kinetics than WT and did not differ from the KI-NT. The kinetics of the KI-S282 were lower than KI-NT and similar to the WT. As for the force under electrical pacing the kinetics of KI-D282 were intermediate between WT and KI-NT (Figure 32).

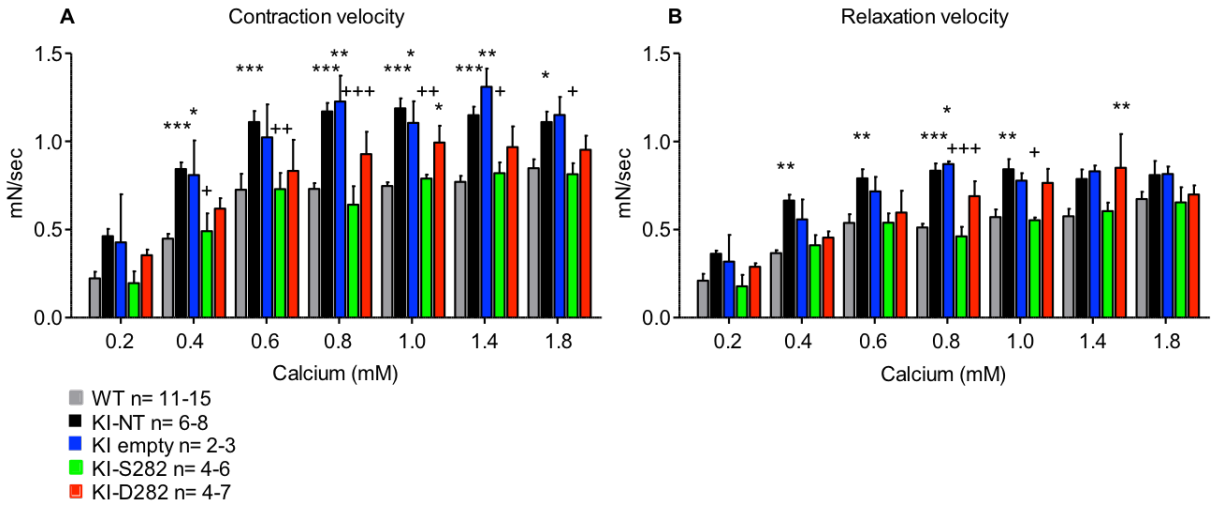

Figure 32: Contractile phenotype in terms of CV and RV of EHTs with electrical pacing (6 Hz) in Tyrode's solution. Development of **[A]** CV and **[B]** RV in the different groups of EHTs at different external [Ca^{2+}] in Tyrode's solution under electrical pacing (6 Hz). Data are expressed as mean±SEM. **P*<0.05, ***P*<0.01, ****P*<0.001 vs. WT, same condition; +*P*<0.05, ++*P*<0.01, +++*P*<0.001 vs. KI-NT, same condition (two-way ANOVA plus Bonferroni post test). WT, wild-type; KI, knock-in; NT, non-transduced.

There was no difference in $T1_{20}$ or $T2_{20}$ between the groups under electrical pacing at any calcium concentration (data not shown).

3.5.2 Response to rising external [Ca^{2+}] and calcium sensitivity

In addition to the contractile parameters, the sensitivity of the different groups towards external [Ca^{2+}] was investigated. For this aim all forces were normalized to the maximal forces in each group at a certain calcium concentration and EC_{50} values were calculated. Calculated EC_{50} values were 0.39, 0.28, 0.30, 0.40 and 0.32 mM in WT, KI-NT, KI empty, KI-S282 and KI-D282, respectively (Figure 33). KI-NT were known to exhibit a higher sensitivity to external [Ca^{2+}] than the WT (Stohr et al. 2013) and indeed their curve showed a shift to the left. Whereas transduction of KI-S282 resulted in the same sensitivity to external [Ca^{2+}] as the WT. The curves for KI empty and KI-D282 were between KI-NT and WT with slight shifts to the left.

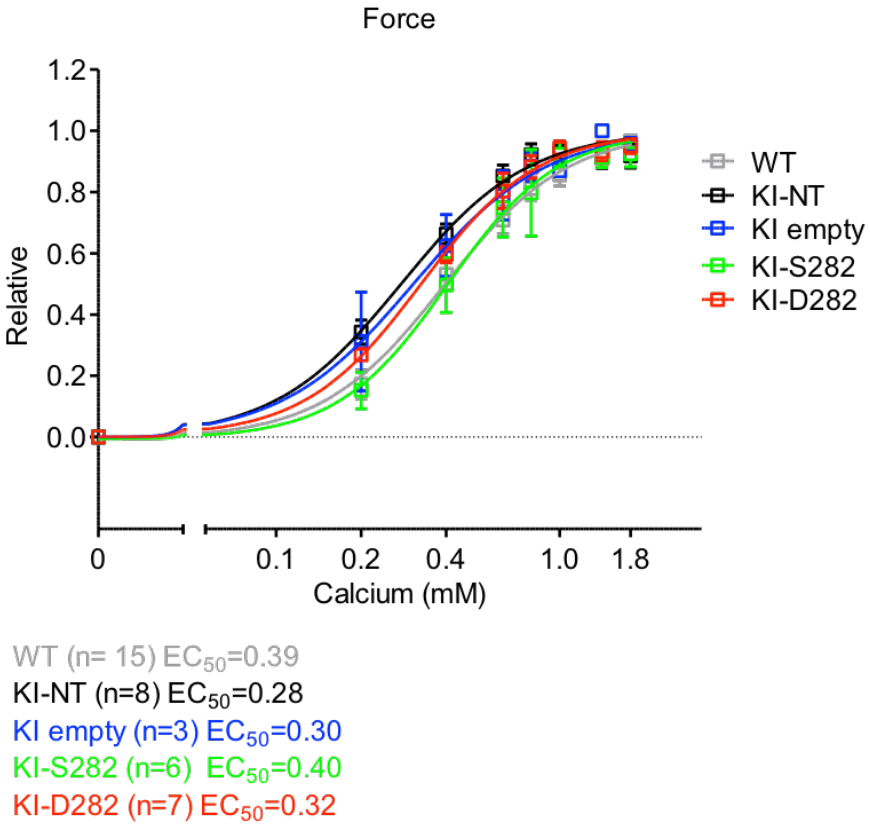

Figure 33: Calcium-sensitivity in EHTs. Normalized relative force (same data as Figure 31) to external [Ca^{2+}] (0.2 – 1.8 mM). All data expressed as mean±SEM. Log-EC_{50} was different for each data set. *P*= 0.0008 (F-test). WT, wild-type; KI, knock-in; NT, non-transduced.

3.5.3 Response to isoprenaline at submaximal external [Ca^{2+}]

To investigate the behavior of the different EHTs in the presence of external stressors, EHTs were subjected to isoprenaline and EMD 57033 (3.5.4). Isoprenaline as a β-adrenergic agonist is mainly known as positive inotropic and chronotropic agent. Thus an increase of force in EHTs was expected after treatment (Stohr et al. 2013). Therefore a submaximal external [Ca^{2+}] around the calculated EC_{50} values (~0.4 mM) was chosen. This should enable to capture the effect on force. In order to prevent the confounding effect of frequency that might be mediated by both drugs on EHTs, experiments were performed under electrical pacing (6 Hz in Tyrode's solution). First EHTs were measured in Tyrode's solution of 0.4 mM external [Ca^{2+}]. Then isoprenaline was added (final concentration 100 nM) and EHTs were measured after 15 and 30 min of incubation. An effect was already expected after 15 min, but to evaluate the stability of the effect, the additional measurement after 30 min was performed. However after the addition of isoprenaline even more EHTs became

arrhythmic and did not properly follow the pacing rhythm any more. Several EHTs were still present for analysis at baseline, but had to be excluded from the analysis after treatment (Figure 34).

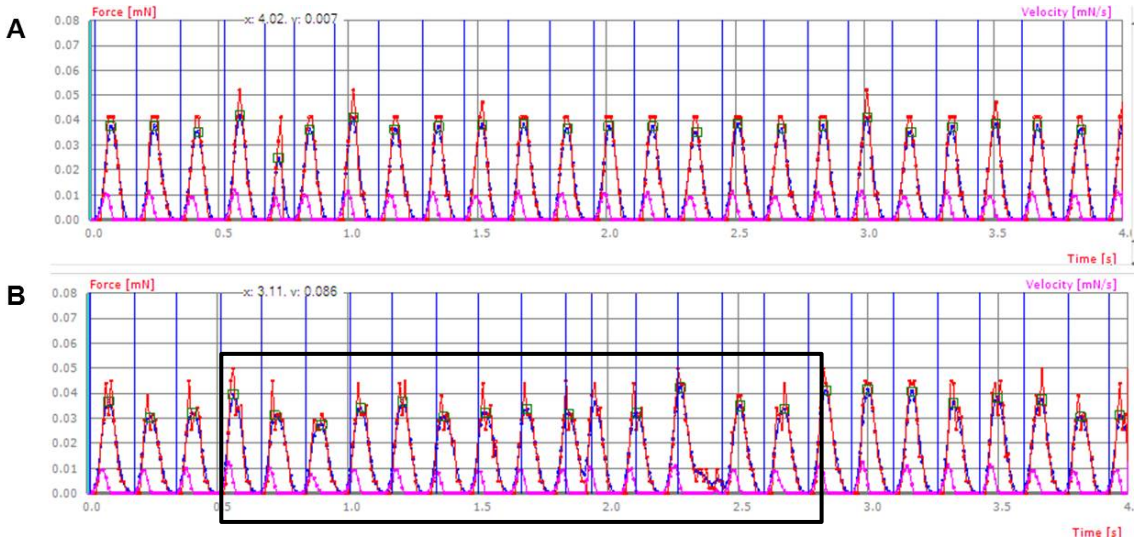

Figure 34: Paced EHTs in the presence of isoprenaline. Representative 4 sec segments of paced EHTs after 15 min incubation with isoprenaline. **[A]** Well paced EHT with a stable force development and **[B]** an arrhythmic EHT after isoprenaline treatment. Black rectangle shows the arrhythmic segment. Blue lines depict the pulse of the pacing unit.

Although dealing with small n numbers, in WT EHTs an increase of force of at least 2-fold compared to baseline was observed in the presence of isoprenaline, which was also stable over time. This effect was blunted in the KI-NT with only an increase of 1.2-fold compared to baseline. In KI empty the effect of isoprenaline was more pronounced (1.4-fold increase compared to baseline), but less than in WT. In both KI-S282 and KI-D282 an increase in force of 1.7-fold compared to baseline was seen after 15 min. This increase was lost after 30 min (not shown), since almost all EHTs became arrhythmic (Figure 35).

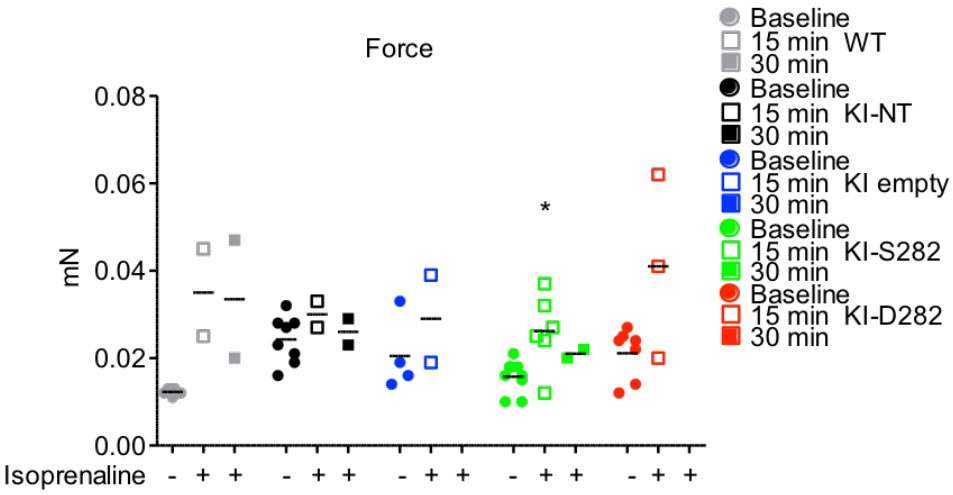

Figure 35: Force response to isoprenaline at submaximal [Ca^{2+}] in EHTs under electrical pacing. EHTs from different groups were measured under electrical pacing (6 Hz) at submaximal external [Ca^{2+}] (0.4 mM) in Tyrode's solution first at baseline and with treatment of isoprenaline (final concentration 100 nM) after 15 and 30 min of incubation. *P<0.05 vs. corresponding baseline (paired Student's t-test). WT, wild-type; KI, knock-in; NT, non-transduced.

In line with the effect on force, CV and RV showed similar tendencies. $T1_{20}$ did not differ between the groups, whereas $T2_{20}$ was decreased in WT, KI-S282 and KI-D282 in the presence of isoprenaline. This revealed the positive lusitropic effect (=faster relaxation) of isoprenaline. No changes were seen for KI-NT and KI empty EHTs (Figure 36).

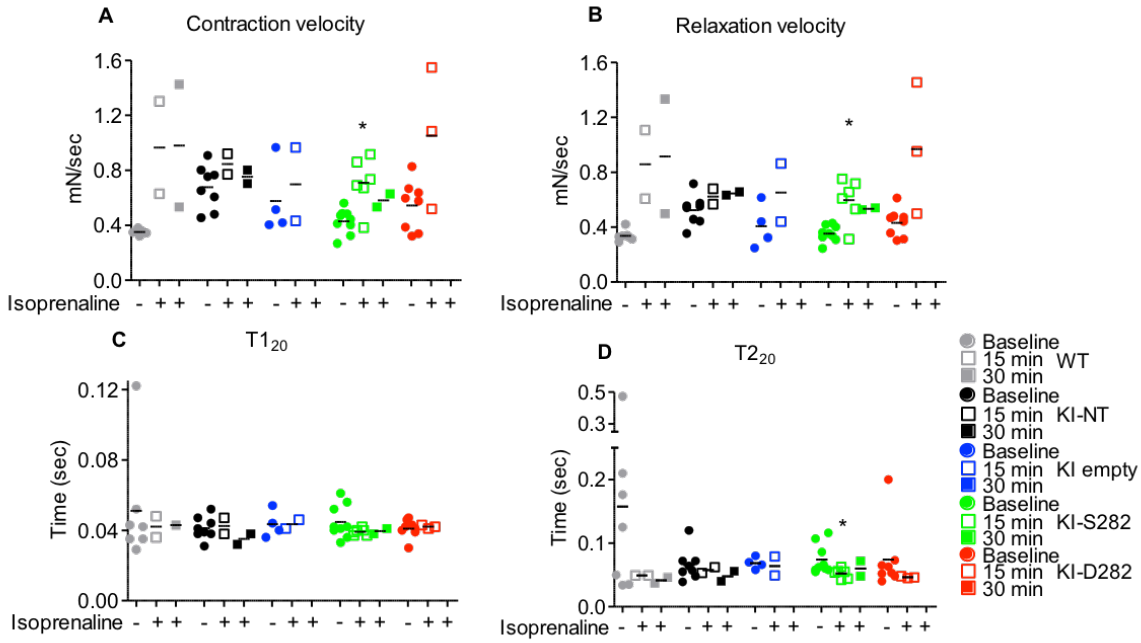

Figure 36: Response of kinetics of contraction to isoprenaline at submaximal [Ca^{2+}] in EHTs under electrical pacing. EHTs from different groups were measured under electrical pacing (6 Hz) at submaximal external [Ca^{2+}] (0.4 mM) in Tyrode's solution first at baseline and after addition of isoprenaline (final concentration 100 nM) after 15 and 30 min of incubation. Shown are data for **[A]** CV, **[B]** RV, **[C]** T1 (20), **[D]** T2 (20). *P<0.05 vs. corresponding baseline (paired Student's t-test). WT, wild-type; KI, knock-in; NT, non-transduced.

3.5.4 Response to EMD 57033 at submaximal external [Ca^{2+}]

EMD 57033 is a calcium-sensitizer and has positive inotropic effects. Therefore as for isoprenaline an increase in force in EHTs after treatment was expected (Stohr et al. 2013). As for isoprenaline treatment, EHTs were measured at submaximal external [Ca^{2+}] of 0.4 mM at 6 Hz pacing. EMD 57033 was added (final concentration 10 µM) and measurements were performed 15 min and 30 min after treatment. In contrast to isoprenaline treatment almost all EHTs that were treated with EMD could be taken into account for the analysis, since only few became arrhythmic. However, changes in force were not as pronounced as they were after treatment with isoprenaline. Nevertheless the WT-EHTs showed a 1.3-fold increase in force after 15 min incubation with isoprenaline, which was even stronger after 30 min (1.4-fold) compared to baseline. In contrast, KI-NT showed a blunted response to EMD 57033. However KI empty similar to WT-EHTs showed a 1.4-fold increase in force after treatment with EMD 57033. Similarly, EMD 57033 treamtent induced a 1.3-fold increase in force, which was stable over time in KI-S282 EHTs. KI-D282 EHTs did not remarkably differ from baseline after the addition of EMD 57033 (Figure 37).

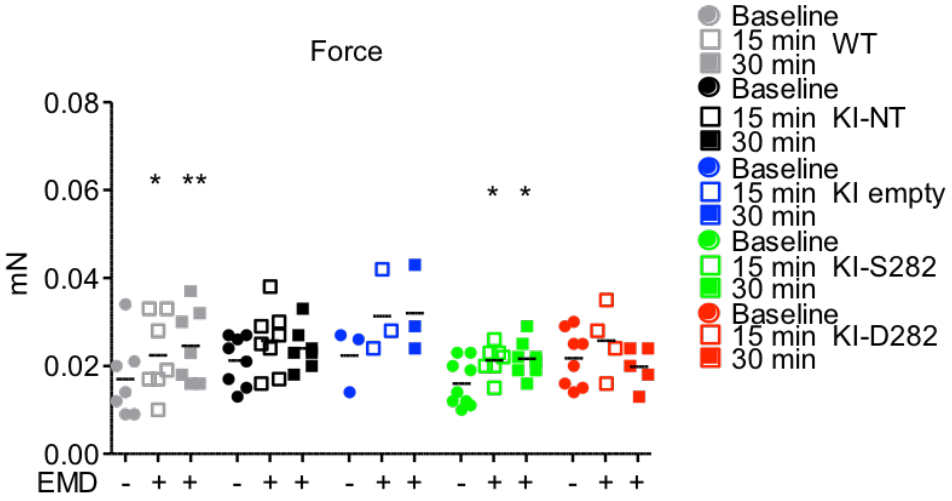

Figure 37: Force response to EMD 57033 at submaximal [Ca^{2+}] in EHTs under electrical pacing. EHTs from different groups were measured under electrical pacing (6 Hz) at submaximal external [Ca^{2+}] (0.4 mM) in Tyrode's solution first at baseline and after addition of EMD 57033 (final concentration 10 µM) after 15 and 30 min of incubation. *P<0.05, **P<0.01 vs. corresponding baseline (paired Student's t-test). WT, wild-type; KI, knock-in; NT, non-transduced.

The positive inotropic effect of EMD 57033 on CV and RV was also visible in the different EHTs. The same development patterns were observed in these parameters. $T1_{20}$ was significantly increased after 15 min of incubation with EMD 57033 in the KI-NT as well as in the KI-S282, but not in the other groups. However $T2_{20}$ was decreased by 50% (*P*= 0.1; for WT + EMD 57033 30 min vs. corresponding baseline) but not significantly in the WT after incubation with EMD 57033. Significantly increased values for $T2_{20}$ were only seen for KI-NT and KI-S282 by 1.5-fold both, 15 min after treatment with EMD 57033. No remarkable changes were observed in both KI empty and KI-D282 (Figure 38).

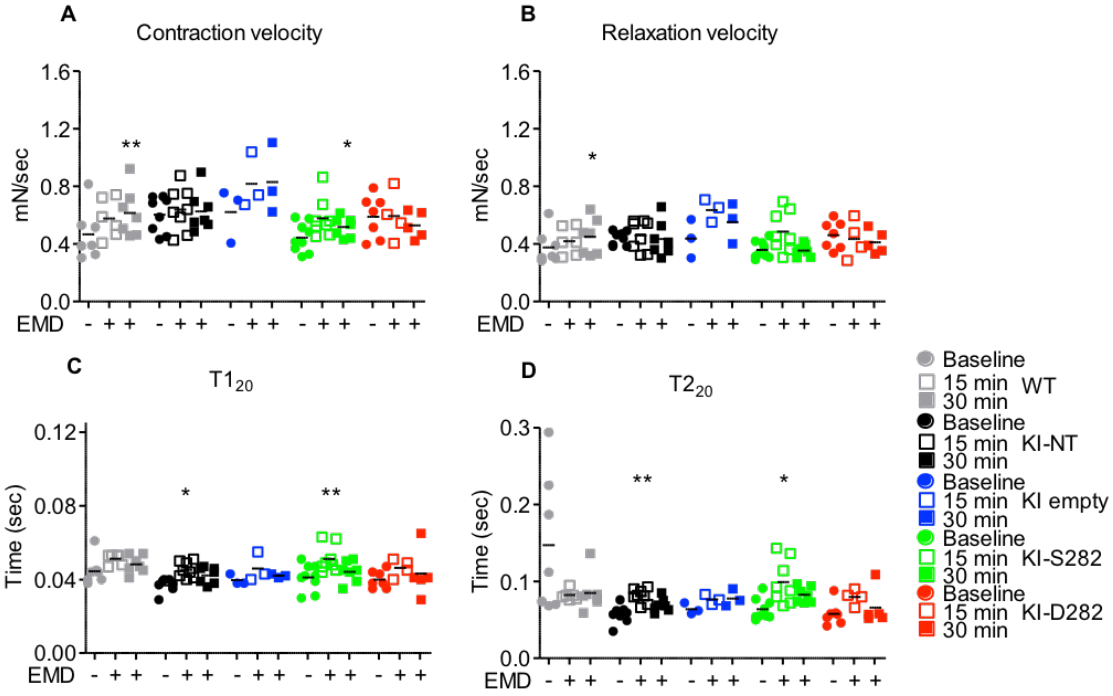

Figure 38: Response of contractile parameter to EMD 57033 at submaximal [Ca^{2+}] in EHTs under electrical pacing. EHTs from different groups were measured under electrical pacing (6 Hz) at submaximal external [Ca^{2+}] (0.4 mM) in Tyrode's solution first at baseline and with addition of EMD 57033 (final concentration 10 µM) after 15 and 30 min of incubation. Shown are data for **[A]** CV, **[B]** RV, **[C]** T1 (20), **[D]** T2 (20). **P*<0.05, ***P*<0.01 vs. corresponding baseline (paired Student's t-test). WT, wild-type; KI, knock-in; NT, non-transduced.

All in all, with treatment of both drugs KI-S282 and KI-D282 exhibited contractile kinetics, which were close to the WT kinetics.

3.6 Evaluation of *Mybpc3* and hypertrophic markers

In order to validate the efficacy of gene therapy at molecular level in the different EHTs, RNA was extracted with TRIzol® from the EHTs and subjected either to RT-PCR or qPCR. Experiments were performed in RNA-pools of EHTs (n= 3).

3.6.1 Total *Mybpc3* mRNA and prevention of accumulation of mutant mRNAs

To evaluate whether transduction of EHTs with AAV6 (S282 and D282) lead to an increase in total *Mybpc3* mRNA level, qPCR using the SYBR Green technology with primers located in *Mybpc3* exons 2 and 3 was performed. *Gnas* was used as a housekeeping gene for normalization and the data were related to the WT. Total *Mybpc3* mRNA level was 75% lower in KI-NT than in WT. After gene transfer, total *Mybpc3* mRNA level was 6-fold and 3.5-fold higher in KI-S282 and KI-D282 than in WT, respectively (Figure 39A). KI empty showed no major difference with the KI-NT (data not shown).

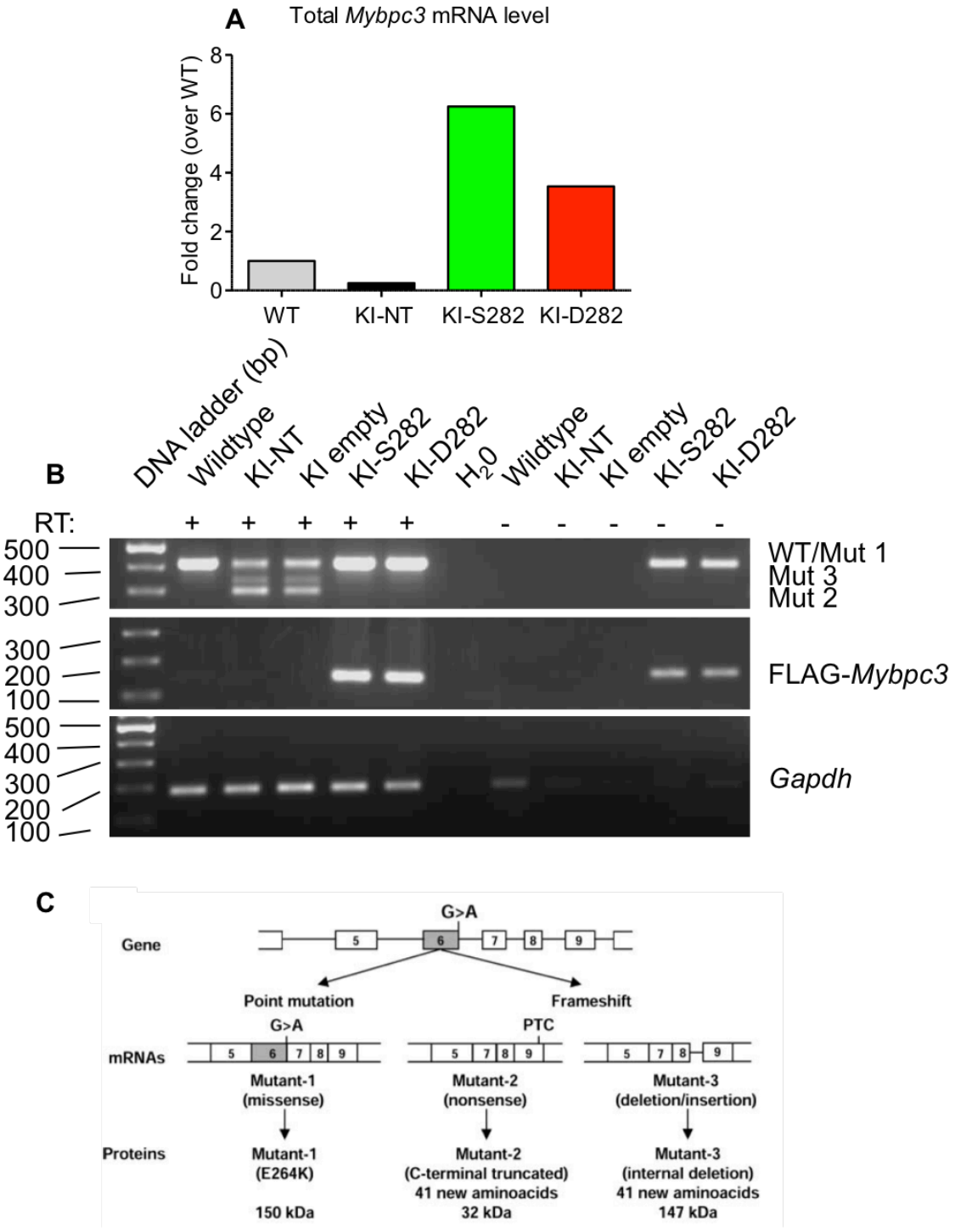

Figure 39: Total *Mybpc3* mRNA level and evaluation of mutant mRNAs. [A] Quantification of total *Mybpc3* mRNA levels. mRNA levels were determined by SYBR Green qPCR with primers located in exon 2/3 of the *Mybpc3* cDNA using RNA pools (n= 3); **[B]** Representative agarose gels of RT-PCR on total RNA of the different EHT groups. Expected fragments are: Mutant-1 (missense)/WT: 415 bp, Mutant-3 (frameshift): 334 bp, Mutant-2 (297) bp, FLAG: 155 bp, *Gapdh*: 185 bp; **[C]** G>A transition at the last nucleotide of exon 6 in *Mybpc3* leads to three different mutant mRNAs and three different mutant proteins (Vignier et al. 2009). WT, wild-type; KI, knock-in; NT, non-transduced; bp, base pairs.

The KI-NT typically show three different mutant mRNAs resulting from different RNA splicing (Figure 39C) and the effect of gene therapy on these was investigated. This was determined by RT-PCR with primers recognizing total *Mybpc3* mRNAs (WT,

missense and frameshift). As a control for amplification of exogenous *Mybpc3,* primers recognizing the FLAG-tag sequence of the transgenic products were used. As a loading control primers for recognition of *Gapdh* mRNA were chosen. Representative agarose gels for these RT-PCR are shown in Figure 39B. The KI-NT showed the presence of the three different mutant mRNAs (Mutant-1 (missense), Mutant-3 (frameshift), Mutant-2 (frameshift) with 415 bp, 334 bp, 297 bp length, respectively). In contrast, only one band of 415 bp was detected in the WT, KI-S282 and KI-D282. No amplification was observed without RT, except for KI-S282 and KI-D282 corresponding to the amplification of the transgene (genomic DNA or cDNA contamination). In addition only those EHTs that received exogenous *Mybpc3* cDNA (WT or D282) showed a signal with the primer in the FLAG-tag sequence with residuals of the transgene in the –RT lane. Amplification of *Gapdh* was comparable in all groups.

3.6.2 Evaluation of mutant *Mybpc3* mRNAs

To evaluate the amount of mutant mRNAs, a qPCR with specific probes for WT, missense or frameshift *Mybpc3* mRNAs was performed. The binding sites of these probes are schematically shown in Figure 40 (bottom part). *Gnas* was used as a housekeeping gene. Data on WT *Mybpc3* mRNA levels were related to the WT, whereas data on the different mutant *Mybpc3* mRNAs levels were related to the KI-NT. The KI-D282 and KI-S282 showed a 4.8-fold and 10-fold higher WT *Mybpc3* mRNA than in WT EHTs, respectively. As expected no WT *Mybpc3* mRNA was detected in the KI-NT. Missense *Mybpc3* mRNA level was absent in the WT, but also in KI-S282 and KI-D282. Frameshift *Mybpc3* mRNAs were absent in the WT and dropped to only 20% of KI-NT in the KI-S282 and KI-D282 (Figure 40). KI empty showed no major difference with the KI-NT (data not shown).

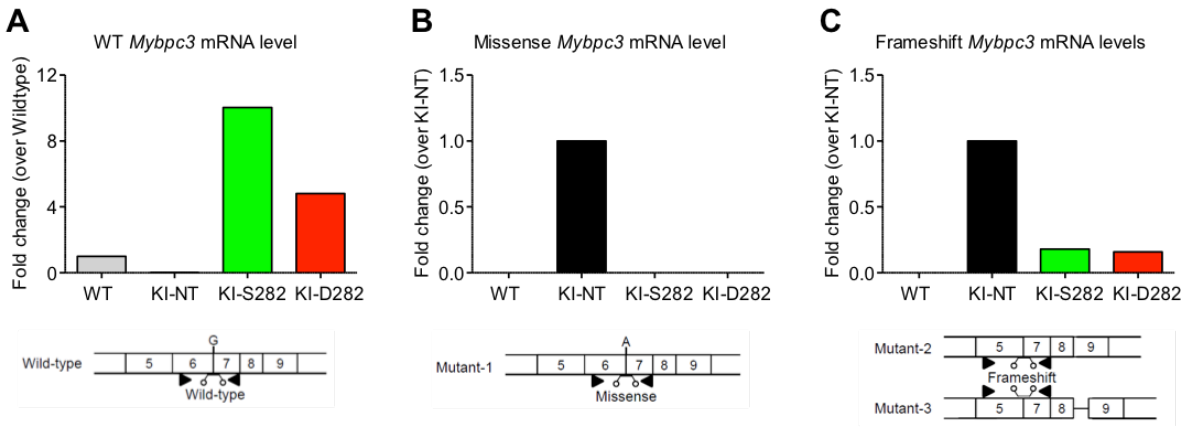

Figure 40: Determination of mutant *Mybpc3* mRNAs in EHTs. Levels of **[A]** WT *Mybpc3* mRNA, **[B]** missense *Mybpc3* mRNA and **[C]** frameshift *Mybpc3* mRNAs in the different groups with the binding sites of the specific probes, that are schematically depicted below the corresponding analysis. RNA pools (n= 3). WT, wild-type; KI, knock-in; NT, non-transduced.

3.6.3 Hypertrophic markers

A hallmark of hypertrophy in cardiac tissue is the reactivation of the fetal gene program. Several markers (*Acta1*, *Myh7* and *NppA*) are known to be upregulated in the *Mybpc3*-targeted KI mouse model (Vignier et al. 2009). These mRNA levels of hypertrophic markers were investigated in RNA pools of the different groups. SYBR Green technology with primers for *Acta1*, *Myh7* and *NppA* was used. *Acta1* mRNA level were 2-fold higher in the KI-NT than in WT, whereas it did not differ between KI-S282, KI-D282 and WT. Similarly, *Myh7* mRNA level was 1.5-fold higher in the KI-NT than in WT and did not differ between KI-S282 and KI-D282. There was no upregulation of *NppA* mRNA level in the KI-NT, but the level was 50% lower in KI-S282 and KI-D282 than in WT (Figure 41). KI empty showed no major difference with the KI-NT (data not shown).

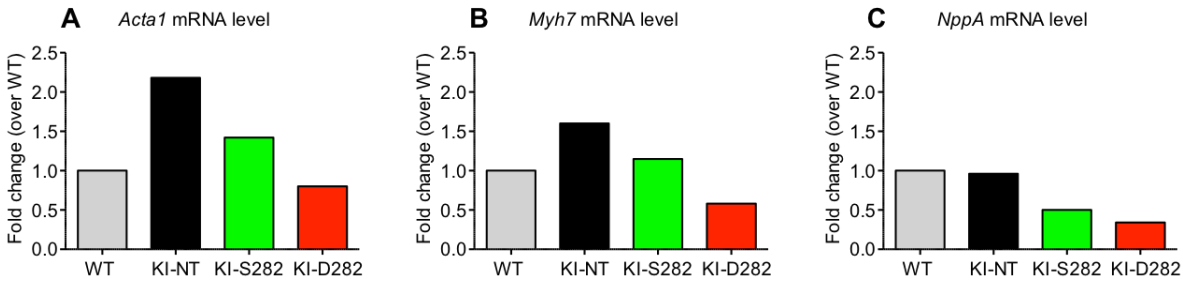

Figure 41: Evaluation of hypertrophic markers in EHTs. Pools of total RNA from EHTs extracted with Trizol. Specific primers for **[A]** *Acta1*, **[B]** *Myh7* and **[C]** *NppA* were used with SYBR Green technology. All data related to WT, (n= 3-4). WT, wild-type; KI, knock-in; NT, non-transduced.

3.7 Evaluation of cMyBP-C protein level

To assess whether the exogenous *Mybpc3* is also translated into proteins, Western Blots were performed on protein lysates from EHTs. Antibodies directed either against the FLAG epitope or against the Mybpc-Motif of cMyBP-C were used to evaluate the level of exogenous and total cMyBP-C protein, respectively, in the different groups. For a cardiac specific loading control, the samples were stained with an antibody directed against α-actinin. For quantification, bands for exogenous and total cMyBP-C were normalized to the α-actinin signals. Expression of FLAG-tagged exogenous protein was only observed in the EHTs that were transduced with AAV6 (S282 or D282). To assess the effect of gene therapy on total cMyBP-C in KI-S282 and KI-D282, data were related to the WT. KI-NT and KI empty showed a 80% and 76% lower cMyBP-C amount than the WT, respectively. Level of cMyBP-C in KI-S282 and the KI-D282 did not differ from the WT level (Figure 42).

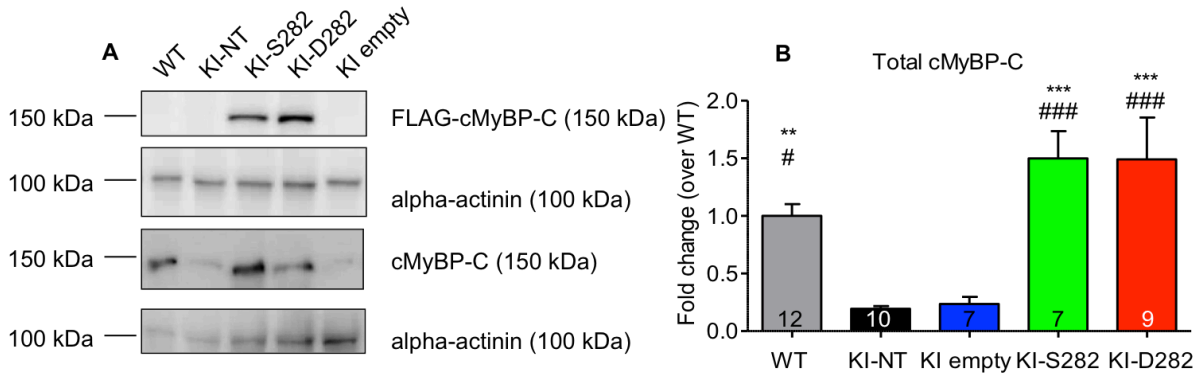

Figure 42: Evaluation of exogenous and endogenous cMyBP-C level in EHTs. Proteins were extracted from EHTs and used for Western Blot analysis. **[A]** Representative Blots with antibodies directed against the FLAG epitope (upper part) or against the Mybpc-Motif (bottom part) were used for detection of exogenous or total cMyBP-C, respectively. α-actinin served as a cardiac specific loading control. **[B]** To compare the total cMyBP-C in the groups, signals were normalized to alpha-actinin. Number of samples is indicated in the bars. All data are expressed as mean±SEM. ***P*<0.01, ****P*<0.001 vs. KI-NT; #*P*<0.05, ###*P*<0.001 vs. KI empty; (one-way ANOVA plus Bonferroni post test). WT, wild-type; KI, knock-in; NT, non-transduced.

3.8 Evaluation of phosphorylation state of serine residues in the Mybpc-Motif

In order to evaluate the role of constitutive Ser-282 phosphorylation, Western Blot analysis with specific antibodies directed against phosphorylated serine residues was used. Western Blots were performed on proteins extracted from EHTs in basal condition with antibodies directed against the phosphorylated serines 273, 282 and

302, but differences in phosphorylation levels were hardly seen (data not shown). Therefore EHTs were stimulated with 100 nM isoprenaline prior to harvesting to elicit protein phosphorylation via PKA activation. Western Blots with specific phospho-antibodies showed stronger signals after isoprenaline treatment especially in the WT and in KI-S282. Overall low signals were detected in both KI-NT and KI empty EHTs. KI-D282 neither showed a signal at baseline nor after stimulation for Ser-282 but a stronger signal for Ser-302. Staining for α-actinin served as a loading control (Figure 43).

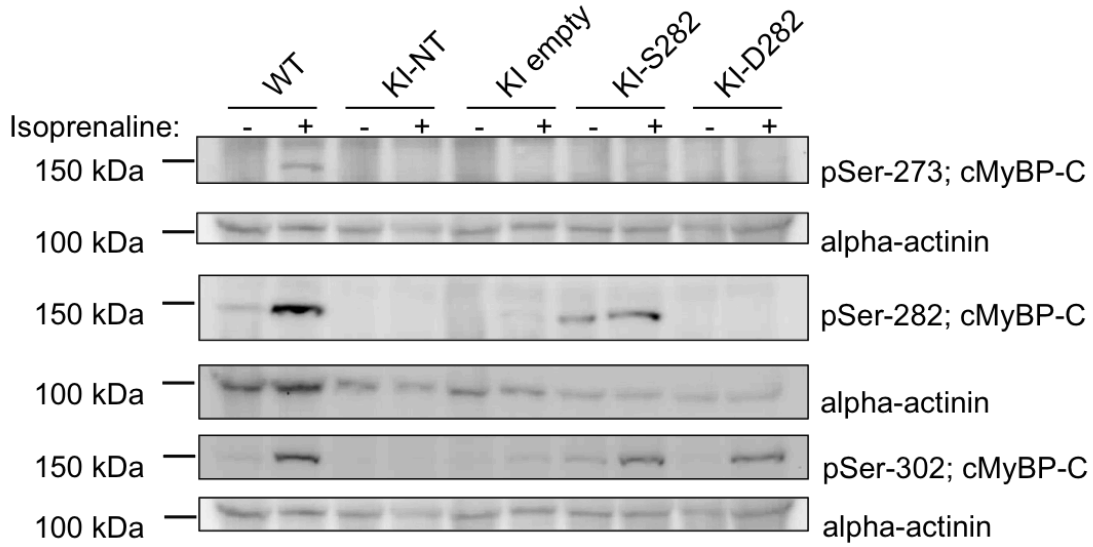

Figure 43: Phosphorylation of different serines in the Mybpc-Motif at baseline and after stimulation with isoprenaline. Representative Western Blot on proteins extracted from EHTs using antibodies directed against phosphorylated Mybpc-Motif Ser-273, Ser-282, Ser-302 residues. EHTs were treated for 15 min with isoprenaline (final concentration 100 nM) prior to harvesting. Alpha-actinin served as a cardiac specific loading control. WT, wild-type; KI, knock-in; NT, non-transduced.

In order to compare the different signals from different groups, a densitometric quantification was performed. Signals of phosphorylated serine residues were normalized to the associated α-actinin signals, then membranes were stripped and restained for total cMyBP-C. Phospho/α-actinin ratios were then normalized to the corresponding total cMyBP-C/α-actinin ratio and all data were afterwards related to the KI-S282 plus isoprenaline. No quantification for Ser-273 was possible since the software was not able to distinguish faint bands from background. For both WT and KI-S282 an increase of Ser-282 and Ser-302 phosphorylation was observed with stimulation of isoprenaline to almost the same extent. They did also differ neither at baseline nor after stimulation. No great changes in phosphorylation of Ser-282 or Ser-302 were seen in both KI-NT and KI empty. The phosphorylation at baseline,

however, was already higher than in WT and to KI-S282 (35-50% of KI-S282 phosphorylation). No signal was detected for KI-D282 with the pSer-282 antibody at baseline and upon isoprenaline treatment before harvesting. The phosphorylation of Ser-302 in KI-D282 EHTs was only slighty elevated (33% of KI-S282 phosphorylation at this residue; Figure 44).

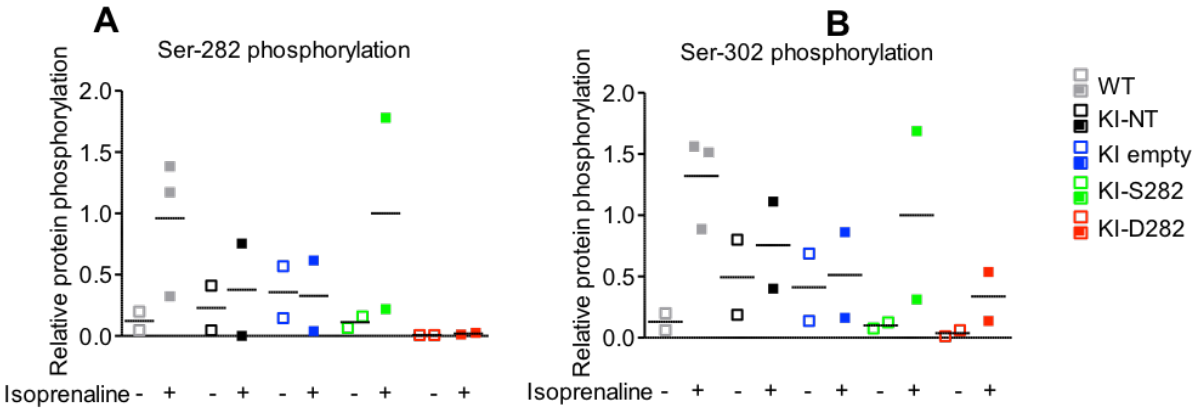

Figure 44: Relative phosphorylation of Ser-282 and Ser-302 at baseline and after stimulation. Data from densitometric quantification of the signals, obtained by Western Blot analysis. Signals were obtained using specific antibodies for phosphorylated **[A]** Ser-282 and **[B]** Ser-302. All data related to KI-S282 + isoprenaline. WT, wild-type; KI, knock-in; NT, non-transduced.

3.9 Sarcomeric localization of cMyBP-C in EHTs

To evaluate the localization of exogenous cMyBP-C protein, EHTs were subjected to immunofluorescence analysis. Antibodies directed against the Mybpc-Motif for recognition of total cMyBP-C or against the FLAG epitope of the exogenous protein were used as primary antibodies. To display the Z-discs in sarcomeres, EHTs were costained with an antibody directed against α-actinin. There was much less total cMyBP-C detectable in the KI-NT and KI empty compared to the WT. No differences were seen between KI-S282, KI-D282 and WT. In these three groups, cMyBP-C was properly incorporated in the A-band of the sarcomere in form of doublets (Figure 45).

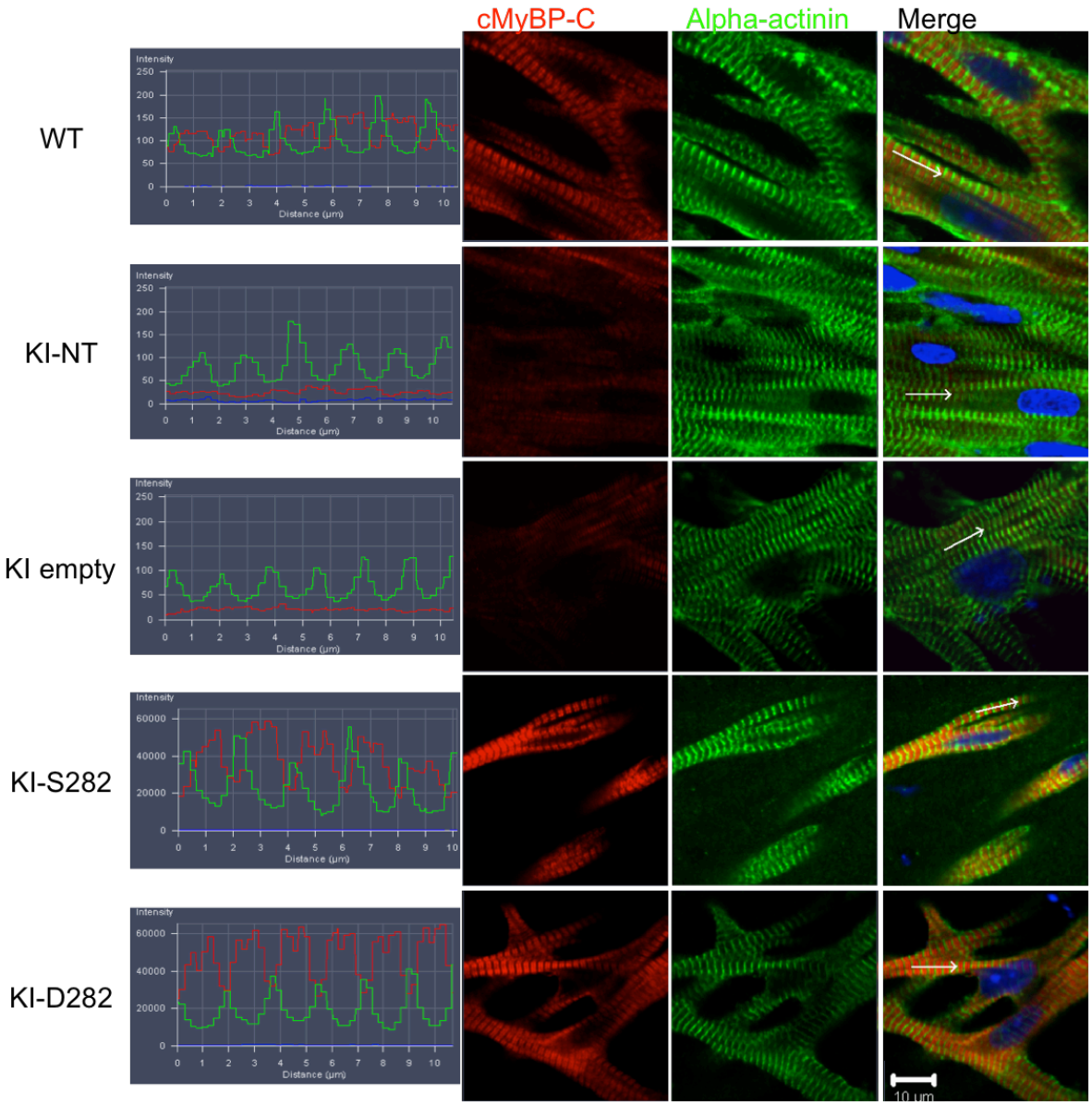

Figure 45: Localization of cMyBP-C in EHTs. Immunoflourescence pictures of EHTs from the different groups. Antibodies directed against the Mybpc-Motif for total cMyBP-C (red) and α -actinin for Z-disc (green) staining were used. Nuclei were stained with DRAQ 5 (blue). Flourescence profiles (left panel) show alternation of cMyBP-C (red lines) and α-actinin (green lines). White arrow indicates the place, where fluorescence profiles were taken. WT, wild-type; KI, knock-in; NT, non-transduced.

FLAG-cMyBP-C protein was found only in KI-S282 and KI-D282 EHTs, confirming the Western Blot data and with proper A-band localization. Only background signal was detected in the WT or in the KI empty (Figure 46).

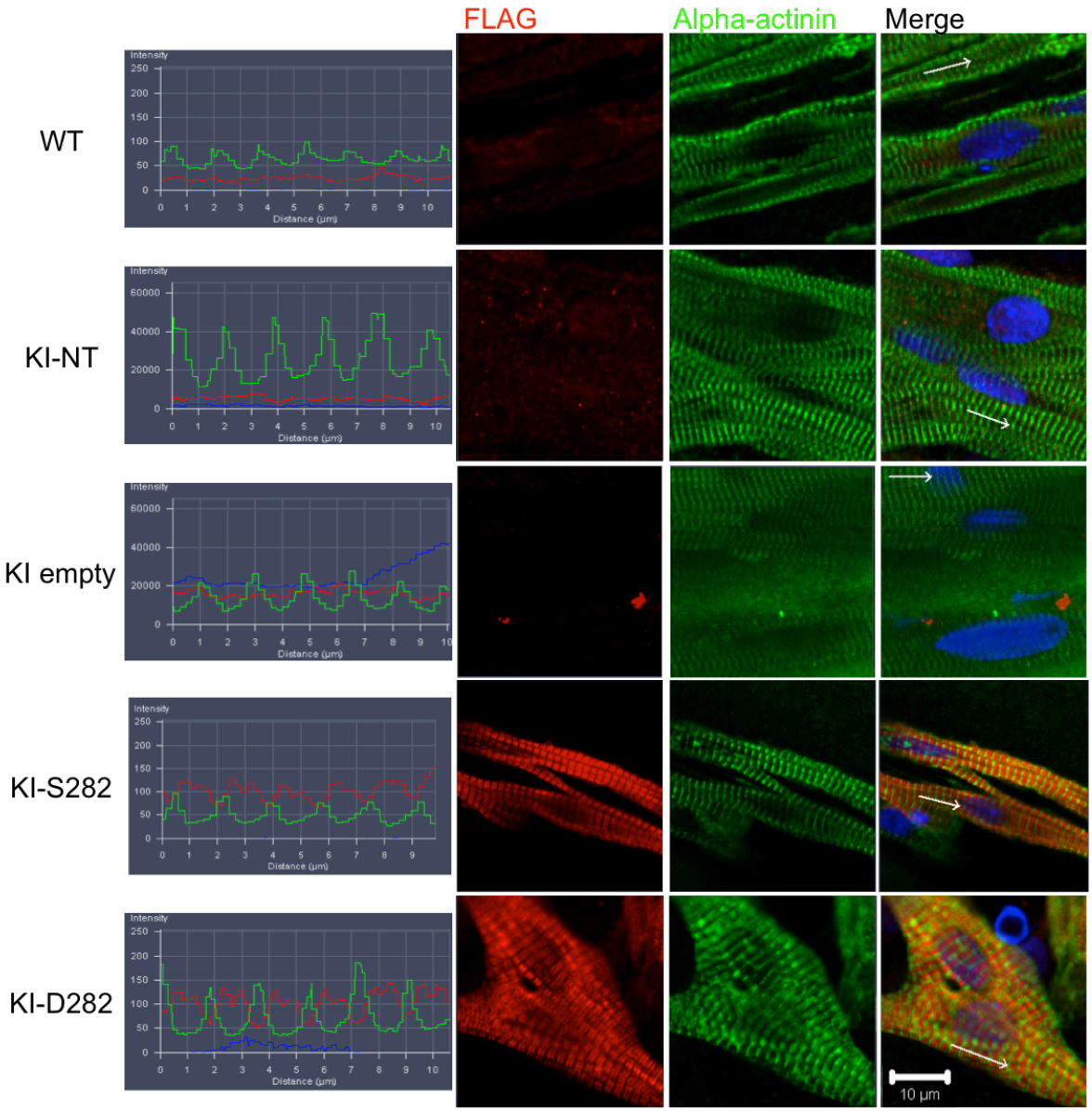

Figure 46: Localization of FLAG-cMyBP-C in EHTs. Immunoflourescence pictures of EHTs from the different groups. Antibodies directed against the FLAG-tag for exogenous cMyBP-C (red) and α-actinin for Z-disc (green) staining were used. Nuclei were stained with DRAQ 5 (blue). Flourescence profiles (left panel) show alternation of cMyBP-C (red lines) and α-actinin (green lines). White arrow indicates the place, where fluorescence profiles were taken. WT, wild-type; KI, knock-in; NT, non-transduced.

To verify the colocalization of exogenous and endogenous cMyBP-C protein, KI-S282 and KI-D282 were costained with antibodies directed against the Mybpc-Motif and the FLAG epitope. For both KI-S282 and KI-D282 the two signals were observed at the same place, showing the colocalization (Figure 47).

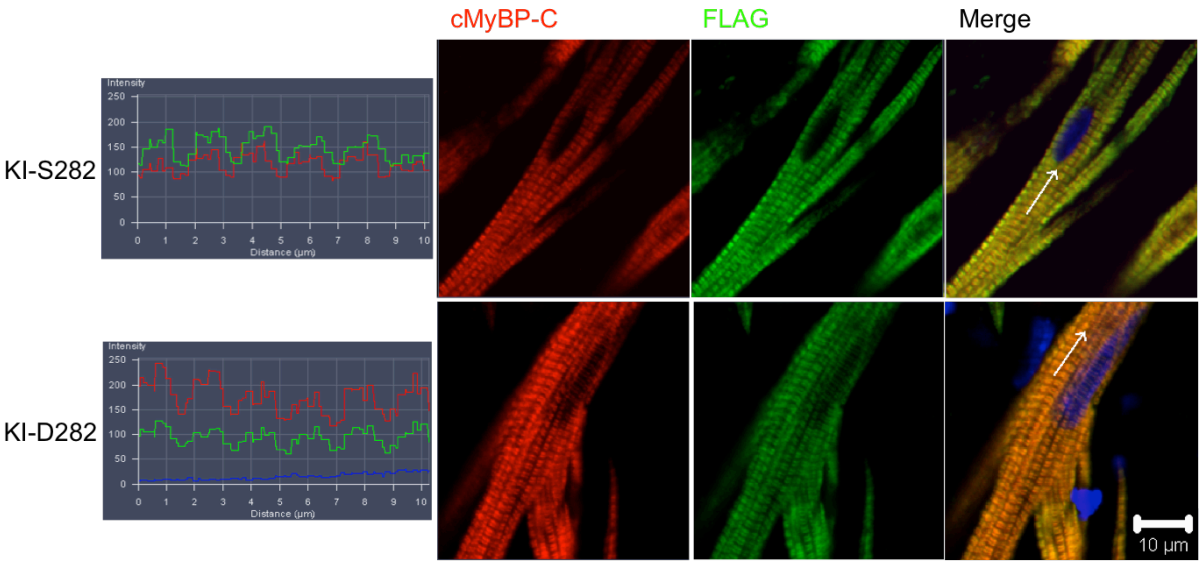

Figure 47: Colocalization of endogenous and exogenous cMyBP-C in KI-S282 and KI-D282. Immunoflourescence pictures of EHTs from the different groups. Antibodies directed against the Mybpc-Motif for total cMyBP-C (red) and α-actinin for Z-disc (green) staining were used. Nuclei were stained with DRAQ 5 (blue). Flourescence profiles (left panel) show parralelism of cMyBP-C (red lines) and FLAG epitope (green lines). White arrow indicates the place, where fluorescence profiles were taken. WT, wild-type; KI, knock-in; NT, non-transduced.

4 Discussion

The first description of the familial form of HCM was made by Teare (Teare 1958). The discovery of the main protein (cMyBP-C) that is responsible (if abnormal) for the onset of HCM followed (Offer et al. 1973). The first characterization of the genomic localization of the *MYBPC3* gene on chromosome 11 was done in 1995 (Gautel et al. 1995), immediately after it was reported to be a novel locus for the onset of HCM (Carrier et al. 1993). The whole *MYBPC3* DNA-sequence was characterized in 1997 by Lucie Carrier and colleagues (Carrier et al. 1997). Until today a great progress has been done in investigation and treatment of HCM. To date at least 19 genes are known to cause HCM if they are affected (Schlossarek et al. 2011). Among them, as stated above, the *MYBPC3* is the major affected gene. Thus it became clear that this "root of all evil" for the disease would be one of the main targets of investigations. In the clinical daily routine a causal therapy for the disease is still missing (Authors/Task Force et al. 2014). The way towards a causal therapy for HCM might be paved (Merkulov et al. 2012, Mearini et al. 2014). The approach via conventional gene therapy by Mearini and colleagues could give rise to a larger patient population since the transfer of the whole gene was performed into homozygous *Mypbc3* KI-mice, displaying a HCM phenotype. Merkulov and colleagues also report successful gene transfer of cMyBP-C via lentiviral-driven transduction of cardiomyocytes *in vivo*. In contrast to Mearini et al. they used mice completely lacking cMyBP-C, which does not represent the HCM phenotype in detail.

It remained unclear so far, whether gene therapy of constitutively phosphorylated cMyBP-C would also lead to a rescue of HCM affected individuals. The role of phosphorylation in cMyBP-C has been studied to a great extent. Phosphorylation was shown to be essential for maintaining a proper cardiac function, even at rest (Barefield and Sadayappan 2010, James and Robbins 2011, Bardswell et al. 2012, Sadayappan and de Tombe 2012). Additionally phosphorylation was shown to be cardioprotective (Sadayappan et al. 2006) and stabilizes cMyBP-C, protecting it from degradation (Barefield and Sadayappan 2010).

Therefore, the goal of this work was to study the effect and feasibility of gene therapy with a constitutively phosphorylated cMyBP-C (Ser-282) in an *in vitro*-model. The established model of EHTs was chosen (Hansen et al. 2010, Stohr et al. 2013). They

were based on murine cardiomyocytes, extracted from homozygous *Mybpc3* KI mice carrying a frequent human mutation for HCM (Girolami et al. 2006).
The main findings of this work are as follows:

1. The contractile parameters of EHTs were significantly different under electrical pacing (6 Hz) but did not differ in spontaneous contraction.
    a. Under pacing KI showed a hypercontractile phenotype. This was corrected by AAV-mediated transduction of WT (S282) or D282
    b. KI had a higher sensitivity towards external [Ca^{2+}] compared to WT. This was also corrected towards WT sensitivity by transduction of either S282 or D282.
    c. KI showed a blunted response towards the application of isoprenaline or EMD under pacing. KI-S282 and KI-D282 behaved in the same way like WT.
    d. Pacing of EHTs in many cases lead to arrhythmic contraction patterns.
2. KI-S282 and KI-D282 showed a 5-10-fold increase in total and WT *Mybpc3* mRNA levels and restored levels of full-length cMyBP-C protein
    a. The accumulation of mutant mRNAs in KI-S282 and KI-D282 was prevented by gene therapy.
    b. Exogenous cMyBP-C was properly incorporated into the sarcomere and showed colocalization with endogenous cMyBP-C.

4.1 Mouse-EHTs – a relatively young model

The first model of EHT was described by Eschenhagen and colleagues (Eschenhagen et al. 1997). Since then, the principle of cardiac tissue engineering has been improved over the years with many different approaches that were tried (Hirt et al. 2014). The established technology in our Department of Experimental Pharmacology and Toxicology is a fibrin-based mini format of cardiac tissue, which was elaborated especially for rat cardiomyocytes (Hansen et al. 2010). Since Yamanaka was able to show the generation of induced-pluripotent stem cells (iPSC) in 2007 (Okita et al. 2007), the focus will be set more on the investigation of iPSC-derived cardiomyocytes. However, not much investigation was performed using mouse EHTs in the past. Two different approaches were published recently (de

Lange et al. 2011, Stohr et al. 2013) using mouse Engineered Cardiac Tissue (ECTs) or EHTs, respectively, of which the latter ones were generated in our Department.

That was the basis for this work, following the established protocol for casting and culturing of mouse EHTs. Nevertheless some details were still not certainly defined concerning the handling of mouse EHTs. Especially in the beginning, although following the protocol, EHTs did not develop forces that were measured previously (Stohr et al. 2013). A weakness of the established protocol might be, that in none of the cases the amount of cardiomyocytes was determined, e.g. by FACS analysis. Admittedly this seems to be quite challenging during the process of EHT production. Although cardiac cell numbers were counted, the assumption may be suggested, that the number of cardiomyocytes from preparation to preparation of EHTs heavily differed. This can be due to any step of the cardiomyocyte isolation. Nonetheless the experiments were all performed under the same conditions. This reduced the variability of the different batches only to the fact of potentially different numbers of cardiomyocytes. During the period of culture, it became clear that not all EHTs developed in the same way. Therefore all EHTs, that did not develop measurable forces, were not mentioned in the analysis. Additionally, a clear cut-off point was set for the EHTs. Overall the forces of mouse EHTs were lower than in rat or iPSC-derived EHTs. Too low forces due to incoherent contraction patterns were also not mentioned. Since the development of the EHTs was different, the contractile parameters on the day of highest force development were shown. Then forces obtained under spontaneous contractions were almost comparable to those from 2013 (Stohr et al. 2013). Nonetheless they remained quite low. Higher forces would most likely reveal effects more easily, but the video-optical recording system also has its limitations, in terms of figure recognition. It needs to be mentioned, however, that in at least one batch of WT EHTs, no force was measurable at all. The reasons remain unclear.

Even more difficult in handling were WT EHTs derived from mice on the C57BL/6J genetic background. They did not develop forces three times in a row (data not shown, Paul Wijnker). This is a critical point in the assessment of the EHTs that did beat. Since reasons for the lack of contractions are not known, casting of mouse EHTs always implicates a risk of an unknown outcome. Better force developments

could be obtained by elaborated standards of the protocol with (1) validation of the amount of cardiomyocytes among the cardiac cells after extraction from murine hearts and (2) a higher predictability of the development of EHTs in culture, which will be indeed not easy to achieve. If this can be managed, mouse EHTs are, besides the iPSC-derived EHTs a very interesting model for investigation. Genetic engineering in mice is a standard method for years and is still cheaper and less complex than iPSC handling.

4.2 Hypercontractile HCM-phenotype of KI-EHTs

It was known that both *Mybpc3*-targeted KI and KO mouse EHTs showed a hypercontractile phenotype compared to WT mice, displayed by a higher force development under spontaneous contractions (Stohr et al. 2013, Mearini et al. 2014, Wijnker et al. 2016). In the present work this was not visible under spontaneous contractions. Forces between the different groups did unexpectedly not differ and were all around 0.040 mN. No correction of the KI-phenotype was observed in the KI-S282 and KI-D282 under these conditions. CV and RV did also not reveal the hypercontractile phenotype, but only showed a tendency. The trend in CV was underlined by a shorter $T1_{20}$ in KI-NT and KI empty compared to WT. And additionally the frequency of the KI-NT was higher than in WT EHTs. A clear evidence for the hypercontractile phenotype of the KI-NT was only revealed when EHTs were electrically paced. Since the frequencies between different EHTs were extremely different under spontaneous contractions (range from 58 to 352 bpm) they were subjected to electrical pacing at 6 Hz. An overpacing of the intrinsic frequency for EHTs was needed. At lower frequencies (4 Hz) not all EHTs were properly following the pacing rhythm (data not shown). The evidence for hypercontractility only under pacing is in contrast to what was previously shown in our Department (Stohr et al. 2013), but is in line with what was shown by de Lange in KO ECTs (de Lange et al. 2011). The KI-NT EHTs (and KI empty) clearly display the hypercontractility in terms of force, CV and RV compared to the WT. It can even be seen at different external $[Ca^{2+}]$. *In vitro,* under normal conditions, the KI-NT reflected the situation that can be seen in HCM patients. Some patients show strong symptoms and some live unaffected by the disease. That's why this model seems inappropriate at first sight, but is actually quite close to real situation. Especially these patients, missing any symptoms and without knowledge of their disease, are the critical mass. Under

stress, the devastating consequence, sudden cardiac death, can appear (Spinney 2004). The HCM phenotype was present in the KI-NT, but only revealed under acute challenging conditions, such as electrical pacing. It should be noted, however, that the results obtained by pacing need to be critically assessed. Many EHTs were removed from the analysis (independent from treatment) since they were not capable to follow the experimental procedure of electrical stimulation. This seems to support the hypothesis of a general variability in mouse EHTs.

4.2.1 Feasibility of AAV6-mediated gene therapy in EHTs

AAV6 transduction of EHTs was performed according to previous work (Friedrich et al. 2012, Crocini et al. 2013, Mearini et al. 2014, Wijnker et al. 2016), in which cardiac cells were transduced, before they were casted into the EHT format (MOI of 1000 for each virus). An adequate virus titer is mandatory, because a small titer enables few experiments only and requires the production of new virus creating a new experimental variable. AAV6 was shown to efficiently transduce cardiac cells that were used for EHT generation (Friedrich et al. 2012, Mearini et al. 2014, Wijnker et al. 2016). Based on the observations, promoter and vector backbone of the construct were the same (Mearini et al. 2014). The empty virus, used in this work, however, is an exception. Instead of the *TNNT2* promoter, it contained a CMV promoter and no functional gene downstream. This was chosen to investigate the virus toxicity effect itself. Although the promoters were different, the virus properties were the same. It was previously shown that rat EHTs transduced with this empty control virus did not differ from the non-transduced control group (Simon Braumann, unpublished data).

Although no impairment on the appearance or on the physiological function was observed by the transduction with the virus itself, in KO EHTs an MOI of 300 already lead to cMyBP-C levels comparable to those in WT (Wijnker et al. 2016). It remains unclear, however, whether this MOI would also be sufficient for gene therapy in KI cardiomyocytes. In contrast to KO, KI cardiomyocytes do not completely lack cMyBP-C (Carrier et al. 2004) but still contain about 10% in the homozygous state (Vignier et al. 2009). Additionally, there are mutant proteins expressed that might have a harmful effect in the KI. These are obviously missing in the KO. A proof in the KI with a titration between MOI of 300 to 1000 as a sufficient MOI is still missing but would be an attractive investigation, since virus and money could be saved using a lower MOI.

4.2.2 Rescue of the hypercontractile phenotype in KI-EHTs

No correction of the KI phenotype was visible under spontaneous contraction in KI-S282 and KI-D282. This was unexpected because a rescue of this phenotype was already shown by transduction of KI-EHTs with full-length WT *Mybpc3* at an MOI of 1000 (Mearini et al. 2014). Nevertheless, the phenotype of the different groups might have been masked under spontaneous contractions and was revealed by electrical pacing. Herein a prevention of the hypercontractile phenotype of KI EHTs towards a WT phenotype was achieved in the KI-S282 EHTs. This was in line with the results obtained from KI mice treated with different doses of AAV9 encoding full-length cMyBP-C (Mearini et al. 2014). The KI-D282 also showed a tendency towards lower contractile parameters, but were intermediate the KI-NT and WT.

Myofilament [Ca^{2+}] sensitivity is a characteristic parameter that is increased in HCM, especially in cases of cardiac troponin I and T and α-tropomyosin mutations (reviewed in Hernandez et al. 2001). But a lack of cMyBP-C was also shown to cause a higher myofilament [Ca^{2+}] sensitivity (van Dijk et al. 2012). This was also observed in the *Mybpc3*-targeted KI model (Fraysse et al. 2012). Sensitivity towards external [Ca^{2+}] was already assessed in both KI-NT and WT EHTs. EC_{50} were 0.34 mM for KI and 0.66 mM for WT (Stohr et al. 2013). In the present work, EC_{50} were 0.28 mM and 0.39 mM for KI-NT and WT, respectively. This might be due to a different experimental setup, although mice were bred from the same genetic background.

In another study [Ca^{2+}] sensitivity was determined comparing mouse, rat and human WT EHTs (Stoehr et al. 2014). Herein the EC_{50} for mouse EHTs was determined as 0.39 mM. The EC_{50} for WT in this work matched the value published in 2014. No matching values were obtained in the KI-NT, however. Nevertheless, in the present work, the KI-NT revealed an increased sensitivity towards external [Ca^{2+}], which was corrected in the KI-S282 (EC_{50}= 0.40 mM).

The effect of phosphorylation of cMyBP-C on myofilament [Ca^{2+}] sensitivity is controversially discussed in the literature (Barefield and Sadayappan 2010, Bardswell et al. 2012, Kuster et al. 2012, Sequeira et al. 2014). In the present study KI-D282 showed a slightly lower sensitivity to external [Ca^{2+}] than the KI-NT (EC_{50}=

0.32 mM). This argues for a role of cMyBP-C in regulation of calcium sensitivity, but not uniquely mediated by it, like shown elsewhere (Chen et al. 2010). However in the present work, an indirect stimulation with PKA was only achieved by administration of isoprenaline, since EHTs were not skinned. Side effects of mutant proteins, that might be still existent in this background, could not be excluded, because they remain undetectable. In addition to that, the influence of cTnI and the interaction between cMyBP-C and cTnI and other contractile proteins in this model remains unclear. Especially an investigation on these interactions would shed more light on the regulatory function of cMyBP-C (and phospho-cMyBP-C) in [Ca^{2+}] sensitivity of the cell.

Pacing revealed the important difference between the different genotypes, such as the hypercontractility of KI-NT and so should the exposition to drugs. The administration of isoprenaline (final concentration 100 nM, according to Stohr et al. 2013) lead to arrhythmias in many EHTs, though, preventing the potential analysis of the data. None of the groups was preferably affected. Only the KI-S282 seemed to be resistant towards arrhythmias at least for 15 min after subjection to isoprenaline. The evaluable numbers of EHTs reduced to a minimum of two per group (except KI-S282) after 15 min but still showed the expected tendencies of an increase of force. In KI-NT (and KI empty) the effect of isoprenaline was blunted whereas in the WT and its correlate, the KI-S282, isoprenaline mediated a positive inotropic and lusitropic effect. The absolute increase in force in KI-D282 was comparable with the increase observed in WT and thus can be seen as a successful prevention of the KI phenotype. In general these data confirm the role of cMyBP-C as a mediator of contraction and relaxation, which is regulated upon phosphorylation. Most likely a greater effect on contractility is mediated with transduction of constitutively phosphorylated cMyBP-C into KI, but this needs to be proven in larger numbers of EHTs. At least a clear tendency was visible.

The drug therapy of HCM includes calcium antagonists such as verapamil, as calcium sensitivity is increased in HCM affected individuals. As an indirect proof for increased sensitivity towards external calcium, EHTs were subjected to the calcium sensitizer EMD 57033 (final concentration 10 µM, according to Stohr et al. 2013) to unmask the different phenotypes. As shown by A. Stoehr, the response was less

pronounced in every group compared to the response to isoprenaline. Clear effects, however, on the force in terms of positive inotropy were only observed in WT and KI-S282. KI-NT, KI-D282 and KI empty showed a blunted response towards the positive inotropic effect mediated by EMD. The increase in force in WT and KI-S282 and the lack of increase in force in KI-NT, KI-D282 and KI empty (after EMD 57033 administration maximal forces almost equalized to the same level (~ 0.025 – 0.03 mN)) confirmed the assumption of a higher [Ca^{2+}] sensitivity in the KI. Otherwise a marked increase in force would have been expected after EMD 57033 administration to the KI-NT. Interestingly the KI-NT showed prolonged times of contraction and relaxation as well as the KI-S282, which was not visible in the corresponding velocities. Only WT EHTs showed increased kinetics. These data suggest that EMD mediates different effects in the different groups according to their properties. Unexplainable remains the influence of EMD in KI-NT with regards to the impact of the different mutant proteins that might be affected in different ways by EMD.

Other alterations within the KI phenotype are molecular changes. It was known that KI mice showed lower levels of both *Mybpc3* mRNA and cMyBP-C protein than WT (Vignier et al. 2009, Fraysse et al. 2012). In this work, in both KI-S282 and KI-D282 a strong increase in both total and WT *Mybpc3* mRNA levels over the WT was observed. Total *Mybpc3* mRNA levels remained low in KI-NT (25% of WT level) and KI empty (data not shown). The cMyBP-C protein levels in both KI-S282 and KI-D282 did not differ from the WT, whereas low levels of cMyBP-C were found in the KI-NT and KI empty (20% and 24% of WT level, respectively). This argues for a successful prevention and a rescue of the molecular KI phenotype in both KI-S282 and KI-D282. In terms of cMyBP-C protein not only a restoration of normal cMyBP-C back to WT levels, but also the inhibiton of the presence of mutant or toxic proteins that are present in the KI-NT, might be achieved. A verification of this hypothesis is not possible, though, since the mutant proteins were not detectable.

Surprisingly there is a discrepancy between mRNA levels and the resulting protein levels. Several explanations may be possible. mRNA underlies a very quick turnover. After the translation into proteins, these are much more long-lasting in the cell as they fulfill structural tasks. Therefore the extraction of RNA from cells within a phase of a high production can distort the result. But since the RNA was that much higher

detectable in this work in the different groups, this seems unlikely. Most likely, within the process after transcription, until translation into the protein or even beyond the protein translation there may be machineries of the cell involved in preventing an overproduction. Especially the sarcomere requires a control element, because its stoichiometry underlies a tight regulation (reviewed in Schlossarek et al. 2011). This might be heavily disturbed in the KI-NT, due to the little amount of cMyBP-C. In this work, the exogenous protein was found properly incorporated into the sarcomere in cardiomyocytes, respecting the stoichiometry. This was proven by the immunofluorescence analysis with different stainings either for total, exogenous cMyBP-C or both. In line with previous results, the different mutant *Mybpc3* mRNAs were not or hardly detectable with RT-PCR or qPCR in the KI-S282 and KI-D282, suggesting that gene transfer not only rescued the deficiency of WT cMyBP-C but also prevented accumulation of likely toxic mutant *Mybpc3* mRNA (Mearini et al. 2014). Thus a preference for the transcription of the transgene and its translation into functional protein revealed by *Mybpc3* gene therapy.

Further confirmation for a prevention of the hypercontractile phenotype was obtained by analysis of markers of the fetal gene program. In hypertrophic cardiac tissue these are known to be upregulated, as a kind of compensatory mechanism due to increased stress levels. Especially in the KI mice some of these markers (*Acta1*, *Myh7*, *NppA*) were shown to be upregulated (Vignier et al. 2009, Stohr et al. 2013). In the present study, in the KI-S282 and KI-D282 the markers did not differ from the WT, particularly for *Acta1* and *Myh7*. In both cases there was even slightly less mRNA detectable in the total RNA pools of KI-D282 than in the WT.

4.2.3 Impact of constitutive phosphorylation *in vitro*

The focus of this work was set on gene therapy of the HCM phenotype in KI EHTs in general, but particularly using a consitutively phosphorylated cMyBP-C (D282) due to its beneficial effects on cardiac function (Sadayappan et al. 2006, Sadayappan et al. 2011, Gupta et al. 2013). Phosphorylation of the Mybpc-Motif serines of cMyBP-C is known to abolish its break function on the actin-myosin interaction (Schlossarek et al. 2011). Interestingly the KI-S282 had an advantage over the KI-D282 *in vitro*. Herein the correction of the hypercontractile phenotype towards the WT was much more efficient. Certainly the cardiac performance is overall bad in HCM patients, especially

in the neonatal forms with severe presentations (Xin et al. 2007, Wessels et al. 2015). To improve the output as well as a facilitation of the relaxation of the heart, a prior phosphorylated cMyBP-C would have an invaluable advantage over the WT. Although mice with a constitutively phosphorylated cMyBP-C (D282) did not differ from WT mice in terms of their cardiac performance measured by echocardiography under basal conditions (Gupta et al. 2013), evidence is given that under β-adrenergic stimulation a lack of the opportunity for phosphorylation leads to a poorer cardiac performance (Gresham et al. 2014). It should be noted that these results were obtained in transgenic mice bred from a null background (cMyBP-$C^{-/-}$). In our KI-model, 10 % of WT cMyBP-C are still detectable by Western Blot (Vignier et al. 2009).

Hints for a better performance on force development under β-adrenergic stimulation were given in this work by the subjection of EHTs to isoprenaline under pacing conditions. Here the KI-D282 exhibited a stronger response to isoprenaline than KI-S282 (at least a trend), which may reflect the situation *in vivo*. It remains to be investigated how cardiac performance will develop in mice that received gene therapy with constitutively phosphorylated cMyBP-C. Therefore a valid comparison of the different treatment strategies (either transduction of KI-S282 or KI-D282) would be more appropriate *in vivo* only.

4.3 Role of M-Motif serine 282: trigger or serine as any other?

The phosphorylation of cMyBP-C has been the focus of many investigations in the past. Its importance for cardiac performance was shown by several groups. It is known that the phosphorylation of cMyBP-C is cardioprotective, in terms of ischemic reperfusion injury. Dephosphorylation of cMyBP-C induces its cleavage (Govindan et al. 2013). Recently another kinase, the glycogen synthase kinase 3β (GSK3β), was identified to phosphorylate a serine residue (Ser-131) in the Pro-Ala-rich region upstream of the M-Motif with an influence on the contractility of the filaments (Kuster et al. 2013). For phosphorylation sites and other posttranslational modifications on cMyBP-C see Figure 7.

The majority of kinases act on the M-Motif, which underlines its relevance. Indeed most target the main serine (Ser-282), except PKD. The function of the different serine residues and their impact in terms of a hierarchy are controversially discussed (Gresham et al. 2014, Gupta and Robbins 2014). Especially the Ser-282 has been evoked as the serine residue with the main position in the M-Motif (Gautel et al. 1995). However, the importance of the phosphorylation of all M-Motif serines together should not be neglected (Ser-273, Ser-282, Ser-302 and Ser-307). To investigate a potential impact of constitutive phosphorylation of Ser-282 on the remaining M-Motif serines, proteins were extracted from EHTs. WT and KI-S282 showed an increase in protein phosphorylation upon isoprenaline treatment for all serine residues, suggesting no major difference between those two groups. In the KI-NT and KI empty the baseline phosphorylation was already higher compared to the baseline phosphorylation of KI-S282 and WT for each serine. Even after subjection to isoprenaline the phosphorylation of cMyBP-C remained incomplete in these groups. It should be noted that not only the amount of WT protein is lower in KI-NT, but also the relative serine phosphorylation (Ser-282) is much lower than in WT (Fraysse et al. 2012). As expected no signal was measured for Ser-282 phosphorylation in the KI-D282 and only small changes compared to baseline were observed for both Ser-273 and Ser-302 phosphorylation. At least for Ser-282 this was not surprising, because the epitope of the antibody (usually recognizing pSer-282) was changed to Asp-282. This is an indirect proof, besides the other proofs given in this work, for a successful exchange of the amino acids. However, the lack of an increase in phosphorylation of Ser-273 and Ser-302 was not expected for KI-D282, since even phosphorylation of Ser-282 was shown to facilitate the phosphorylation of at least Ser-273 (Gupta et al. 2013). A recently published work showed that the presence of Ser-282 is not mandatory for the phosphorylation of Ser-273 or Ser-302 (Gresham et al. 2014). In a non-phosphorylatable Ala-282 mutant, the levels of phosphorylated Ser-273 or Ser-302 did not differ from WT controls after PKA stimulation. This argues strongly against the hypothesis of an outstanding role of Ser-282.

It remains unexplainable why in the KI-D282 less phosphorylation of Ser-302 was observed compared to WT and KI-S282 although phosphorylation should enable a facilitation for phosphorylation of the remaining serines.

In this work isoprenaline as a β-adrenergic agonist was used to induce phosphorylation of the serines via PKA activation. But there are also other kinases that mediate an effect on the M-Motif. Thus isoprenaline might not show the whole extent of serine interaction upon phosphorylation. Additionally a weak point in this work is the Western Blot analysis on Ser-273 phosphorylation. The signals were almost indistinguishable from the background signal and therefore the quantification with the software was not possible. Furthermore, the number of analyzed samples was too low to draw sustainable conclusions. Nevertheless tendencies were visible. These are merely hints that need to be confirmed with further experiments.

4.4 From bench to bedside – HCM gene therapy in humans

The way towards clinical application of gene therapy has become reality with the approval of Glybera in 2012 (Pleger et al. 2013). The knowledge about diseases and their causes gives rise to the opportunity for causal therapies. It should be noted however, that conventional gene therapy might not be feasible for every protein of interest (Zhu et al. 2001). Here the overexpression of a WT protein was even associated with a worse phenotype in mice.

Since cardiovascular diseases are still the main cause of death in the industrial countries (Figure 1), the treatment of cardiac diseases does not only have social but also economical implications. A milestone on the way of a causal treatment for an inherited cardiac disease was the work of our group (Mearini et al. 2014). For the first time a feasible strategy for the prevention of HCM was performed in mice. Homozygous KI mice were treated with AAV9 at different doses and followed up over a period of 34 weeks. KI mice that received a dose at the age of 1 day of AAV9 with WT *Mybpc3* DNA did significantly profit from the treatment, in terms of cardiac performance and molecular changes (mRNA, protein levels). In the same study data are included that were obtained from AAV6 transduced KI EHTs.
The present work provides a proof of principle for this treatment of KI EHTs. Both KI-S282 and KI-D282 were able to prevent the KI phenotype. In both cases and studies the onset of the disease was successfully prevented both in EHTs and in mice, independent from the treatment. This gives rise to the potential treatment of severe neonatal forms of HCM that still have a bad outcome and no treatment, except heart

transplantation (Lekanne Deprez et al. 2006, Xin et al. 2007). Both studies, however, do not include the majority of patients in which the disease is already present, namely adults. It is not clear whether these patients would also profit from gene therapy, particularly those, in which structural changes of the heart are already present.

4.5 Conclusion and future directions

This work was stringently performed following the example of previous studies on conventional gene therapy. Here the aim was to test the effect of constitutively phosphorylated cMyBP-C in a KI background and to rule out potential advantages and disadvantages compared to the effect of WT cMyBP-C transduction into a KI background. This work provides insight into the functional role of constitutively phosphorylated cMyBP-C in HCM. The beneficial effects for cardiac contractility parameters were present both in transduced WT cMyBP-C and transduced phosphorylated cMyBP-C. However, the performance of phosphorylated cMyBP-C was weaker than WT cMyBP-C. Nevertheless, the EHTs are an *in vitro* model and every model has its weaknesses. Additionally, there are indications that make it even more interesting to study the transduction of constitutively phosphorylated cMyBP-C as a treatment strategy, such as its cardioprotective effect, the tendency of less cleavage and its beneficial impact on contractility (Sadayappan et al. 2006).
Therefore the effect of constitutive phosphorylation in a model that is either closer to the human situation, such as human EHTs derived from iPS cells or an *in vivo* model should be used in the future. Some *in vivo* models do already exist for experiments, such as the KI mouse of our group (Vignier et al. 2009). Large animal models, such as sheep or pigs would be even closer to the human situation, but are quite challenging in genetic engineering. The first spontaneous large animal model known to date is the Maine Coon cat (Meurs et al. 2005). These cats give the opportunity to relinquish genetic engineering, because sick individuals can be bred from the natural mutation carrier. Nevertheless, costs for keeping of animals is much higher for large animals compared to small animals. To achieve a transfer to the clinics, work in large animals is mandatory, though. In parallel to gene therapy, using the WT, the constitutively phosphorylated (D282) could be tested then, to reveal the effect potential advantages *in vivo*.

5 Zusammenfassung

Die hypertrophische Kardiomyopathie (HCM) ist die häufigiste genetisch bedingte kardiale Erkrankung (Prävalenz 1:500), charakterisiert durch eine linksventrikuläre Hypertrophie, eine diastolische Dysfunktion sowie durch eine ungeordnete myokardiale Struktur. Das *MYBPC3* Gen ist das am häufigsten betroffene Gen. Die meisten Mutationen führen zu einem *frameshift* auf mRNA-Ebene und folglich zu einem vorzeitigen Stoppcodon, was zu der Expression von verkürzten oder trunkierten cMyBP-C Proteinen führt. Der Mangel an normalem cMyBP-C Protein bzw. das Vorkommen potenziell schädlicher trunkierter Formen ist grundlegend für die Entstehung der HCM. cMyBP-C ist das Ziel einer Vielzahl von unterschiedlichen Formen der posttranslationalen Modifikation, unter anderem der Phosphorylierung. Es konnte gezeigt werden, dass vor allem die Phosphorylierung vom Ser-282 im M-Motif des cMyBP-C sich sowohl kardioprotektiv als auch grundsätzlich positiv für die Funktion des Herzens auswirkt.

In der vorliegenden Arbeit sollte der Fokus auf eine Form der molekularen Therapie (Gentherapie) in dem *in vitro* Modell engineered heart tissue (EHT) gelegt werden. Die Fragestellung der vorliegenden Arbeit war, ob es einen Unterschied bezüglich der Gentherapie durch Transduktion von KI-EHTs mittels WT cMyBP-C (S282) oder konstitutiv phosphoryliertem cMyBP-C Protein (D282) gibt und welche der Formen geeigneter als Therapie ist.

Kardiale Zellen, für die Generierung von EHTs, wurden sowohl von *Mybpc3*-knock-in (KI) Mäusen, welche eine beim Menschen häufig auftretende HCM Mutation tragen und von WT Mäusen gewonnen. KI Mäuse zeigen typische Charakteristika der Erkrankung, wie etwa kardiale Hypertrophie sowie eine systolische als auch eine diastolische Dysfunktion.

Eine Behebung des hyperkontraktilen Phänotyps von KI-EHTs (höhere Werte für Kraft sowie Geschwindigkeit von Kontraktion und Relaxation) in den transduzierten EHTs (entweder WT (S282) oder konstitutiv phosphorylierter WT (D282)) war nur unter elektrischer Stimulation (6 Hz) sichtbar (folglich reduzierte Werte für Kraft und Geschwindigkeiten), nicht jedoch bei spontaner Kontraktion der EHTs. Eine leichte Rechtsverschiebung der Sensitivität gegenüber externem [Ca^{2+}] in den D282 EHTs

konnte im Vergleich zu den KI-NT beobachtet werden. In den S282 EHTs hingegen war eine komplette Verschiebung bis hin zur WT Sensitivität sichtbar. Sowohl D282, als auch S282 EHTs zeigten einen Kraftzuwachs, wie bereits aus WT Daten zu erwarten, nach der Applikation des β-adrenergen Agonisten Isoprenalin und der calciumsensitivierenden Susbtanz EMD 57033. KI-NT hingegen zeigten einen abgestumpften Effekt nach der Applikation. In D282 und S282 EHTs konnte zudem die Akkumulation von mRNA Mutanten, welche in den KI EHTs/Mäusen zum Tragen kommt, verhindert werden und außerdem die cMyBP-C Proteinmenge der Menge vom WT angeglichen werden. Immunofloureszenzanalysen bestätigten die korrekte Inkorporation der exogenen Proteine in den Sarkomer.

Beide Formen der Therapie waren geeignet die Ausprägung des KI-Phänotyps zu verhindern und diesen somit zu retten. *In vitro* zeigte sich S282 als der, in den getesteten Bedingungen, dem D282 als überlegen. Um allerdings den Effekt von konstitutiver Phosphorylierung zu bestätigen und weitere Unterschiede zwischen den beiden Therapieformen herauszuarbeiten, sind weitere Studien, v.a. *in vivo,* unerlässlich. Dafür hat die diese Arbeit den Grundstein gelegt.

6 Summary

Hypertrophic cardiomyopathy (HCM) is the most common inherited disease of the heart (1:500), characterized by a left ventricular hypertrophy, diastolic dysfunction and a disarray of the myocardium. *MYBPC3* is the major affected gene. Most of the *MYBPC3* mutations lead to a frameshift on mRNA level and result in a premature terminal codon, producing a truncated cMyBP-C protein. The lack of cMyBP-C protein and/or presence of poison polypeptides is thought to be causative for the onset and the progression of HCM. cMyBP-C is a target for many forms of posttranslational modifications, such as phosphorylation. Phosphorylation of Ser-282 in the Mybpc-Motif of the cMyBP-C protein is known to be cardioprotective and beneficial for the function of the heart.

In the present work the focus was set on a molecular therapy (gene therapy) of the disease in the *in vitro* model of engineered heart tissues (EHTs). The main question to address in this thesis was whether there is a difference in gene therapy of KI-EHTs using either WT cMyBP-C (S282) or constitutively phosphorylated WT cMyBP-C (D282) as a treatment of HCM. Cardiac cells for EHT generation were obtained from both *Mybpc3*-targeted knock-in (KI) mice, carrying one of the most frequent mutation for HCM found in humans, and WT mice. KI mice display typical features of HCM, such as hypertrophy and both systolic and diastolic dysfunction.

A rescue of the hypercontractile phenotype of KI-EHTs (accelerated contractile parameters (force, velocities of contraction and relaxation)) in the transduced EHTs (using either WT (S282) or constitutively phosphorylated WT (D282)) was only visible under subjection of EHTs to electrical pacing (6 Hz), but not under spontaneous contractions, showing lower forces and velocities of contraction and relaxation. A slight shift towards higher sensitivity for external [Ca^{2+}] was observed in the D282 compared to the KI-NT. A full shift towards WT sensitivity was observed in the S282. D282 and S282 both showed an increase in force, as observed in the WT, according to the application of the β-adrenergic agonist isoprenaline and the calcium sensitizer EMD 57033. Almost no response was seen in the KI-NT only. In both D282 and S282 the accumulation of mutant mRNAs was prevented and cMyBP-C protein levels were restored to WT levels. Immunoflourescence analysis enabled the proof of their proper incorporation into the sarcomere.

Both treatments were able to rescue and to prevent the KI phenotype and restore contractile functions as well as molecular changes. *In vitro* S282 showed the better outcome and seemed more appropriate for further treatment investigations, however. But to reveal the effect of constitutive phosphorylation *in vivo,* further investigations are necessary. The basis was made in this thesis.

7 Literature

Abozguia, K., P. Elliott, W. McKenna, T. T. Phan, G. Nallur-Shivu, I. Ahmed, A. R. Maher, K. Kaur, J. Taylor, A. Henning, H. Ashrafian, H. Watkins and M. Frenneaux (2010). "Metabolic modulator perhexiline corrects energy deficiency and improves exercise capacity in symptomatic hypertrophic cardiomyopathy." Circulation **122**(16): 1562-1569.

Adelman, A. G., P. M. Shah, R. Gramiak and E. D. Wigle (1970). "Long-term propranolol therapy in muscular subaortic stenosis." Br Heart J **32**(6): 804-811.

Authors/Task Force, m., P. M. Elliott, A. Anastasakis, M. A. Borger, M. Borggrefe, F. Cecchi, P. Charron, A. A. Hagege, A. Lafont, G. Limongelli, H. Mahrholdt, W. J. McKenna, J. Mogensen, P. Nihoyannopoulos, S. Nistri, P. G. Pieper, B. Pieske, C. Rapezzi, F. H. Rutten, C. Tillmanns, H. Watkins and m. Authors/Task Force (2014). "2014 ESC Guidelines on diagnosis and management of hypertrophic cardiomyopathy: The Task Force for the Diagnosis and Management of Hypertrophic Cardiomyopathy of the European Society of Cardiology (ESC)." Eur Heart J.

Bardswell, S. C., F. Cuello, J. C. Kentish and M. Avkiran (2012). "cMyBP-C as a promiscuous substrate: phosphorylation by non-PKA kinases and its potential significance." J Muscle Res Cell Motil **33**(1): 53-60.

Bardswell, S. C., F. Cuello, A. J. Rowland, S. Sadayappan, J. Robbins, M. Gautel, J. W. Walker, J. C. Kentish and M. Avkiran (2010). "Distinct sarcomeric substrates are responsible for protein kinase D-mediated regulation of cardiac myofilament Ca2+ sensitivity and cross-bridge cycling." J Biol Chem **285**(8): 5674-5682.

Barefield, D. and S. Sadayappan (2010). "Phosphorylation and function of cardiac myosin binding protein-C in health and disease." J Mol Cell Cardiol **48**(5): 866-875.

Bers, D. M. (2002). "Cardiac excitation-contraction coupling." Nature **415**(6868): 198-205.

Carrier, L., G. Bonne, E. Bahrend, B. Yu, P. Richard, F. Niel, B. Hainque, C. Cruaud, F. Gary, S. Labeit, J. B. Bouhour, O. Dubourg, M. Desnos, A. A. Hagege, R. J. Trent, M. Komajda, M. Fiszman and K. Schwartz (1997). "Organization and sequence of human cardiac myosin binding protein C gene (MYBPC3) and identification of mutations predicted to produce truncated proteins in familial hypertrophic cardiomyopathy." Circ Res **80**(3): 427-434.

Carrier, L., C. Hengstenberg, J. S. Beckmann, P. Guicheney, C. Dufour, J. Bercovici, E. Dausse, I. Berebbi-Bertrand, C. Wisnewsky, D. Pulvenis and et al. (1993). "Mapping of a novel gene for familial hypertrophic cardiomyopathy to chromosome 11." Nat Genet **4**(3): 311-313.

Carrier, L., R. Knoll, N. Vignier, D. I. Keller, P. Bausero, B. Prudhon, R. Isnard, M. L. Ambroisine, M. Fiszman, J. Ross, Jr., K. Schwartz and K. R. Chien (2004). "Asymmetric septal hypertrophy in heterozygous cMyBP-C null mice." Cardiovasc Res **63**(2): 293-304.

Carrier, L., G. Mearini, K. Stathopoulou and F. Cuello (2015). "Cardiac myosin-binding protein C (MYBPC3) in cardiac pathophysiology." Gene **573**(2): 188-197.

Chen, P. P., J. R. Patel, I. N. Rybakova, J. W. Walker and R. L. Moss (2010). "Protein kinase A-induced myofilament desensitization to Ca(2+) as a result of phosphorylation of cardiac myosin-binding protein C." J Gen Physiol **136**(6): 615-627.

Crocini, C., T. Arimura, S. Reischmann, A. Eder, I. Braren, A. Hansen, T. Eschenhagen, A. Kimura and L. Carrier (2013). "Impact of ANKRD1 mutations associated with hypertrophic cardiomyopathy on contraction parameters of engineered heart tissue." Basic Res Cardiol **108**(3): 349.

Cuello, F., S. C. Bardswell, R. S. Haworth, E. Ehler, S. Sadayappan, J. C. Kentish and M. Avkiran (2011). "Novel role for p90 ribosomal S6 kinase in the regulation of cardiac myofilament phosphorylation." J Biol Chem **286**(7): 5300-5310.

Davis, J., M. V. Westfall, D. Townsend, M. Blankinship, T. J. Herron, G. Guerrero-Serna, W. Wang, E. Devaney and J. M. Metzger (2008). "Designing heart performance by gene transfer." Physiol Rev **88**(4): 1567-1651.

de Lange, W. J., L. F. Hegge, A. C. Grimes, C. W. Tong, T. M. Brost, R. L. Moss and J. C. Ralphe (2011). "Neonatal mouse-derived engineered cardiac tissue: a novel model system for studying genetic heart disease." Circ Res **109**(1): 8-19.

El-Armouche, A., L. Pohlmann, S. Schlossarek, J. Starbatty, Y. H. Yeh, S. Nattel, D. Dobrev, T. Eschenhagen and L. Carrier (2007). "Decreased phosphorylation levels of cardiac myosin-binding protein-C in human and experimental heart failure." J Mol Cell Cardiol **43**(2): 223-229.

Elliott, P., B. Andersson, E. Arbustini, Z. Bilinska, F. Cecchi, P. Charron, O. Dubourg, U. Kuhl, B. Maisch, W. J. McKenna, L. Monserrat, S. Pankuweit, C. Rapezzi, P. Seferovic, L. Tavazzi and A. Keren (2008). "Classification of the cardiomyopathies: a

position statement from the European Society Of Cardiology Working Group on Myocardial and Pericardial Diseases." Eur Heart J **29**(2): 270-276.

Elliott, P. and W. J. McKenna (2004). "Hypertrophic cardiomyopathy." Lancet **363**(9424): 1881-1891.

Eschenhagen, T., C. Fink, U. Remmers, H. Scholz, J. Wattchow, J. Weil, W. Zimmermann, H. H. Dohmen, H. Schafer, N. Bishopric, T. Wakatsuki and E. L. Elson (1997). "Three-dimensional reconstitution of embryonic cardiomyocytes in a collagen matrix: a new heart muscle model system." FASEB J **11**(8): 683-694.

Flashman, E., C. Redwood, J. Moolman-Smook and H. Watkins (2004). "Cardiac myosin binding protein C: its role in physiology and disease." Circ Res **94**(10): 1279-1289.

Fougerousse, F., A. L. Delezoide, M. Y. Fiszman, K. Schwartz, J. S. Beckmann and L. Carrier (1998). "Cardiac myosin binding protein C gene is specifically expressed in heart during murine and human development." Circ Res **82**(1): 130-133.

Fraysse, B., F. Weinberger, S. C. Bardswell, F. Cuello, N. Vignier, B. Geertz, J. Starbatty, E. Kramer, C. Coirault, T. Eschenhagen, J. C. Kentish, M. Avkiran and L. Carrier (2012). "Increased myofilament Ca2+ sensitivity and diastolic dysfunction as early consequences of Mybpc3 mutation in heterozygous knock-in mice." J Mol Cell Cardiol **52**(6): 1299-1307.

Friedrich, F. W., B. R. Wilding, S. Reischmann, C. Crocini, P. Lang, P. Charron, O. J. Muller, M. J. McGrath, I. Vollert, A. Hansen, W. A. Linke, C. Hengstenberg, G. Bonne, S. Morner, T. Wichter, H. Madeira, E. Arbustini, T. Eschenhagen, C. A. Mitchell, R. Isnard and L. Carrier (2012). "Evidence for FHL1 as a novel disease gene for isolated hypertrophic cardiomyopathy." Hum Mol Genet **21**(14): 3237-3254.

Gautel, M., O. Zuffardi, A. Freiburg and S. Labeit (1995). "Phosphorylation switches specific for the cardiac isoform of myosin binding protein-C: a modulator of cardiac contraction?" EMBO J **14**(9): 1952-1960.

Girolami, F., I. Olivotto, I. Passerini, E. Zachara, S. Nistri, F. Re, S. Fantini, K. Baldini, F. Torricelli and F. Cecchi (2006). "A molecular screening strategy based on beta-myosin heavy chain, cardiac myosin binding protein C and troponin T genes in Italian patients with hypertrophic cardiomyopathy." J Cardiovasc Med (Hagerstown) **7**(8): 601-607.

Govindan, S., D. W. Kuster, B. Lin, D. J. Kahn, W. P. Jeske, J. M. Walenga, F. Leya, D. Hoppensteadt, J. Fareed and S. Sadayappan (2013). "Increase in cardiac myosin binding protein-C plasma levels is a sensitive and cardiac-specific biomarker of myocardial infarction." Am J Cardiovasc Dis **3**(2): 60-70.

Gresham, K. S., R. Mamidi and J. E. Stelzer (2014). "The contribution of cardiac myosin binding protein-c Ser282 phosphorylation to the rate of force generation and in vivo cardiac contractility." J Physiol **592**(Pt 17): 3747-3765.

Gupta, M. K., J. Gulick, J. James, H. Osinska, J. N. Lorenz and J. Robbins (2013). "Functional dissection of myosin binding protein C phosphorylation." J Mol Cell Cardiol **64**: 39-50.

Gupta, M. K. and J. Robbins (2014). "Post-translational control of cardiac hemodynamics through myosin binding protein C." Pflugers Arch **466**(2): 231-236.

Hansen, A., A. Eder, M. Bonstrup, M. Flato, M. Mewe, S. Schaaf, B. Aksehirlioglu, A. P. Schwoerer, J. Uebeler and T. Eschenhagen (2010). "Development of a drug screening platform based on engineered heart tissue." Circ Res **107**(1): 35-44.

Harris, K. M., P. Spirito, M. S. Maron, A. G. Zenovich, F. Formisano, J. R. Lesser, S. Mackey-Bojack, W. J. Manning, J. E. Udelson and B. J. Maron (2006). "Prevalence, clinical profile, and significance of left ventricular remodeling in the end-stage phase of hypertrophic cardiomyopathy." Circulation **114**(3): 216-225.

Harris, S. P., R. G. Lyons and K. L. Bezold (2011). "In the thick of it: HCM-causing mutations in myosin binding proteins of the thick filament." Circ Res **108**(6): 751-764.

Hernandez, O. M., P. R. Housmans and J. D. Potter (2001). "Invited Review: pathophysiology of cardiac muscle contraction and relaxation as a result of alterations in thin filament regulation." J Appl Physiol (1985) **90**(3): 1125-1136.

Herron, T. J., E. Rostkova, G. Kunst, R. Chaturvedi, M. Gautel and J. C. Kentish (2006). "Activation of myocardial contraction by the N-terminal domains of myosin binding protein-C." Circ Res **98**(10): 1290-1298.

Hirt, M. N., J. Boeddinghaus, A. Mitchell, S. Schaaf, C. Bornchen, C. Muller, H. Schulz, N. Hubner, J. Stenzig, A. Stoehr, C. Neuber, A. Eder, P. K. Luther, A. Hansen and T. Eschenhagen (2014). "Functional improvement and maturation of rat and human engineered heart tissue by chronic electrical stimulation." J Mol Cell Cardiol **74**: 151-161.

Hirt, M. N., A. Hansen and T. Eschenhagen (2014). "Cardiac tissue engineering: state of the art." Circ Res **114**(2): 354-367.

Ho, C. Y. (2010). "Hypertrophic cardiomyopathy." Heart Fail Clin **6**(2): 141-159.

James, J. and J. Robbins (2011). "Signaling and myosin-binding protein C." J Biol Chem **286**(12): 9913-9919.

Jessup, M., B. Greenberg, D. Mancini, T. Cappola, D. F. Pauly, B. Jaski, A. Yaroshinsky, K. M. Zsebo, H. Dittrich, R. J. Hajjar and I. Calcium Upregulation by Percutaneous Administration of Gene Therapy in Cardiac Disease (2011). "Calcium Upregulation by Percutaneous Administration of Gene Therapy in Cardiac Disease (CUPID): a phase 2 trial of intracoronary gene therapy of sarcoplasmic reticulum Ca2+-ATPase in patients with advanced heart failure." Circulation **124**(3): 304-313.

Jia, W., J. F. Shaffer, S. P. Harris and J. A. Leary (2010). "Identification of novel protein kinase A phosphorylation sites in the M-domain of human and murine cardiac myosin binding protein-C using mass spectrometry analysis." J Proteome Res **9**(4): 1843-1853.

Kaufmann, K. B., H. Buning, A. Galy, A. Schambach and M. Grez (2013). "Gene therapy on the move." EMBO Mol Med **5**(11): 1642-1661.

Kim, J., J. Lim and C. Lee (2013). "Quantitative real-time PCR approaches for microbial community studies in wastewater treatment systems: applications and considerations." Biotechnol Adv **31**(8): 1358-1373.

Kooij, V., R. J. Holewinski, A. M. Murphy and J. E. Van Eyk (2013). "Characterization of the cardiac myosin binding protein-C phosphoproteome in healthy and failing human hearts." J Mol Cell Cardiol **60**: 116-120.

Kuster, D. W., A. C. Bawazeer, R. Zaremba, M. Goebel, N. M. Boontje and J. van der Velden (2012). "Cardiac myosin binding protein C phosphorylation in cardiac disease." J Muscle Res Cell Motil **33**(1): 43-52.

Kuster, D. W., V. Sequeira, A. Najafi, N. M. Boontje, P. J. Wijnker, E. R. Witjas-Paalberends, S. B. Marston, C. G. Dos Remedios, L. Carrier, J. A. Demmers, C. Redwood, S. Sadayappan and J. van der Velden (2013). "GSK3beta phosphorylates newly identified site in the proline-alanine-rich region of cardiac myosin-binding protein C and alters cross-bridge cycling kinetics in human: short communication." Circ Res **112**(4): 633-639.

Lekanne Deprez, R. H., J. J. Muurling-Vlietman, J. Hruda, M. J. Baars, L. C. Wijnaendts, I. Stolte-Dijkstra, M. Alders and J. M. van Hagen (2006). "Two cases of severe neonatal hypertrophic cardiomyopathy caused by compound heterozygous mutations in the MYBPC3 gene." J Med Genet **43**(10): 829-832.

Mamidi, R., J. Li, K. S. Gresham and J. E. Stelzer (2014). "Cardiac myosin binding protein-C: a novel sarcomeric target for gene therapy." Pflugers Arch **466**(2): 225-230.

Maron, B. J., J. M. Gardin, J. M. Flack, S. S. Gidding, T. T. Kurosaki and D. E. Bild (1995). "Prevalence of hypertrophic cardiomyopathy in a general population of young adults. Echocardiographic analysis of 4111 subjects in the CARDIA Study. Coronary Artery Risk Development in (Young) Adults." Circulation **92**(4): 785-789.

Maron, B. J. and M. S. Maron (2013). "Hypertrophic cardiomyopathy." Lancet **381**(9862): 242-255.

Maron, B. J., S. R. Ommen, C. Semsarian, P. Spirito, I. Olivotto and M. S. Maron (2014). "Hypertrophic cardiomyopathy: present and future, with translation into contemporary cardiovascular medicine." J Am Coll Cardiol **64**(1): 83-99.

Maron, B. J., J. Shirani, L. C. Poliac, R. Mathenge, W. C. Roberts and F. O. Mueller (1996). "Sudden death in young competitive athletes. Clinical, demographic, and pathological profiles." JAMA **276**(3): 199-204.

Maron, M. S., B. M. Kalsmith, J. E. Udelson, W. Li and D. DeNofrio (2010). "Survival after cardiac transplantation in patients with hypertrophic cardiomyopathy." Circ Heart Fail **3**(5): 574-579.

Marston, S., O. Copeland, A. Jacques, K. Livesey, V. Tsang, W. J. McKenna, S. Jalilzadeh, S. Carballo, C. Redwood and H. Watkins (2009). "Evidence from human myectomy samples that MYBPC3 mutations cause hypertrophic cardiomyopathy through haploinsufficiency." Circ Res **105**(3): 219-222.

Mearini, G., D. Stimpel, B. Geertz, F. Weinberger, E. Kramer, S. Schlossarek, J. Mourot-Filiatre, A. Stoehr, A. Dutsch, P. J. Wijnker, I. Braren, H. A. Katus, O. J. Muller, T. Voit, T. Eschenhagen and L. Carrier (2014). "Mybpc3 gene therapy for neonatal cardiomyopathy enables long-term disease prevention in mice." Nat Commun **5**: 5515.

Mearini, G., D. Stimpel, E. Kramer, B. Geertz, I. Braren, C. Gedicke-Hornung, G. Precigout, O. J. Muller, H. A. Katus, T. Eschenhagen, T. Voit, L. Garcia, S. Lorain and L. Carrier (2013). "Repair of Mybpc3 mRNA by 5'-trans-splicing in a Mouse Model of Hypertrophic Cardiomyopathy." Mol Ther Nucleic Acids **2**: e102.

Merkulov, S., X. Chen, M. P. Chandler and J. E. Stelzer (2012). "In vivo cardiac myosin binding protein C gene transfer rescues myofilament contractile dysfunction in cardiac myosin binding protein C null mice." Circ Heart Fail **5**(5): 635-644.

Meurs, K. M., X. Sanchez, R. M. David, N. E. Bowles, J. A. Towbin, P. J. Reiser, J. A. Kittleson, M. J. Munro, K. Dryburgh, K. A. Macdonald and M. D. Kittleson (2005). "A cardiac myosin binding protein C mutation in the Maine Coon cat with familial hypertrophic cardiomyopathy." Hum Mol Genet **14**(23): 3587-3593.

Morita, H., H. L. Rehm, A. Menesses, B. McDonough, A. E. Roberts, R. Kucherlapati, J. A. Towbin, J. G. Seidman and C. E. Seidman (2008). "Shared genetic causes of cardiac hypertrophy in children and adults." N Engl J Med **358**(18): 1899-1908.

Mun, J. Y., M. J. Previs, H. Y. Yu, J. Gulick, L. S. Tobacman, S. Beck Previs, J. Robbins, D. M. Warshaw and R. Craig (2014). "Myosin-binding protein C displaces tropomyosin to activate cardiac thin filaments and governs their speed by an independent mechanism." Proc Natl Acad Sci U S A **111**(6): 2170-2175.

Oakley, C. E., B. D. Hambly, P. M. Curmi and L. J. Brown (2004). "Myosin binding protein C: structural abnormalities in familial hypertrophic cardiomyopathy." Cell Res **14**(2): 95-110.

Offer, G., C. Moos and R. Starr (1973). "A new protein of the thick filaments of vertebrate skeletal myofibrils. Extractions, purification and characterization." J Mol Biol **74**(4): 653-676.

Okita, K., T. Ichisaka and S. Yamanaka (2007). "Generation of germline-competent induced pluripotent stem cells." Nature **448**(7151): 313-317.

Pleger, S. T., H. Brinks, J. Ritterhoff, P. Raake, W. J. Koch, H. A. Katus and P. Most (2013). "Heart failure gene therapy: the path to clinical practice." Circ Res **113**(6): 792-809.

Pohlmann, L., I. Kroger, N. Vignier, S. Schlossarek, E. Kramer, C. Coirault, K. R. Sultan, A. El-Armouche, S. Winegrad, T. Eschenhagen and L. Carrier (2007). "Cardiac myosin-binding protein C is required for complete relaxation in intact myocytes." Circ Res **101**(9): 928-938.

Prasad, K. M., Y. Xu, Z. Yang, S. T. Acton and B. A. French (2011). "Robust cardiomyocyte-specific gene expression following systemic injection of AAV: in vivo gene delivery follows a Poisson distribution." Gene Ther **18**(1): 43-52.

Richard, P., P. Charron, L. Carrier, C. Ledeuil, T. Cheav, C. Pichereau, A. Benaiche, R. Isnard, O. Dubourg, M. Burban, J. P. Gueffet, A. Millaire, M. Desnos, K. Schwartz, B. Hainque, M. Komajda and E. H. F. Project (2003). "Hypertrophic cardiomyopathy: distribution of disease genes, spectrum of mutations, and implications for a molecular diagnosis strategy." Circulation **107**(17): 2227-2232.

Richard, P., E. Villard, P. Charron and R. Isnard (2006). "The Genetic Bases of Cardiomyopathies." J Am Coll Cardiol **Vol. 48**(9): A79-89.

Robinson, K., M. P. Frenneaux, B. Stockins, G. Karatasakis, J. D. Poloniecki and W. J. McKenna (1990). "Atrial fibrillation in hypertrophic cardiomyopathy: a longitudinal study." J Am Coll Cardiol **15**(6): 1279-1285.

Sadayappan, S. and P. P. de Tombe (2012). "Cardiac myosin binding protein-C: redefining its structure and function." Biophys Rev **4**(2): 93-106.

Sadayappan, S., J. Gulick, H. Osinska, D. Barefield, F. Cuello, M. Avkiran, V. M. Lasko, J. N. Lorenz, M. Maillet, J. L. Martin, J. H. Brown, D. M. Bers, J. D. Molkentin, J. James and J. Robbins (2011). "A critical function for Ser-282 in cardiac Myosin binding protein-C phosphorylation and cardiac function." Circ Res **109**(2): 141-150.

Sadayappan, S., H. Osinska, R. Klevitsky, J. N. Lorenz, M. Sargent, J. D. Molkentin, C. E. Seidman, J. G. Seidman and J. Robbins (2006). "Cardiac myosin binding protein C phosphorylation is cardioprotective." Proc Natl Acad Sci U S A **103**(45): 16918-16923.

Sarikas, A., L. Carrier, C. Schenke, D. Doll, J. Flavigny, K. S. Lindenberg, T. Eschenhagen and O. Zolk (2005). "Impairment of the ubiquitin-proteasome system by truncated cardiac myosin binding protein C mutants." Cardiovasc Res **66**(1): 33-44.

Schlender, K. K. and L. J. Bean (1991). "Phosphorylation of chicken cardiac C-protein by calcium/calmodulin-dependent protein kinase II." J Biol Chem **266**(5): 2811-2817.

Schlossarek, S., N. Frey and L. Carrier (2014). "Ubiquitin-proteasome system and hereditary cardiomyopathies." J Mol Cell Cardiol **71**: 25-31.

Schlossarek, S., G. Mearini and L. Carrier (2011). "Cardiac myosin-binding protein C in hypertrophic cardiomyopathy: mechanisms and therapeutic opportunities." J Mol Cell Cardiol **50**(4): 613-620.

Sequeira, V., E. R. Witjas-Paalberends, D. W. Kuster and J. van der Velden (2014). "Cardiac myosin-binding protein C: hypertrophic cardiomyopathy mutations and structure-function relationships." Pflugers Arch **466**(2): 201-206.

Shaffer, E. M., A. P. Rocchini, R. L. Spicer, J. Juni, R. Snider, D. C. Crowley and A. Rosenthal (1988). "Effects of verapamil on left ventricular diastolic filling in children with hypertrophic cardiomyopathy." Am J Cardiol **61**(6): 413-417.

Spinney, L. (2004). "Heart-stopping action." Nature **430**(7000): 606-607.

Stoehr, A., C. Neuber, C. Baldauf, I. Vollert, F. W. Friedrich, F. Flenner, L. Carrier, A. Eder, S. Schaaf, M. N. Hirt, B. Aksehirlioglu, C. W. Tong, A. Moretti, T. Eschenhagen and A. Hansen (2014). "Automated analysis of contractile force and Ca2+ transients in engineered heart tissue." Am J Physiol Heart Circ Physiol **306**(9): H1353-1363.

Stohr, A., F. W. Friedrich, F. Flenner, B. Geertz, A. Eder, S. Schaaf, M. N. Hirt, J. Uebeler, S. Schlossarek, L. Carrier, A. Hansen and T. Eschenhagen (2013). "Contractile abnormalities and altered drug response in engineered heart tissue from Mybpc3-targeted knock-in mice." J Mol Cell Cardiol **63**: 189-198.

Teare, D. (1958). "Asymmetrical hypertrophy of the heart in young adults." Br Heart J **20**(1): 1-8.

Tendera, M., A. Wycisk, A. Schneeweiss, L. Polonski and J. Wodniecki (1993). "Effect of sotalol on arrhythmias and exercise tolerance in patients with hypertrophic cardiomyopathy." Cardiology **82**(5): 335-342.

van Dijk, S. J., E. R. Paalberends, A. Najafi, M. Michels, S. Sadayappan, L. Carrier, N. M. Boontje, D. W. Kuster, M. van Slegtenhorst, D. Dooijes, C. dos Remedios, F. J. ten Cate, G. J. Stienen and J. van der Velden (2012). "Contractile dysfunction irrespective of the mutant protein in human hypertrophic cardiomyopathy with normal systolic function." Circ Heart Fail **5**(1): 36-46.

Vandenburgh, H., J. Shansky, F. Benesch-Lee, V. Barbata, J. Reid, L. Thorrez, R. Valentini and G. Crawford (2008). "Drug-screening platform based on the contractility of tissue-engineered muscle." Muscle Nerve **37**(4): 438-447.

Vannucci, L., M. Lai, F. Chiuppesi, L. Ceccherini-Nelli and M. Pistello (2013). "Viral vectors: a look back and ahead on gene transfer technology." New Microbiol **36**(1): 1-22.

Vignier, N., S. Schlossarek, B. Fraysse, G. Mearini, E. Kramer, H. Pointu, N. Mougenot, J. Guiard, R. Reimer, H. Hohenberg, K. Schwartz, M. Vernet, T. Eschenhagen and L. Carrier (2009). "Nonsense-mediated mRNA decay and ubiquitin-proteasome system regulate cardiac myosin-binding protein C mutant levels in cardiomyopathic mice." Circ Res **105**(3): 239-248.

Wang, W., W. Li, N. Ma and G. Steinhoff (2013). "Non-viral gene delivery methods." Curr Pharm Biotechnol **14**(1): 46-60.

Wessels, M. W., J. C. Herkert, I. M. Frohn-Mulder, M. Dalinghaus, A. van den Wijngaard, R. R. de Krijger, M. Michels, I. F. de Coo, Y. M. Hoedemaekers and D. Dooijes (2015). "Compound heterozygous or homozygous truncating MYBPC3 mutations cause lethal cardiomyopathy with features of noncompaction and septal defects." Eur J Hum Genet **23**(7): 922-928.

Wijnker, P. J., F. W. Friedrich, A. Dutsch, S. Reischmann, A. Eder, I. Mannhardt, G. Mearini, T. Eschenhagen, J. van der Velden and L. Carrier (2016). "Comparison of the effects of a truncating and a missense MYBPC3 mutation on contractile parameters of engineered heart tissue." J Mol Cell Cardiol **97**: 82-92.

Winegrad, S. (1999). "Cardiac myosin binding protein C." Circ Res **84**(10): 1117-1126.

Xin, B., E. Puffenberger, J. Tumbush, J. R. Bockoven and H. Wang (2007). "Homozygosity for a novel splice site mutation in the cardiac myosin-binding protein C gene causes severe neonatal hypertrophic cardiomyopathy." Am J Med Genet A **143A**(22): 2662-2667.

Yamamoto, K. and C. Moos (1983). "The C-proteins of rabbit red, white, and cardiac muscles." J Biol Chem **258**(13): 8395-8401.

Zhu, X., M. Hadhazy, M. E. Groh, M. T. Wheeler, R. Wollmann and E. M. McNally (2001). "Overexpression of gamma-sarcoglycan induces severe muscular dystrophy.

Implications for the regulation of Sarcoglycan assembly." J Biol Chem **276**(24): 21785-21790.

8 Own publications

G. Mearini, D. Stimpel, B. Geertz, F. Weinberger, E. Kramer, S. Schlossarek, J. Mourot-Filiatre, A. Stoehr, A. Dutsch, P. J. Wijnker, I. Braren, H. A. Katus, O. J. Muller, T. Voit, T. Eschenhagen and L. Carrier (2014). "Mybpc3 gene therapy for neonatal cardiomyopathy enables long-term disease prevention in mice." Nat Commun **5**: 5515.

P. J. Wijnker, F.W. Friedrich, A. Dutsch, S. Reischmann, A. Eder, I. Mannhardt, G. Mearini, T. Eschenhagen, J. van der Velden, L. Carrier (2016). "Comparison of the effects of a truncating and a missense MYBPC3 mutation on contractile parameters of engineered heart tissue." J Mol Cell Cardiol **10**: 1016.

9 Acknowledgements

This thesis would not have been possible without many people that supported me in this time. I've learned a lot about scientific work but I've also learned a lot about myself and got to know many people that became more than just colleagues to me during the time in the lab.

I'd like to thank the CVRC for giving me the opportunity of a scholarship to perform the work for this thesis in a full time job for a whole year.

I thank Prof. Dr. Thomas Eschenhagen for the opportunity to work on my thesis in the Department of Experimental Pharmacology and Toxicology, University Medical Center, Hamburg-Eppendorf. I appreciate his support for the work with mouse EHTs, which were admittedly not the easiest model to deal with.

From the beginning I knew I wanted to join the research group of Prof. Dr. Lucie Carrier. And I was lucky to be able to. Lucie has been a great support to me infecting me with her excitement for science. Especially in stressful situations she was a calm anchor encouraging me that I could make it. I will always remember her words, which were more or less like this: "Science is like a river. It can be calm but it can also be rough and quite hard to swim in. But you have to keep on swimming."

Another person without this work would have not been possible, is Giulia Mearini. She was a wonderful supervisor to me. She helped me throughout the whole time, I knew I could always ask her, no matter how simple the question was. I appreciate her patience and her commitment she had for me and the project. She always assuaged my sorrows and with her optimism was a source of inspiration to me.

Special thanks I would like to say to the whole AG Carrier. It did not feel like going to work every day with all of the people around. Without Lisa Krämer this thesis would definitely not be like it is today. With her effort and support I managed to learn scientific techniques and she always had an appropriate solution for every problem also apart from the work in the lab.
Especially Paul Wijnker was more than just a colleague for me. I'm very happy that I could learn a lot with him and a lot from him about science. I think we were a great

team on the work with mouse EHTs although we also had our disagreements. Moreover I want to mention all the other people that also supported me during my lab work made this unique atmosphere in the research group possible: Felix Friedrich, Maksimilian Prondzynski, Sonia Singh, Frederik Flenner, Mahtab Naisb, Verena Behrens-Gawlik, Silke Reischmann, Birgit Geertz, Saskia Schlossarek and Simon Braumann.

Additionally I would also like to thank the whole Department of Experimental Pharmacology and Toxicology. The warm and friendly atmosphere made working pleasant and not a duty. Particularly I want to thank Marc Hirt, Arne Hansen, Alexandra Eder, Ingra Vollert, David Letuffe-Breniere, Ann-Cathrin Kunze and Tessa Werner for their support on EHTs.

I also want to thank the HEXT Core Facility (Ingke Braren, Claudia Schob) in the basement of the Department of Experimental Pharmacology and Toxicology for the production of the AAV.

Not only people from science made this work possible. Also my very best friends Timo and Stefan shall be named here. They always had an open ear for my sorrows and never were angry if they needed to relinquish me.
And finally I want to thank my family. It is invaluable to mention what my parents make possible for me. I dedicate this work to my parents, to give thanks to what they did for me, to make them proud of me and happy.

10 Curriculum vitae

Personal data

Name:	Alexander Dutsch
Date of birth:	12th March 1990
Place of birth:	Henstedt-Ulzburg

Education

2009	Abitur, Dietrich-Bonhoeffer Gymnasium, Quickborn
since 2010	Medicine, University Hamburg
08/2012	1st Medical Examinations, Hamburg
10/2013-10/2014	MD scholarship student, Cardiovascular Research Center, Institute for Pharmacology and Toxicology (Research group of Prof. Dr. Lucie Carrier), Hamburg
12/2014	Co-Author on “Mybpc3 gene therapy for neonatal cardiomyopathy enables long-term disease prevention in mice.", Mearini et al., published in Nat Commun
04/2016	2nd Medical Examinations, Hamburg
04/2016	Co-Author on "Comparison of the effects of a truncating and a missense MYBPC3 mutation on contractile parameters of engineered heart tissue.", Wijnker et al., published in J Mol Cell Cardiol
05-09/2016	Practical year, Anaesthesiology, Asklepios Klinik Barmbek, Hamburg
09-12/2016	Practical year, Surgery, Universitätsspital Basel, Switzerland
12/2016-04/2017	Practical year, Internal Medicine, Albertinen-Krankenhaus, Hamburg

11 Appendix

11.1 List of abbreviations

°C	Degree Celsius
3D	3-dimensional
A	Adenine
AAV	Adeno-associated virus
AC	Adenylyl cyclase
Acta1	Mouse α –skeletal actin gene
APS	Ammonium persulfate
ATP	Adenosine triphosphate
AV block	Atrioventricular block
bp	Base pair(s)
bpm	Beats per minute
BSA	Bovine serum albumin
C-protein	cMyBP-C
Ca^{2+}	Calcium
CaMKII	calcium calmodulin-dependent protein kinase II
cAMP	3'-5'-Cyclic adenosine monophosphate
cDNA	Complementary desoxyribonucleic acid
CK 2	Casein kinase II
CMV	Cytomegalovirus
cMyBP-C	Cardiac Myosin binding protein C
C_t	Cycle threshold
cTnC	Cardiac troponin C
cTnI	Cardiac troponin I
cTnT	Cardiac troponin T
CV	Contraction velocity
DMEM	Dulbecco's Modified Eagle's Medium
DMSO	Dimethyl sulfoxide

DNA	Desoxyribonucleic acid
dNTP	Deoxynucleoside triphosphate
ECC	Excitation contraction coupling
ECL-Prime Kit	Enhanced chemiluminescence
ECT	Engineered cardiac tissue
EHT	Engineered Heart Tissue
EMD	EMD 57033
EMD 57033	5-(1-(3,4-dimethoxybenzoyl)-1,2,3,4-tetrahydroquinolin-6-yl)-6-methyl-3,6-dihydro-2H-1,3,4-thiadiazin-2-one
ESC	European Society of Cardiology
FACS	Flourescence-activated cell sorting
FCS	Fetal calf serum
G	Guanine
g	gram
g	Gravitational constant
G_i	Inhibitory GTP-binding protein
G_s	Stimulating GTP-binding protein
GAPDH	Glyceraldehyde 3-phosphate dehydrogenase
GTP	Guanosine triphosphate
HBSS	Hank's balanced salt solution
HCM	Hypertrophic cardiomyopathy
HEPES	4-(2-Hydroxyethyl)-1-piperazineethanesulfonic acid
HS	Horse serum
HW/BW	Heart weight/body weight
Hz	Frequency in Hertz
iPS	Induced pluripotent stem cells
kbp	Kilobase pair(s)
kDa	Kilodalton
KI	Knock-in
KI-D282	KI transduced with full-length WT

	constitutively phosphorylated *Mybpc3* cDNA
KI-NT	KI non-transduced
KI-S282	KI transduced with full-length WT *Mybpc3* cDNA
KO	Knock-out
l	Liter
LB medium	Lysogeny broth medium
LED	Light-emitting diode
LV	Left ventricle
M	Molar
m	Meter
M-Motif	Mybpc-Motif of cMyBP-C
min	Minutes
MOI	Multiplicity of infection
mRNA	Messenger ribonucleic acid
MYBPC3	Human cMyBP-C gene
Mybpc3	Mouse cMyBP-C gene
Myh7	Mouse β-myosin heavy chain gene
N	Force in Newton
NKM	Non cardiac myocyte medium
NppA	Mouse atrial natriuretic peptide gene
NYHA	New York Heart Association
Pa	Pascal
PBS	Phosphate buffered saline
PCR	Polymerase chain reaction
PKA	cAMP-dependent protein kinase
PKC	Protein kinase C
PKD	Protein kinase D
PLB	Phospholamban
Pro-Ala	Proline-Alanine
qPCR	Quantitative Polymerase chain reaction

RNA	Ribonucleic acid
rpm	Revolutions per minute
RSK	ribosomal S6 kinse
RT-PCR	Reverse transcriptase PCR
RV	Relaxation velocity
RyR	Ryanodine receptor
SDS-PAGE	Sodium dodecyl sulfate polyacrylamide gel electrophoresis
sec	Second
SEM	Standard error of the mean
Ser	Serine
SOC-medium	Super Optimal Broth medium with 20 mM Glucose
SR	Sarcoplasmatic reticulum
TBS	Tris buffered saline
TBS-T	TBS-Tween
TEMED	N,N,N',N'-Tetramethylethylenediamine
TNNT2	Human cardiac troponin T gene
U	Unit
V	Volt
WT	wild-type
β-AR	β-adrenergic receptor
α-MHC	α-Myosin heavy chain
β-MHC	β-Myosin heavy chain

11.2 SI Prefixes

k	Kilo (10^{3})
m	Mili (10^{-3})
µ	Micro (10^{-6})
n	Nano (10^{-9})

Eidesstattliche Versicherung

Ich versichere ausdrücklich, dass ich die Arbeit selbständig und ohne fremde Hilfe verfasst, andere als die von mir angegebenen Quellen und Hilfsmittel nicht benutzt und die aus den benutzten Werken wörtlich oder inhaltlich entnommenen Stellen einzeln nach Ausgabe (Auflage und Jahr des Erscheinens), Band und Seite des benutzten Werkes kenntlich gemacht habe.
Ferner versichere ich, dass ich die Dissertation bisher nicht einem Fachvertreter an einer anderen Hochschule zur Überprüfung vorgelegt oder mich anderweitig um Zulassung zur Promotion beworben habe.
Ich erkläre mich einverstanden, dass meine Dissertation vom Dekanat der Medizinischen Fakultät mit einer gängigen Software zur Erkennung von Plagiaten überprüft werden kann.

Datum: …… Unterschrift: .....